ENERGY LABORATORY

MASSACHUSETTS INSTITUTE
OF TECHNOLOGY

EULERIAN-LAGRANGIAN ANALYSIS OF POLLUTANT TRANSPORT IN SHALLOW WATER

by

Antonio E. de M. Baptista, E. Eric Adams
and Keith D. Stolzenbach

Energy Laboratory Report No. MIT-EL 84-008
June 1984

EULERIAN-LAGRANGIAN ANALYSIS OF POLLUTANT TRANSPORT IN SHALLOW WATER

by

Antonio E. de M. Baptista

E. Eric Adams

Keith D. Stolzenbach

Energy Laboratory

and

R.M. Parsons Laboratory for
Water Resources and Hydrodynamics

Department of Civil Engineering
Massachusetts Institute of Technology
Cambridge, Massachusetts 02139

Sponsored by

Northeast Utilities Service Company
and
New England Power Service Company

under the
MIT Energy Laboratory Electric Utility Program

Energy Laboratory Report MIT-EL 84-008

June 1984

EULERIAN-LAGRANGIAN ANALYSIS OF POLLUTANT TRANSPORT IN SHALLOW WATER

ABSTRACT

A numerical method for the solution of the two-dimensional, unsteady, transport equation is formulated, and its accuracy is tested.

The method uses a Eulerian-Lagrangian approach, in which the transport equation is divided into a diffusion equation (solved by a finite element method) and a convection equation (solved by the method of characteristics). This approach leads to results that are free of spurious oscillations and excessive numerical damping, even in the case where advection strongly dominates diffusion. For pure diffusion problems, optimal accuracy is approached as the time-step, Δt, goes to zero; conversely, for pure-convection problems, accuracy improves with increasing Δt; for convection-diffusion problems the Δt leading to optimal accuracy depends on the characteristics of the spatial discretization and on the relative importance of convection and diffusion.

The method is cost-effective in modeling pollutant transport in coastal waters, as demonstrated by two prototype applications: hypothetical sludge dumping in Massachusetts Bay and the thermal discharge from Brayton Point Generating Station in Narragansett Bay. Numerical diffusion is eliminated or greatly reduced, raising the need for realistic estimation of dispersion coefficients. Costs (based on CPU time) should not exceed those of conventional Eulerian methods and, in some cases (e.g., problems involving predictions over several tidal cycles), considerable savings may even be achieved.

ACKNOWLEDGEMENTS

This study was performed in connection with the project "Near and Far Field Interaction of Thermal Discharges", through the MIT Energy Laboratory Electric Utility Program. The sponsorship of Northeast Utilities Service Company and New England Power Service Company is acknowledged and greatly appreciated. Thanks are due to Mssrs. Andrew Aitken, Robert Gowing, Ronald Klattenberg, Ernesto Lorda, Martin Pitek and William Renfro and Ms. Linda Bireley, members of the project steering committee, for their cooperation and encouragement.

The typing of the manuscript was done by Miss Diane Hardy, and figures that were not directly generated by computer were drawn by Mrs. Izildinha Baptista.

The material contained in this report was submitted by Mr. Baptista in partial fulfillment of the requirements for the degree of Master of Science at M.I.T.

TABLE OF CONTENTS

LIST OF FIGURES

5.13 Convection and diffusion in a sinusoidal uniform flow. Numerical solutions at different times (M = 7; N = 288; T = 36864 s; $Pe_{max} = \infty$).

5.14 Convection and diffusion in a sinusoidal uniform flow. Error measures as a function of time.

5.15 Convection and diffusion of a continuous source in a steady uniform flow. Numerical solutions for different values of Pe ($t \equiv T = 9216$ s; M = 7; N = 72).

5.16 Diffusion in a depth-variable medium. Numerical solutions ($t \equiv T = 9216$ s; M = 7; N = 72).

5.17 Advancing front. Numerical solution for different Pe.

5.18 Convection in a flow in rigid-body rotation.

6.1 Massachusetts Bay. Finite Element Grid.

6.2 Massachusetts Bay. Velocity field at maximum ebb.

6.3 Massachusetts Bay. Velocity field at maximum flood.

6.4 Massachusetts Bay. Sludge plumes for discharge at Site 1.

6.5 Massachusetts Bay. Sludge plumes for discharge at Site 2.

6.6 Brayton Point. Complete finite element grid for Mt. Hope Bay.

6.7 Brayton Point. Detail of the finite element grid near the discharge.

6.8 Brayton Point. Circulation computed by TEA at maximum ebb.

6.9 Brayton Point. Detail of circulation computed by TEA at high tide.

6.10 Brayton Point. Detail of circulation computed by TEA at maximum ebb.

6.11 Brayton Point. Finite element grid used for transport calculations.

6.12 Brayton Point. Excess temperatures computed at high tide and maximum ebb.

7.1 Optimal time step. Illustrative sketches.

A.1 Linear discretization scheme.

A.2 Amplitude and phase errors per time step, for 1-D linear expansions.

A.3 Quadratic discretization scheme.

A.4 Amplitude and phase errors per time step, for 1-D quadratic expansions.

LIST OF TABLES

1. INTRODUCTION

The last few decades have seen an upsurge of numerical models for circulation and pollutant transport in natural waters. Their popularity is easily understandable: numerical models are relatively inexpensive, versatile and easy to use; yet they are based on rather complete forms of the equations of fluid mechanics, and therefore describe the relevant phenomena with good detail.

However, recent years have found users and developers of numerical models progressively more conscious of the limitations of their tools. Indeed, it has often been stressed (although not so much implemented) that models need to be calibrated and verified based on field data. Also, drawbacks of available numerical techniques have been identified and have become the subject of research.

One such drawback concerns the solution of the transport equation, when convection is dominant over diffusion (or other diffusion-like mechanisms). Most available numerical methods avoid spurious oscillations only at the expense of artificial diffusion, introduced explicitly in the data, or self-generated by the method. As a result, plumes of pollutants tend to be, especially in the so-called intermediate field, excessively diffused and damped.

The present work describes, tests and demonstrates the cost-effectiveness of a numerical method characterized by low artificial diffusion, even for convection-dominated transport problems.

The mathematical problem is stated in Chapter 2. The 2-D unsteady form of the transport equation is selected, given that we are primarily

interested in the analysis of shallow coastal waters; however, no conceptual difficulties should arise if the method is extended to 3-D.

Chapter 3 presents a brief review of methods available for the solution of the stated problem. A clear distinction is made between Eulerian, Eulerian-Lagrangian and Lagrangian methods; each of these categories of methods represents a rather different solution approach and results are likely to reflect these differences.

Chapter 4 describes the method developed in this study, which is Eulerian-Lagrangian in concept. The method is based on the decomposition of the transport equation into a diffusion equation, solved by a finite element method, and a convection equation, solved by the method of characteristics.

Chapter 5 presents the results of tests, performed by using the proposed method to solve several problems with known exact solutions. Results are rather satisfactory, showing a good ability in handling even strongly convection-dominated problems with neither excessive damping nor spurious oscillations.

Chapter 6 describes the application of the method to two prototype examples: sludge dumping in Massachusetts Bay and thermal plume calculations in Narragansett Bay. These applications are presented as illustrations of the potential and drawbacks of the method, and are not intended for direct impact assessment.

Chapter 7 presents the conclusions of our work, and identifies future research needs.

2. MATHEMATICAL STATEMENT OF THE PROBLEM

The fate of a passive pollutant discharged in shallow water is often appropriately described by the 2-D (depth-averaged) transport equation

$$\frac{\partial c}{\partial t} + u_i \frac{\partial c}{\partial x_i} = \frac{1}{h} \frac{\partial}{\partial x_i} \left(h \, D_{ij} \frac{\partial c}{\partial x_j} \right) + Q \qquad (2.1)$$

where

$c(x,y,t)$ - is the unknown depth-averaged concentration of the pollutant

$u_i(x,y,t)$ - is the flow velocity in the i-direction

$h(x,y,t)$ - is the flow depth

$D_{ij}(x,y,t)$ - are diffusion coefficients, forming a 2×2 tensor

$Q(c,x,y,t)$ - represents internal sources and sinks, and vertical fluxes through the bottom and the surface of the flow

($i = 1,2$; $j = 1,2$; $x_1 \equiv x$; $y_2 \equiv y$; $u_1 \equiv u$; $u_2 \equiv v$; summation implied over repeated indices)

To complete the formulation, initial and boundary conditions must be imposed. Such conditions will be considered to be of the form (Fig. 2.1)

$$c(x,y,t) = c_o(x,y) \qquad \text{at } t = 0, \text{ in } \Omega \qquad (2.2)$$

$$c(x,y,t) = \bar{c}(x,y,t) \qquad \text{at } t > 0, \text{ on } \Gamma_1 \qquad (2.3)$$

$$q_n(x,y,t) = \bar{q}_n(x,y,t) \qquad \text{at } t > 0, \text{ on } \Gamma_2 \qquad (2.4)$$

where an overbar denotes a known quantity; q_n represents a flux normal to the boundary, and is defined as

$$q_n = - D_{ij} \frac{\partial c}{\partial x_j} \cos(\hat{n}, \hat{x}_i) \qquad (2.5)$$

Eq. (2.1) results from the principle of mass conservation, applied to a pollutant dissolved or suspended passively in a turbulent quasi-horizontal host fluid. The well-known derivation involves two averaging processes: one over the time-scale of turbulence, and the other over the flow depth (e.g., see Daily and Harleman, 1966). Two diffusion-like mechanisms (turbulent diffusion, and shear-diffusion or dispersion) result from these averages, each representing the bulk transport effect of the part of the flow which is not explicitly represented. Turbulent and shear diffusion are, in general, unsteady, non-homogeneous, and orthotropic (with principal axis that do not necessarily coincide with x and y, at each point). However, the ability to evaluate the appropriate coefficients in natural waters is rather limited, which has often lead to the assumption that D_{ij} are constant in time and space.

Although turbulent and shear diffusion are several orders of magnitude more efficient than molecular diffusion, their transport ability is typically still secondary to convection by the part of the flow that is explicitly represented by u, v and h. This leads to the dominance, in Eq. (2.1), of hyperbolic (e.g. $u\,\partial c/\partial x$) over parabolic (e.g. $D_{xx}\,\partial^2 c/\partial x^2$) operators, which constitutes a major difficulty for the numerical solution of the transport equation (see Chapter 3).

The term Q(c,x,y,t) that appears on the right-hand side of Eq. (2.1) is problem-dependent but typically introduces little challenge as far as the numerical solution of the transport equation is concerned.

In the present work we will set

$$Q(c,x,y,t) = p(x,y,t) - \kappa(x,y,t)\, c(x,y,t) \qquad (2.6)$$

where p represents a source, and $-\kappa c$ a first-order decay mechanism.

3. REVIEW OF AVAILABLE SOLUTION METHODS

3.1 Introduction

Several numerical methods have been proposed to solve numerically the transport equation. They typically fit in one of three categories: Eulerian, Lagrangian, and Eulerian-Lagrangian methods.

Eulerian methods solve the Eulerian form of the transport equation (e.g., Eq. 2.1) in the nodes of a fixed grid. As a consequence, they require the simultaneous solution of hyperbolic and parabolic operators, which has proved to be a hard task when the former dominate the latter (see §3.2).

Lagrangian methods avoid the explicit treatment of hyperbolic operators by solving the transport equation in a grid moving with the flow. Although potentially very accurate, this approach leads, in many situations of interest (e.g., continuous sources and complex reversing flows), to practical difficulties, linked to the grid displacement and deformation.

Eulerian-Lagrangian methods constitute an intermediate approach. The convenience of a fixed grid is retained, but, at some point of the numerical procedure, the transport equation is treated in Lagrangian form to avoid the explicit treatment of the hyperbolic operators.

Eulerian methods (EM) are currently the most popular ones, much because of historical reasons. However, a major shift towards the use of Eulerian-Lagrangian methods (ELM) may occur in the near future. The review presented in the next section will be restricted to these two categories. For completeness, we mention Varoglu and Finn, 1980, and O'Neill and Lynch, 1980, as references on Lagrangian methods.

3.2 Eulerian Methods

Methods in this category are typically based on the build-up and solution of a single system of algebraic equations, where both convective and diffusive terms are represented; unknowns are the concentrations at a finite number of fixed locations (nodes) in the computational domain. The transformation of the original differential equation into such a system of algebraic equations is usually achieved using either finite difference methods (FDM) or finite element methods (FEM).

Relative merits of FDM and FEM have been widely discussed for several years. While few uniformly accepted conclusions have been reached, it is usually recognized that FEM

- handle more efficiently complicated land boundaries and internal grid refinements;
- are more consistent in the treatment of boundary conditions and in the set-up of interpolation procedures over the whole computational domain;

while FDM

- are more intuitive to formulate, and tend to require less memory capacity and CPU time, for a similar number of nodes;
- result in significantly easier procedures concerning preparation and input of data.

FDM have been used in the solution of the transport equation since the late 1950's. They typically discretize the computational domain through the use of an orthogonal grid. Stretching transformations may be used to provide some grid refinement. Over each grid element, the differential transport equation is replaced by an algebraic equation,

where both the space- and time-derivatives are approximated by finite-differences. The resulting system of algebraic equations is adjusted to take into account the appropriate boundary conditions, and is then solved to give the nodal concentrations.

Initial FDM used centered schemes to approximate both the convection and the diffusion terms (e.g., $u \left.\frac{\partial c}{\partial x}\right|_j \simeq u_j \frac{c_{j+1} - c_{j-1}}{2\Delta x}$; $D \left.\frac{\partial^2 c}{\partial x^2}\right|_j \simeq D_j \frac{c_{j+1} - 2c_j + c_{j-1}}{\Delta x^2}$, where j denotes an arbitrary node). Such methods were typically plagued with spurious spatial oscillations (wiggles). A careful analysis of the production of wiggles is presented in Roache (1982) in the context of a one-dimensional, steady problem, using a regular grid; major conclusions have proved to hold for higher-dimensions, unsteady conditions, and (in a less straightforward way) irregular grids. Wiggles are produced when

$$Pe = \frac{u\Delta x}{D} \geq 2$$

where Pe is the Peclet (or cell-Reynolds) number. The usefulness of centered FDM is then reduced to the solution of diffusion-dominated problems (where $Pe < 2$, with Δx in some practical range).

As a remedy for wiggles in convection-dominated problems ($Pe \geq 2$), more recent FDM have used centered finite-differences only for the diffusion terms, replacing the convective derivatives by upwinding differences (e.g., $u \frac{\partial c}{\partial x} \simeq u_j \frac{(c_j - c_{j-1})}{\Delta x}$ if $u_j > 0$, and $u_j \frac{c_{j+1} - c_j}{\Delta x}$ if $u_j < 0$). Upwinding methods do avoid wiggles; however, they introduce numerical diffusion in a way that increases with Pe and may easily overshadow physical diffusion (Roache, 1982). The use of such methods, therefore, corresponds to a re-statement of the physical

problem, which may not be acceptable. In spite of this limitation, upwinding FDM have become popular tools in engineering practice.

An alternative approach (Flux-Corrected Transport Method) was proposed by Book et al. (1975) in the form of the addition of "optimal" artificial diffusion (the magnitude of the artificial diffusion is systematically selected over the domain only as required to avoid wiggles). Again, this approach leads to a re-statement of the problem.

FEM have become popular for the solution of the transport equation since the early 1970's. The computational domain is divided into elements of convenient shape, such as triangles or quadrilaterals. Within each element information is concentrated in nodes, but may be unambiguously interpolated to any other point using pre-selected interpolation functions. The original partial differential equation is then transformed into a system of ordinary differential equations in time, using a weighted residual method. Numerical integration of this system leads finally to a system of algebraic equations, whose solution gives the nodal values of the concentration field.

The use of the weighted residual method requires the definition of elementary weighted residuals; these result from the integration over each element of the errors made in approximating the actual concentration field, weighted by pre-selected weighting functions; the sum over the whole computational domain of the elementary residuals is then forced to be zero, to minimize the approximation errors. Different FEM result from different choices of interpolation and weighting functions. In the early 1970's, most FEM solved the transport equation using the same interpolation and weighting functions; such methods are

known as Galerkin-FEM (GA-FEM). They are the basis for the models DISPER (Leimkuhler, 1974) and FETRA (Onishi, 1981), among others.

GA-FEM lead to "centered" approximations of the advective terms, and present the same limitations as centered FDM: wiggles are produced when the Peclet number exceeds a small critical value. Users of GA-FEM have tried to extend the application of the method to convection-dominated problems, through the adoption of uniform diffusion coefficients which may be 1 to 2 orders of magnitude larger than the physical ones.

In the late 1970's several attempts were made to account for the flow direction, i.e., to "upwind" FEM. Petrov-Galerkin FEM (PG-FEM), as presented by Christie et al. (1976) and extended by Heinrich et al. (1977) and Heinrich and Zienkiewicz (1977) constitute one such attempt which has been successful in avoiding wiggles. In these methods, the weighting functions are not equal to the interpolation functions, but are obtained from them by a change in shape that increases the relative weight of upstream information in a way that depends on the element geometry and the flow characteristics. Limitations of PG-FEM methods include (a) introduction of artificial diffusion, as a function of the local Peclet number (similar to upwinding FDM); (b) increased computational effort required to generate the weighting functions from the interpolation functions, at each element and at each time step, and (c) difficulty in handling elements other than quadrilaterals.

A different upwinding procedure (much in the line of the Flux-Corrected Transport Method in FDM) was proposed by Hughes (1979) for 1-D, and was later extended to 2-D (Hughes and Brooks, 1979 and Kelly et al., 1980). In this procedure, the weighting and interpola-

tion funtions are equal, like in standard GA-FEM. However, an artificial anisotropic diffusion term, equivalent to the one that is implicitely introduced by the PG-FEM, is computed and added to each element at each time step. Methods using this procedure have not received a unique designation, being sometimes referred to as Balanced-Dissipation - FEM (BD-FEM). Results of BD-FEM have been reported as indistinguishable from results obtained with PG-FEM. However, BD-FEM are much less expensive and are more easily applied to elements of any shape and dimensionality.

3.3 Eulerian-Lagrangian Methods

Eulerian-Lagrangian methods (ELM) represent an attempt to combine the convenience of an Eulerian grid with the accuracy of a Lagrangian treatment of convection. Typically, ELM decouple the transport equation into two components (pure-convection and pure-diffusion), each being solved by an appropriate technique. Most often, the convection equation is solved by a backwards method of characteristics, while the diffusion equation is solved by FDM (Holly and Preissmann, 1977; Glass and Rodi, 1982; Holly and Polatera, 1984). A few ELM using FEM to solve the diffusion equation have been studied in recent years (Newman, 1981; Newman and Sorek, 1982, Hasbani et al., 1983).

The general procedure behind a ELM is illustrated in Fig. 3.1. At time t_n parcels of fluid are identified with each node of the numerical grid, and followed backwards along a streamline, until a previous time t_{n-1} where the nodal concentrations are all known. Concentrations of the parcels at t_{n-1} are then found by interpolation, and directly associated with the nodal concentrations at t_n

(Fig. 3.1a). This completes the solution of the convection equation. A conventional centered FDM or FEM is then used to solve the diffusion equation, using the newly computed concentrations as initial conditions (Fig. 3.1b).

Cheng et al. 1984 uses a different Eulerian-Lagrangian approach. The transport equation is written in Lagrangian form, but is not decoupled. As above, at any given time t_n a parcel is associated with each node and followed backwards, along a streamline, until t_{n-1}. Now, however, instead of using a numerical procedure for the diffusion step, concentrations at t_n are computed as the weighted average of concentrations within clouds surrounding the parcels' position at t_{n-1}. As the size of the clouds is defined by means of the diffusion coefficients and the time step, this procedure allows the simultaneous solution of both convection and diffusion.

A systematic comparison of ELM, among themselves and with respect to Eulerian and Lagrangian methods, is yet to be performed. Nevertheless, reported results suggest that ELM represent the most cost-efficient solution technique to solve transport problems. In general, solutions tend to be "wiggle-free" and remarkably accurate (very low numerical damping and diffusion) even for high Peclet numbers, and the computer costs seem comparable to those of Eulerian methods.

4. DESCRIPTION OF THE METHOD

4.1 Introduction

The method described in the next sections is Eulerian-Lagrangian, in the terminology of Chapter 3. The transport equation is split into a convection and a diffusion equation - the former being solved by the method of characteristics, and the latter by a Galerkin finite element method.

4.2 The Splitting Technique

The transport equation, Eq. 2.1, may be rewritten by expansion of the derivatives on the right-hand side, and rearranged as

$$\frac{\partial c}{\partial t} + u_i^* \frac{\partial c}{\partial x_i} = D_{ij} \frac{\partial^2 c}{\partial x_i \partial x_j} + Q \tag{4.1}$$

where the apparent velocity u_i^* is given by

$$u_i^* = u_i - \frac{1}{h} \frac{\partial}{\partial x_j} (hD_{ij}) \tag{4.2}$$

We will discretize Eq. 4.1 in time, according to the scheme

$$\frac{c^n - c^{n-1}}{\Delta t} + \left\{ u_i^* \frac{\partial c}{\partial x_i} \right\}_{n-1} = \left\{ D_{ij} \frac{\partial^2 c}{\partial x_i \partial x_j} \right\}_n + \{Q\}_n \tag{4.3}$$

which introduces an error of order (Δt). In the above, n denotes current time, and n-1 a previous time, a time-step, Δt, apart.

Defining an auxiliary variable c^f, and making use of the linearity of the transport equation, it is possible to decompose Eq. 4.3 into a convection and a diffusion equation,

$$\frac{c^f - c^{n-1}}{\Delta t} + \left\{ u_i^* \frac{\partial c}{\partial x_i} \right\}_{n-1} = 0 \qquad (4.4)$$

$$\frac{c^n - c^f}{\Delta t} = \left\{ D_{ij} \frac{\partial^2 c}{\partial x_i \partial x_j} \right\}_n + \{Q\}_n \qquad (4.5)$$

No error is directly introduced by decomposing Eq. 4.3, providing that at each time step, Eq. 4.4 is solved first, by an explicit technique, and Eq. 4.5 is solved next, by an implicit technique.

The variable c^f may be interpreted as the concentration that would be obtained at time n, if the only transport mechanism between n-1 and n was convection by the apparent velocity u_i^*. However, c^f can not be rigidly identified with time n, as it becomes an initial condition for the solution of the diffusion equation.

The initial (at the beginning of each step) and boundary conditions of the full problem may be written in discretized form, as

$$c = c^{n-1} \qquad \text{at } n-1, \text{ in } \Omega \qquad (4.6)$$

$$c^n = \bar{c} \qquad \text{at } n, \text{ on } \Gamma_1 \qquad (4.7)$$

$$q_n^n = \bar{q}_n \qquad \text{at } n, \text{ on } \Gamma_2 \qquad (4.8)$$

Using the auxiliary variable c^f, we may take advantage of the linearity of the problem to obtain, again without any decomposition error, the two following sets of conditions

$$c = c^{n-1} \qquad \text{at } n-1, \text{ in } \Omega \qquad \text{for convection} \tag{4.9}$$

$$c^f = \bar{c} \qquad \text{at } n, \text{ on } \Gamma_1 \tag{4.10}$$

$$c = c^f \qquad \text{at } n-1, \text{ in } \Omega \tag{4.11}$$

$$c^n = c^f \qquad \text{at } n, \text{ on } \Gamma_1 \qquad \text{for diffusion} \tag{4.12}$$

$$q_n^n = \bar{q}_n \qquad \text{at } n, \text{ on } \Gamma_2 \tag{4.13}$$

The splitting technique used in most ELM is based on the same idea of discretizing the original transport equation in time, and taking advantage of the time-discrete form to decompose the equation.[1] Typically, however, the time-discretization is performed on the transport equation written in the form of Eq. 2.1, rather than that of Eq. 4.1. The splitting leads then to the equations

$$\frac{c^f - c^{n-1}}{\Delta t} + \left\{ u_i \frac{\partial c}{\partial x_i} \right\}_{n-1} = 0 \tag{4.14}$$

$$\frac{c^n - c^f}{\Delta t} = \left\{ \frac{1}{h} \frac{\partial}{\partial x_i} \left(h D_{ij} \frac{\partial c}{\partial x_j} \right) \right\} + \{ Q \}_n \tag{4.15}$$

For the general case where hD_{ij} is space-dependent the above decomposition does not avoid the presence of hyperbolic components in the diffusion equation, as is clear by expanding the derivatives in the right-hand side of Eq. 4.15:

---

[1] An exception is the method described by Neuman and Sorek (1982), where the decomposition is performed over the continuous form of the equation.

$$\frac{c^n - c^f}{\Delta t} = \left\{\left(\frac{1}{h}\frac{\partial h D_{ij}}{\partial x_i}\right)\frac{\partial c}{\partial x_j} + D_{ij}\frac{\partial^2 c}{\partial x_i \partial x_j}\right\} + \{Q\}_n \qquad (4.16)$$

Clearly, if the hyperbolic terms in Eq. 4.16 dominate the parabolic ones (e.g., due to large gradients in the flow depth), significant numerical diffusion will occur.

4.3 Solution of the Diffusion Equation

4.3.1 Introduction

The diffusion equation is solved by a standard FEM, based on a weighted residual Galerkin formulation. The time-discretization scheme is implicit, based on a backward Euler's formula. § 4.3.2 to 4.3.4 present the details of the solution technique.

The selection of a FEM rather than a FDM (more conventional in an Eulerian-Lagrangian context) was recommended by the superior ability of the former to deal with irregular domains, and with internal grid refinements.

It should be noticed that the use of an irregular FE grid increases the complexity of the particle tracking algorithm required to solve the convection equation (see §4.4.2). On the other hand, FEM, unlike FDM, lead to the unambiguous definition of interpolation functions that cover the whole domain. These functions are natural candidates to become the basis of the interpolation procedure required to solve the convection equation (see §4.4.3).

4.3.2 The Weighted-Residual Statement

The diffusion problem will be stated as governed by the differential equation[1]

$$\frac{\partial c}{\partial t} = D_{ij} \frac{\partial^2 c}{\partial x_i \partial x_j} - \kappa c + p \qquad (4.17)$$

with initial conditions

$$c(x,y,t) = \bar{c}_o(x,y) \qquad \text{at } t = 0, \text{ in } \Omega \qquad (4.18)$$

and boundary conditions

$$c(x,y,t) = \bar{c}(x,y,t) \qquad \text{at } t > 0, \text{ on } \Gamma_1 \qquad (4.19)$$

$$q_n(x,y,t) = \bar{q}_n(x,y,t) \qquad \text{at } t > 0, \text{ on } \Gamma_2 \qquad (4.20)$$

A discrete representation of the space-domain is adopted, such that the concentration is approximated by

$$c(x,y,t) \simeq \hat{c}(x,y,t) = \bar{c}(x,y,t) + \sum_{j=1}^{N_T} \alpha_j(t)\, \phi^j(x,y) \qquad (4.21)$$

---

[1] Formally, the problem should be stated in the time-discrete form that results from the splitting of operators - Eqs. 4.5 and 4.11-13. The non-discretized form is adopted for the sake of simplicity; it introduces no errors, providing that the discretization scheme used before is kept while actually solving the equations (see §4.3.4).

where $\hat{}$ - denotes approximation due to the spatial discretization

$\bar{c}(x,y,t)$ - is zero outside Γ_1, and is known everywhere on Γ_1

$\alpha_j(t)$ - are unknown coefficients

$\phi^j(x,y)$ - are known interpolation functions

N_T - is the number of nodes in the domain

This approximation introduces residuals over Ω, Γ_1 and Γ_2, defined as

$$R(x,y) = \frac{\partial \hat{c}}{\partial t} - D_{ij} \frac{\partial^2 \hat{c}}{\partial x_i \partial x_j} + \kappa \hat{c} - p \qquad \text{in } \Omega \qquad (4.22)$$

$$T(x,y) = \hat{c} - \bar{c} \qquad \text{on } \Gamma_1 \qquad (4.23)$$

$$S(x,y) = \bar{q}_n - \hat{q}_n \qquad \text{on } \Gamma_2 \qquad (4.24)$$

We will satisfy the essential boundary condition Eq. 4.19 exactly, which implies that the residual $T(x,y)$ and the functions ϕ^j must vanish identically on Γ_1. The errors in Ω and on Γ_2 will be minimized in a weighting residual sense, by letting

$$W = \iint_{\Omega} w\, R(x,y)\, dA + \int_{\Gamma_2} w\, S(x,y)\, ds = 0 \qquad (4.25)$$

where W is the weighted-residual over the domain, and w is an arbitrary weighting function.

Introducing the definitions of the residuals R(x,y) and S(x,y) into Eq. 4.25, the weighted residual over the whole domain becomes

$$W = \iint_{\Omega} \{ w \frac{\partial \hat{c}}{\partial t} dA - D_{ij} w \frac{\partial^2 \hat{c}}{\partial x_i \partial x_j} + \kappa w \hat{c} - wp \} dA + \int_{\Gamma_2} w(\bar{q}_n - \hat{q}_n) ds \qquad (4.26)$$

Integration by parts of the term involving second derivatives, and re-arrangement leads to the balanced weak form of the weighted residual statement retained for our finite element formulation:

$$W = \iint_{\Omega} \{ w \frac{\partial \hat{c}}{\partial t} dA + D_{ij} \frac{\partial w}{\partial x_i} \frac{\partial \hat{c}}{\partial x_j} + \kappa w \hat{c} - wp \} dA + \int_{\Gamma_1} w \hat{q}_n ds + \int_{\Gamma_2} w \bar{q}_n ds = 0 \qquad (4.27)$$

4.3.3 The FEM Formulation

As in any FEM formulation, the domain is divided into elements. The weighted residual over the domain, W, which is required to vanish by Eq. 4.27, is evaluated as the sum of the elementary residuals, W^e.

Following a Galerkin approach, we will restrict the weighting functions to have the same shape as the interpolation functions, over each element. Clearly, the weighting functions must now vanish on

Γ_1, as the interpolation functions do. Therefore, the integral over Γ_1 on the right-hand side of the weighted residual statement, $\int_{\Gamma_1} w\, \hat{q}_n ds$ vanishes identically. Also, we may write over an element, in a way consistent with Eq. 4.21,

$$\hat{c} = \underline{\phi}(x,y)\, \underline{\alpha}_e(t) \tag{4.28}$$

$$w = \underline{\phi}(x,y)\, \underline{w}_e(t) \equiv \underline{w}_e^T(t)\, \underline{\phi}^T(x,y) \tag{4.29}$$

where $\underline{\alpha}_e$ and $\underline{w}_e$ are column vectors containing the nodal concentrations and the (arbitrary) nodal weights; $\underline{\phi}$ is a row vector containing the interpolation functions.

The weighted residual over an element then becomes:

$$W^e = \underline{w}_e^T \left\{ \left(\iint_{\Omega_e} \underline{\phi}^T \underline{\phi}\, dA \right) \frac{\partial \underline{\alpha}_e}{\partial t} + \left(\iint_{\Omega_e} D_{ij} \frac{\partial \underline{\phi}^T}{\partial x_i} \frac{\partial \underline{\phi}}{\partial x_j}\, dA \right) \underline{\alpha}_e + \right.$$

$$\left. + \left(\iint_{\Omega_e} \kappa \underline{\phi}^T \underline{\phi}\, dA \right) \underline{\alpha}_e - \iint_{\Omega_e} \underline{\phi}^T p\, dA + \int_{\Gamma_2} \underline{\phi}^T \bar{q}_n ds \right. \tag{4.30}$$

or equivalently,

$$W^e = \underline{w}_e^T \left\{ \underline{\underline{M}}_e \dot{\underline{\alpha}}_e + (\underline{\underline{A}}_e + \underline{\underline{B}}_e)\, \underline{\alpha}_e - \underline{P}_e \right\} \tag{4.31}$$

where

$$\underline{\underline{M}}_e^T = \iint_{\Omega_e} \underline{\phi}^T \underline{\phi}\, dA \qquad \text{geometric matrix} \tag{4.32}$$

$$\underline{\underline{A}}_e = \iint_{\Omega_e} D_{ij} \frac{\partial \underline{\phi}^T}{\partial x_i} \frac{\partial \underline{\phi}}{\partial x_j}\, dA \qquad \text{diffusion matrix} \tag{4.33}$$

$$\underline{\underline{B}}_e = \iint_{\Omega_e} \kappa \underline{\phi}^T \underline{\phi}\, dA \qquad \text{decay matrix} \tag{4.34}$$

$$\underline{P}_e = \iint_{\Omega_e} \underline{\phi}^T p \, dA - \int_{\Gamma_2} \underline{\phi}^T \bar{q}_n \, ds \quad \text{source/boundary vector} \quad (4.35)$$

The sum, over the whole domain, of the individual contributions of the elements to the global weighted residual leads to the system of ordinary differential equations

$$\underline{\underline{M}} \, \dot{\underline{\alpha}} + (\underline{\underline{B}} + \underline{\underline{A}}) \, \underline{\alpha} = \underline{P} \quad (4.36)$$

where each global matrix represents the assemblage of the corresponding elementary matrices.

In the above formulation, the highest derivatives involved in the selected weighted residual statement are of first order. Therefore, space-continuity requires that the interpolation functions be first-derivative square integrable, i.e., have piece-wise continuous first derivatives. In addition, convergence in the mean-square sense requires that, within each element, the interpolation functions be at least linear.

Linear interpolation functions, although admissible, were found to be inadequate. Indeed, they allow an accurate solution of the diffusion equation, but tend to introduce excessive numerical diffusion and damping in the solution of the convection equation (see §4.4). The use of at least quadratic interpolation functions is strongly recommended.

4.3.4 Time-Discretization Scheme. Solution Strategy

To transform Eq. 4.36 into a system of algebraic equations, we have adopted an implicit time-discretization scheme, based on a backward Euler's formula:

$$[\underline{\underline{M}} + \Delta t(\underline{\underline{A}}^n + \underline{\underline{B}}^n)]\underline{\alpha}^n = \underline{\underline{M}}\,\alpha^f + \Delta t\,\underline{P}^n \qquad (4.37)$$

where the superscripts n and f denote current time and "previous" time (after the convection equation has been solved).

The scheme is unconditionally stable and is consistent with the splitting procedure described in §4.2.

From the analysis of Eqs. 4.32 to 4.34, we recognize that $\underline{\underline{M}}$ is always a symmetric, time-independent matrix, while in general $\underline{\underline{A}}$ and $\underline{\underline{B}}$ are non-symmetric, time-dependent matrices. However, $\underline{\underline{A}}$ will be time-independent if D_{ij} are time-independent. The same applies to $\underline{\underline{B}}$ with regard to κ. Also, $\underline{\underline{A}}$ will be symmetric if the diffusion coefficients D_{ij} (a) constitute a symmetric tensor and (b) are uniform over each element (although they may vary from element to element). Similarly, $\underline{\underline{B}}$ will be symmetric if κ may be considered uniform over each element.

The best strategy for the solution of the system of Eq. 4.37 depends on the characteristics of the matrix $\underline{\underline{Z}} = \underline{\underline{M}} + \Delta t(\underline{\underline{A}}^n + \underline{\underline{B}}^n)$. In the present work, we have dealt only with situations where $\underline{\underline{Z}}$ is symmetric and time-independent. To take advantage of this property, we have solved the system by using an appropriate LL^T - decomposition method. The decomposition of $\underline{\underline{Z}}$ is done only once; in each additional time step, the required operations are limited to updating the load vector, $\underline{P}$, and performing appropriate forward and backward substitutions to obtain the vector of nodal concentrations.

It should be noted that, if the conventional splitting procedure mentioned in §4.2 had been adopted, the definition of $\underline{\underline{A}}$ would include not only the diffusion coefficients D_{ij}, as before, but also the flow depth, h. Therefore, $\underline{\underline{A}}$ would be time-independent only when D_{ij} is time-independent, as before, and either (a) h is constant over each element (in which case the explicit dependence of $\underline{\underline{A}}$ on h vanishes), or (b) h is time-independent. In many situations of interest (e.g., estuaries and coastal waters, with non-negligible depth gradients), the requirements on D_{ij} are much weaker than the requirement in h; as a consequence, the splitting procedure used in this work may lead to a time-independent $\underline{\underline{Z}}$, while the conventional splitting procedure would lead to a time-dependent $\underline{\underline{Z}}$, and therefore to less computational efficiency.

4.4 Solution of the Convection Equation

4.4.1 Introduction

The convection equation, which in continuous form may be written as

$$\frac{Dc}{Dt} \equiv \frac{\partial c}{\partial t} + u_i^* \frac{\partial c}{\partial x_i} = 0 \tag{4.38}$$

with

$$u_i^* = u_i - \frac{1}{h} \frac{\partial}{\partial x_j} (D_{ij} h) \tag{4.39}$$

states that the concentration of a particle following the apparent flow (u*,v*) remains constant, i.e., that the concentration remains constant along trajectories or characteristic lines defined by

$$\frac{dx_i}{dt} = u_i^*(x,y,t) \tag{4.40}$$

We will solve the equation using this property. In each time step, we allocate a fluid particle to each node of the finite element grid used to solve the diffusion equation, and we proceed as illustrated below.

Consider, at time n, the particle at node j, located at $P \equiv (x_j, y_j)$ (Fig. 4.1). This particle was previously at position (P', n-1), having been driven from there by the apparent flow, along a characteristic line. Tracking the characteristic line backwards, we can determine P', and then determine c(P',n-1) by spatial interpolation at time n-1 (where the concentrations at the nodes of the finite element grid are known). But by Eq. 4.38, $c(P,n) \equiv c(P',n-1)$ and the problem is solved for node j; the procedure must now be repeated for each of the remaining nodes.

The same basic procedure applies even if an inflow boundary is crossed during the back-tracking (case of node Q, Fig. 4.1). Now, however, the concentration at (Q,n) is imposed directly from the boundary condition, i.e., $c(Q,n) \equiv \bar{c}(Q',n')$. In outflow or closed boundaries the back-trajectory of a particle is towards the interior of the domain, and boundary conditions are not required.

The approach described has been called "step-wise method of characteristics", "reverse method of characteristics" or "streakline method". It clearly includes two main tasks:

- the stepwise back-tracking of the particles along the characteristic lines, starting at each node of the fixed computational grid, at each time n, and being carried until time n-1 (or until an inflow boundary is crossed);
- the spatial interpolation required to find the concentration carried along the characteristic line.

4.4.2 The Stepwise Particle-Tracking Algorithm

The stepwise tracking of a particle constitutes an initial-value problem, governed by the set of ordinary differential equations

$$\frac{dx_i}{dt} = u_i^* (x,y,t) \qquad \{i=1,2\} \qquad (4.41)$$

which must be solved backwards in time, with boundary conditions

$$x_i = \bar{x}_i^{\bullet} \qquad \text{at time } n \qquad (4.42)$$

In most FEM, the driving flow field (u,v,h) is given explicitely only at the nodes of a (often irregular) grid; however, interpolation functions that apply to each element allow the unambiguous definition of (u*,v*) in the whole domain. Also, most FE circulation models only compute the flow field at fixed times, requiring time-interpolation procedures to complete the flow description. Exceptions include models based on frequency-domain approaches, that explicitly establish the time dependence on the u,v,h.

We have developed an element-per-element tracking algorithm that accounts for the need of an element-based spatial interpolation of the flow field, and is flexible to accomodate time-interpolation schemes, when required.

We will refer to Fig. 4.2 to describe this algorithm. Consider a particle at position (P, n) where P coincides with a node of the finite element grid; at time n-1 this particle was at (P'''', n-1), which we want to determine. We first follow the particle backwards along its characteristic line, until position (P', $n-\beta_1$).

As only element K_1 is involved, we may write:

$$u_i(x,y,t) = \sum_{\ell=1}^{m} \psi_\ell(x,y;K_1)\, u_{i\ell}(t;K_1) \tag{4.43}$$

$$h(x,y,t) = \sum_{\ell=1}^{m} \tau_\ell(x,y;K_1)\, h_\ell(t;K_1) \tag{4.44}$$

$$D_{ij}(x,y,t) = \sum_{\ell=1}^{m} \theta_\ell(x,y;K_1)\, D_{ij\ell}(t;K_1) \tag{4.45}$$

where ψ_ℓ, τ_ℓ and θ_ℓ are elementary interpolation functions; $u_{i\ell}$, h_ℓ and $D_{ij\ell}$ represent nodal values of u_i, h and D_{ij}; and m is the number of nodes of the element. If the nodal quantities $u_{i\ell}$, h_ℓ and $D_{ij\ell}$ are known at all times between n and n-α (either directly or by time-interpolation), $u^*_{i\ell}$ may be computed everywhere, using Eq. 4.39.

Because we were constrained by the choice of circulation models, we have used in this work linear interpolation of velocities and flow depths, over 3-noded triangular elements. The diffusion coefficients D_{ij} were assumed constant over each element. The procedure is rather general, though, and may be applied to any other consistent choice of interpolation functions and element shapes.

Once u* and v* are defined, the solution of the initial-value problem governed by Eqs. 4.41 and 4.42 determines (P', n-β_1). Several numerical solution techniques are available; we have selected a 4th order Runge-Kutta method, with constant time-stepping. The time step, δt^{K_1} is selected to limit the truncation error per step to a prescribed value. Once (P', n-β_1) is obtained, an evaluation of (P, n) given (P', n-β_1) is performed, to assess the total error between n and n-β_1; if the total error is not found satisfactory,

the time-step is reset, and the tracking between (P, n) and (P', $n-\beta_1$) is repeated.

Once (P', $n-\beta_1$) is known within satisfactory accuracy, the functions u^* and v^* are replaced by equivalent ones applying over element K_2, and the particle is tracked along this element, back to (P'', $n-\beta_2$). The tracking is accomplished as before; a new Runge-Kutta time step δt^{K_2} is selected in an attempt to account for the variation of the flow characteristics from element to element.

The element-per-element tracking is continued until time n-1 is reached, or a boundary is crossed (whichever happens first).

4.4.3 The Interpolation Scheme

Consider again the finite element grid shown in Figure 4.2. Assume that (P'''', n-1) was found by the particle tracking procedure, and lies in element K_4, say.

The concentration at (P'''', n-1) will not, in general, be explicitly known. However, concentrations at the nodes of elements K_4 are known at time n-1, and the finite element approximation used to solve the diffusion equation inherently supplies a consistent way of interpolating concentrations over the element.

Therefore,

$$c(P,n) \equiv c(P'''',n-1) = \sum_{i=1}^{m} \phi_i(x,y;\ K_4)\ c_i(n-1;\ K_4) \qquad (4.46)$$

where $\phi_i(x,y;\ K_4)$ are interpolation functions, associated with the finite element approximation for concentrations; c_i are nodal concentrations; and m is the number of nodes of the element.

Preliminary tests showed that the use of linear interpolation functions introduced too much numerical damping. This is supported by the brief accuracy analysis for the solution of the convection equation, presented in the appendix. We have therefore adopted quadratic interpolation functions, defined to be consistent with the interpolation functions for velocity and flow depth over triangular elements (now with 6 rather than 3 nodes).

4.5 Comments on Stability and Accuracy

The method has no stability limitations on the time step, Δt. For the convection equation, unconditional stability is assured by the fact that the concentration at the foot (P', say) of each characteristic line is found by interpolation (over the element that contains P') rather than by extrapolation. For the diffusion equation, unconditional stability is assured by the implicit time-discretization scheme that was adopted.

A formal analysis of the accuracy of the method is beyond the scope of our work. Errors may arise in each of the three major components of the method: the splitting technique, the solution of the diffusion equation and the solution of the convection equation.

The error associated with the splitting technique results exclusively from the time-discrete form adopted for the transport equation (as pointed out in §4.2, for such discrete form, no additional errors arise from the splitting of the full equation into two sub-equations) and is of order $O(\Delta t)$.

The diffusion equation that results from the splitting is already in a time-discrete form. Errors inherent to the solution of this equation are therefore due only to spatial approximations, and are

estimated to be of order $O(\Delta\ell)^3$, for quadratic interpolation functions. This estimate is based on the theoretical bound of the mean-square error in 1-D

$$\left|\left|c-\hat{c}\right|\right| = \{\int_{\Omega_e} (c-\hat{c})^2 \, dA\}^{1/2} \leq (\Delta\ell)^{p+1}\{\int_{\Omega_e} (\frac{d^{p+1}c}{dx^{p+1}})^2 dA\}^{1/2} \qquad (4.47)$$

where p is the order of the interpolation function.

Errors inherent to the solution of the convection equation may be associated with both time and space discretizations. Time-discretization errors arise during the particle tracking, where the time-step for the solution of the hyperbolic equation, Δt, is broken into sub-steps, δt; as a 4th order Runge-Kutta method is used, errors are estimated to be of order $(\delta t)^4$.

Space-discretization errors arise in connection with the interpolation of the concentrations at the feet of the characteristic line. The magitude of these errors depends on factors such as shape and length of the original concentration distribution or the source term, the order of the interpolation functions and the discretization steps in space and time. A simplified error analysis is presented in the appendix, in which the damping error per time step is calculated for a harmonic concentration field, as a function of the dimensionless wavelength, M, and the decimal part of the Courant number, α.

Results obtained indicate that (a) the damping error per time step decreases with the increase of the dimensionless wavelength, M;

(b) the damping error per time step does not depend on the Courant number, but on its decimal part, α; therefore the error per time step is essentially independent of the order of magnitude of the time-step and the total error after a given time decreases with increasing Δt (decreasing number of time steps); (c) the damping error decreases significantly when the order of the interpolation functions goes from linear to quadratic.

5. SOLUTION OF TEST PROBLEMS

5.1 Introduction

The numerical method described in Chapter 4 was used to solve several problems with known exact solution. The analysis of the results provides useful information on the characteristics of the method, that is out of the reach of a theoretical accuracy analysis.

A quantitative basis for the analysis of the results is provided by the set of error measures defined in Table 5.1. These measures concern a variety of characteristics of the numerical solution: overall accuracy, artificial damping (reduction of peak concentrations), spreading and shifting of the concentration field, and spurious oscillations. This variety of error measures is felt to be necessary, because (a) different numerical methods introduce different types of errors, and (b) the property of the exact solution that is of most interest depends on the specific engineering application.

Test problems were solved using 2-D regular grids, with 6-noded triangular elements. Each grid is characterized by its length, L, and width, W, and by the size of the right-sides of the triangular elements, $\Delta\ell$ (which is twice the nodal spacing in the x and y directions, Δx and Δy).

Most problems are, however, essentially 1-D, involving transport in the x-direction alone. To assure proper dimensionality in these cases, the initial and boundary conditions were imposed uniformly along the y-axis; in addition, no-flux conditions were imposed at the lateral boundaries, and high lateral diffusion was introduced.

5.2 Pure Convection in a Steady Uniform Flow

We will consider first the 1-D transport of an instantaneous Gaussian source of initial variance σ_{ox}^2, by a uniform, steady flow. The governing equation is

$$\frac{\partial c(x,t)}{\partial t} + u \frac{\partial c(x,t)}{\partial x} = 0 \qquad -\infty < x < \infty \qquad (5.1)$$

with initial and boundary conditions

$$c(x,t) = \frac{m}{\sqrt{2\pi}\ \sigma_{ox}} \exp\left\{-\frac{(x - x_o)^2}{2\sigma_{ox}^2}\right\} \qquad t=0,\ -\infty < x < \infty \qquad (5.2)$$

$$c(x,t) = 0 \qquad t>0,\ |x| \to \infty \qquad (5.3)$$

where m represents total mass (per unit width and depth and divided by density), and x_o is the original position of the center of mass. These definitions yield concentrations in dimensionless units for this and subsequent examples.

The exact solution corresponds to the undisturbed transport of the source, i.e.,

$$c(x,t) = \frac{m}{\sqrt{2\pi}\ \sigma_{ox}} \exp\left\{-\frac{(x - x_o - ut)^2}{2\sigma_{ox}^2}\right\} \qquad t>0,\ -\infty < x < \infty \qquad (5.4)$$

Numerical solutions were found for the combinations of parameters shown in Table 5.2. Results are partially documented in Tables 5.3 and 5.4 and Figs. 5.1 to 5.5.

For all runs, the numerical solutions are virtually exact regarding total mass, position of the center of mass, and variance of the concentration field (see in Tables 5.3 and 5.4 the values of the error measures μ_o, μ_x, μ_{xx}, defined in Table 5.1). However, solutions

may exhibit some overdamping and loss of symmetry, the latter in the form of a shift in the position of the peak concentration and of the presence of a quickly damped wake of negative concentrations.

Observed errors were found to be controlled by two major parameters: the number of time steps required to reach the final computational time, $N = T/\Delta t$, and the dimensionless source length, $M \equiv 6\sigma_{ox}/\Delta\ell$. To discuss the influence of N and M, let us consider first the integral error measure ϕ, defined in Table 5.1.

Fig. 5.1 and Table 5.3 show that ϕ decreases when N decreases. This means (as T is fixed) that the numerical solution improves as Δt increases. The reason is that the error per time step results almost entirely from the interpolation procedure required to find the concentration at the feet of the characteristic lines (§4.4.3), and for high enough values of M, is nearly independent of the actual Δt (see Appendix). Therefore, the total error at time T should be roughly proportional to the number of required interpolations, i.e., to N.

Assuming $\phi \propto N^n$, we computed a best-fit value for n, by linear regression of the logarithms of available pairs of (ϕ, N). The result, shown in Fig. 5.2a, suggests that ϕ is indeed nearly linear, being proportional to $N^{0.85}$. The power $n = 0.85$ should not be interpreted too rigidly, as it may vary with T and with the shape and length of the source, for instance. The deviation from strict linear proportionality results from a slight reduction of the error per time step from one time step to the next (Fig. 5.3), which is due to the presence in the solution of progressively lower frequency harmonics, generated by numerical dispersion.

Fig. 5.4 and Table 5.4 show, in turn, that ϕ decreases as M increases (keeping fixed the shape of the source). This is related to

the interpolation procedure required to find the concentration at the feet of the characteristic lines: larger M corresponds to smoother profiles, and therefore to smaller interpolation errors. Fig. 5.5a suggests that $\phi \propto M^{-2.8}$, where, again the value of the power of M should not be taken too rigidly. It is of interest to define a limit $\bar{M}$ above which errors are "small"; although such limit will depend on the actual problem and on the meaning of "small", we tentatively suggest that $\bar{M}$ be taken in the range 7 to 9.

The dependence of ϕ on M and N cannot be extrapolated directly to other error measures. However, striking similarities exist in the behaviour of ϕ and ε, the measure of the damping of the peak concentration: we found $\varepsilon \propto N^{0.85}$ (Fig. 5.2b) and $\varepsilon \propto M^{-2.6}$ (Fig. 5.5b), which are to be compared with $\phi \propto N^{0.85}$ and $\phi \propto M^{-2.8}$.

No significant spurious oscillations are found in the numerical solutions in spite of the infinite Peclet number that characterizes the runs. However, a small region of significant negative concentrations appears in the wake of the source profile. Taking the absolute value of the normalized maximum negative concentration, ψ, as a measure, it is clear that the error decreases when N decreases or M increases; Figs. 5.2c and 5.5c explore the possibility of a simple dependence of the type $\psi \propto N^p$, $\psi \propto M^q$; the former relation, with $p = 1.4$, seems roughly adequate, but the latter is clearly inadequate.

The position of the peak concentration (unlike the position of the center of mass of the concentration profile) is not preserved by the numerical solution. As measured by ξ, the shift error tends to decrease with increasing M (Fig. 5.5). Small values of N tend to keep ξ small, although no monotonic dependence was found (Fig. 5.2d).

5.3 Convection and Diffusion in a Steady Uniform Flow

We will consider now the 1-D convection and diffusion of the same source used in §5.2. The problem is governed by the equation

$$\frac{\partial c(x,t)}{\partial t} + u \frac{\partial c(x,t)}{\partial x} = D \frac{\partial^2 c(x,t)}{\partial x^2} \qquad -\infty < x < \infty \qquad (5.5)$$

and the initial and boundary conditions Eqs. 5.2 and 5.3. The exact solution is

$$c(x,t) = \frac{m}{\sqrt{2\pi}\ \sigma_x} \exp\left\{ - \frac{(x - \bar{x})^2}{2\sigma_x^2} \right\} \qquad -\infty < x < \infty \qquad (5.6)$$

with

$$\sigma_x^2 = \sigma_{ox}^2 + 2Dt \qquad (5.7)$$

$$\bar{x} = x_o + ut \qquad (5.8)$$

The numerical solution of this problem was found for the combinations of parameters shown in Table 5.5. Results are shown in Tables 5.6 to 5.8, and Figs. 5.6 to 5.11.

The analysis of the results indicates clearly that the presence of diffusion tends to improve the numerical solutions. This is due to the fact that diffusion increases progressively the effective source length, making the required interpolations of concentration more accurate.

Fig. 5.7 shows the dependence of ϕ and ε on Pe, for M = 7 and N = 72 (note the logarithmic scale of the axis of Pe). Errors are rather small for low Pe (up to 4, say), increase significantly in the region of moderate to high Pe ($4 < Pe < 100$, say) and then tend

assymptotically to finite values as Pe goes to infinity.

For pure-convection problems, both ϕ and ε decrease monotonically with decreasing N (i.e., increasing Δt). This was explained in §5.2 as a consequence of the leading errors per time step being associated with interpolations of concentration, and being essentially independent of Δt. For convection-diffusion problems, ϕ and ε have minima at some optimal value of N, which increases as Pe decreases (see Fig. 5.9, for Pe = 10). This is explained by the fact that, above the optimal value of N, errors associated with interpolations of concentrations are dominant; however, below the optimal value, errors inherent to the time discretizations of the original differential equation, which are roughly proportional to Δt (i.e. to N^{-1}), become dominant. Clearly, for diffusion dominant problems ϕ and ε should tend to decrease monotonically with increasing N (decreasing Δt), except for round-off errors in the vicinity of $\Delta t = 0$. Thus, unlike Eulerian methods, Eulerian-Lagrangian methods present the challenge of selecting an optimal Δt (see further discussion in §7.2). However, they have the strong computational advantage that the optimal Δt is quite large when convection is dominant.

We have seen that, for pure-convection problems, ϕ and ε strongly depend on M. Such dependence is still present in convection-diffusion problems, but is weaker, as illustrated in Fig. 5.11. This results from the fact that diffusion tends to spread the original source profile, increasing progressively the effective M seen in each computational time. Minimal admissible values of M are therefore Pe-dependent and may be somewhat smaller than those suggested in §5.2.

The dependence of other error measures on Pe, M and N is partially shown in Tables 5.6 to 5.8. Numerical solutions are always virtually exact with regard to mass preservation, position of center of mass and variance of the concentration profiles. Negative concentrations do appear in the wake of the concentration profile, but they loose significance as Pe decreases, N decreases or M increases; furthermore, decreasing Pe decreases the influence of N and M. The same qualitative comments apply to the error in the position of the peak concentration.

5.4 Convection and Diffusion in a Sinusoidal Uniform Flow

We will consider again the problem defined by Eq. 5.5 and the initial and boundary conditions of Eqs. 5.2 and 5.3. However, we will now let u be time-dependent; specifically,

$$u(t) = U_{max} \sin\left(\frac{2\pi t}{P}\right) \tag{5.9}$$

where U_{max} denotes velocity amplitude, and P denotes period.

The exact solution is given by Eq. 5.6, where, now

$$\bar{x} = x_o + \int_o^t u(t)dt \tag{5.10}$$

Numerical solutions were found for two combinations of parameters, corresponding to pure-convection (Pe = ∞) and to convection-dominated (Pe = 20) conditions (Table 5.9). Results are shown in Figs. 5.12 to 5.14 and Table 5.10.

As in previous tests, numerical solutions are virtually exact as regards total mass and variance of the concentration profile. The same is not true for the position of the center of mass, though, which may exhibit a small shift, of the order of 1% of the total travel distance. The shifts are greatest at half periods (t = 0.5P, 1.5P, 2.5P, etc.) and become insignificant at full periods (t = P, 2P, 3P, etc.).

For this test problem, detectable errors have local maxima at half periods, and local minima at full periods; this suggests that the errors depend on the flow direction. As such, errors would accumulate while the flow is in a same direction and would partially cancel out as the direction of the flow reverses. This periodic effect is to be superimposed on a long-term error trend, which depends on the relative importance of convection and diffusion: pure-convection leads to increasing error with time, while even moderate amounts of diffusion lead to decreasing error (Fig. 5.14).

As a consequence of the periodic error trend, symmetry tends to be better preserved for pure-sinusoidal than for steady flows, as suggested by visual analysis of Figs. 5.12 and 5.13 (as compared to Figs. 5.6d and 5.6f), and quantified by the values of the error measures ψ and ξ shown in Table 5.10 (as compared to Table 5.6).

5.5 Convection and Diffusion of a Continuous Source in a Steady Uniform Flow

In previous sections, we have dealt with the transport of instantaneous sources. We will consider now the case of a continuous Gaussian source of strength, $\dot{m}$, in a steady uniform flow. The exact

solution is given by the time integral of solutions of the form of Eq. 5.6, with $m = \dot{m}dt$, i.e.,

$$c(x,t) = \int_{o}^{t} \frac{\dot{m}}{\sqrt{2\pi}\sigma_x} \exp\left\{ - \frac{(x - \bar{x})^2}{2\sigma_x^2} \right\} dt \qquad -\infty < x < \infty \qquad (5.11)$$

with σ_x^2 and $\bar{x}$ given by Eqs. 5.7 and 5.8.

The time-integral on the right-hand side of Eq. 5.11 has no closed form solution, but may be easily solved numerically, supplying an adequate reference solution. Numerical solutions were obtained for the conditions shown in Table 5.11, and results are summarized in Table 5.12 and Fig. 5.15.

As expected, the continuous source problem is easier to solve than the corresponding instantaneous source problem, since the concentration profile is now much wider and smoother.

Numerical solutions show very good agreement with the reference ones, even for Pe as high as 200: mass is preserved in a virtually exact way, the L-2 norm, ϕ, remains low, and no significant negative concentrations appear. It can be seen (Fig. 5.15) that the numerical solutions exhibit a slight overshoot at the front edge of the concentration profile that increases with increasing Pe. However, for Pe = 200, the overshoot is still less than 2% of the maximum concentration.

5.6 Diffusion in a Depth-Variable Channel

To test our approach for handling depth variations (described in §4.2), we will consider the problem of an instantaneous source in a depth-variable channel. Assuming a uniform diffusion coefficient D, the governing equation for the depth-averaged concentration in 1-D is written

$$\frac{\partial c}{\partial t} + u \frac{\partial c}{\partial x} = \frac{D}{h} \frac{\partial}{\partial x} (h \frac{\partial c}{\partial x}) \tag{5.12}$$

with initial and boundary conditions given by Eqs. 5.2 and 5.3.

The above problem does not have a general analytical solution. However, for the case of pure-diffusion (u = 0), and with

$$h(x) = h_o e^{ax} \tag{5.13}$$

Eq. 5.12 reduces to

$$\frac{\partial c}{\partial t} - aD \frac{\partial c}{\partial x} = D \frac{\partial^2 c}{\partial x^2} \tag{5.14}$$

As the apparent velocity, -aD, is uniform, an exact solution is available in the form

$$c(x,y) = \frac{m}{\sqrt{2\pi}\ \sigma_x} \exp\{- \frac{[x - (x_o - aD\ t)]^2}{2\sigma_x^2}\} \quad t>0,\ -\infty < x < \infty \tag{5.15}$$

with $\sigma_x^2 = \sigma_{ox}^2 + 2Dt$.

This solution shows that, as may be expected, depth variation introduces an effective displacement of the depth-averaged concentration profile towards small depths, as a way to preserve the total mass, while net diffusion progresses toward large depths. In the particular

case of a exponential depth-variation (Eq. 5.13), this displacement takes place at a constant rate (see Eq. 5.15), because the effective velocity of displacement is uniform; however, this will not be true for other depth variations, which will in general lead to non-uniform velocities. Table 5.13 characterizes the numerical runs, and results are shown in Fig. 5.16.

We have considered first the case of h_o = 3 m, a = 0.0003 m^{-1}, and x_o = 8000 m. The values of h_o and a correspond to an average slope over the computational domain (0 < x < 16000 m) of 2.25%, and an average slope in the zone of primary interest for the transport of the concentration profile (4000 < x < 12000 m) of 1.25%. These slopes are in the usual range for most coastal zones. The numerical results (Fig. 5.16a) show an excellent agreement with the exact ones, in all regards.

We have then increased the value of a to 0.003 m^{-1}, to test the performance of the method for extremely high slopes, which in coastal zones may occur at local discontinuities (e.g., navigation channels and marine faults). The resulting bottom profile has averaged slopes, over the entire domain (0 < x < 16000 m) and in the region of primary interest (2000 < x < 10000 m), respectively, of 1.3×10^{19}% and 1.3×10^{11}% (either of which approximate an infinite slope).

The numerical solution (Fig. 5.16b) shows good agreement with the exact one, except for a spatial shift. Because depth is a function of space, this shift is quite significant in terms of mass content (20% of the original mass was lost after 9216 seconds). The reason for the

shift error lies in the fact that the piecewise linear representation of the depth variation used in the computation is too rough to simulate the actual exponential form, leading to an incorrect evaluation of the velocity of displacement.

Two alternative approaches are available to reduce the errors: reduce $\Delta\ell$, the characteristic length of the elements, or increase the order of the interpolation functions for h, within each element. Following the latter approach, we used quadratic interpolation for h, and came up with the results shown in Fig. 5.16c, which are in excellent agreement with the exact solution.

It should be emphasized that the mass loss detected when a linear interpolation was used for h, results from ill-representation of the depth-variation, rather than from the order of the interpolation functions. (Indeed, using linear interpolation with smaller $\Delta\ell$ would have solved the problem.)

These results have implications on the expected accuracy of convective diffusion calculations in 2-D variable depth flows where the flow field u(t), v(t), h(t) must be specified (e.g., by a numerical circulation model). In cases where a mass-conserving flow field is computed on the basis of linear interpolations of velocity and depths, the transport model should not result in additional mass loss. Conversely, if the flow field is not conservative, no conservative solution of the 2-D analog of Eq. 5.12 can be expected regardless of the order of the interpolation functions used for u, v and h.

5.7 Advancing Front

We will consider now the problem defined by

$$\frac{\partial c(x,t)}{\partial t} + u \frac{\partial c(x,t)}{\partial x} = D \frac{\partial^2 c(x,t)}{\partial x^2} \qquad 0 \leq x \leq L \qquad (5.16)$$

subject to the initial and boundary conditions

$$c(x,t) = 0 \qquad t=0,\ 0 \leq x \leq L \qquad (5.17)$$

$$c(x,t) = 1 \qquad t>0,\ x=0 \qquad (5.18)$$

$$c(x,t) = 0 \qquad t>0,\ x=L \qquad (5.19)$$

The problem differs from previous ones in that no load is present, the concentration field being imposed by a constant mass flux, specified through constant velocity and upstream concentration. However, it shows some similarity with the continuous load problem (§5.4), which can be seen to result also in an advancing front of concentrations.

The analytical solution, valid for $L \to \infty$, is (Neuman and Sorek, 1982):

$$c(x,t) = \frac{1}{2}\left\{ \operatorname{erfc}\left(\frac{x-ut}{2\sqrt{Dt}}\right) + \exp\left(\frac{ux}{D}\right) \operatorname{erfc}\left(\frac{x+ut}{2\sqrt{Dt}}\right)\right\} \qquad (5.20)$$

The numerical solution was found for the set of parameters defined in Table 5.14. The results obtained demonstrate (Fig. 5.17) that the method can handle satisfactorily advancing front problems, although some overshoot will appear for very high Pe.

5.8 Convection in a Flow in Rigid-Body Rotation

We will consider, as a last test problem, the transport by convection of a 2-D cosine-hill source in a flow of counterclockwise

rigid body rotation. This problem differs from those treated in previous sections in two major ways: (a) it is fully 2-D and (b) it involves a non-uniform flow field; the use of a cosine-hill instead of a Gaussian source is of minor importance and was dictated by expediency in using available auxiliary computer codes.

The problem is defined by

$$\frac{\partial c}{\partial t} + u \frac{\partial c}{\partial x} + v \frac{\partial c}{\partial y} = 0 \tag{5.21}$$

with initial and boundary conditions

$$c(x,y,t) = \begin{cases} 0.5 \left[1 + \cos \frac{2\pi r}{M\Delta\ell}\right] & t=0,\ r \leq M\Delta\ell/2 \\ 0 & t=0,\ r > M\Delta\ell/2 \end{cases} \tag{5.22}$$

$$c(x,y,t) = 0 \qquad t>0,\ r \to \infty \tag{5.23}$$

In the above

$$r = [(x-x_o)^2 + (y-y_o)^2]^{1/2} \tag{5.24}$$

$$u = -\omega y \tag{5.25}$$

$$v = \omega x \tag{5.26}$$

where ω is the angular frequency of rotation.

Numerical solutions were found for the set of parameters indicated below:

$$
\begin{aligned}
L &= W = 1400 \text{ m} \\
\Delta\ell &= 100 \text{ m} \\
\Delta t &= 30 \text{ s} \\
M &= 3 \\
x_o &= 700 \text{ m} \\
y_o &= 1100 \text{ m} \\
\omega &= \frac{2\pi}{3\Delta t} \text{ rad/s}
\end{aligned}
\tag{5.27}
$$

Results are shown in Fig. 5.18. After 5 hours, the cosine-hill distribution has neither collapsed nor distorted excessively, even though a small number of elements (note that M = 3) was used to discretize the source. Mass, variance, and position of center of mass are well reproduced, and no wiggles are present (although negative concentrations do show up). These results suggest the method's adequacy in fully 2-D problems, with non-uniform flow fields.

6. ON THE APPLICATION OF THE METHOD TO THE ANALYSIS OF POLLUTANT TRANSPORT IN COASTAL WATERS

6.1 Introduction

The method described in Chapter 4, and tested in Chapter 5, is the basis for a computer code, whose primary objective is to simulate pollutant transport in shallow coastal waters.

The application of the code will be illustrated in this chapter through the analysis of sludge dumping in Massachusetts Bay and a power plant discharge in Narragansett Bay. Our objective is to demonstrate the cost-effectiveness of the code and to identify limitations and desirable improvements. At this point, we have not attempted to seriously calibrate or verify the model against actual field data (other than by using the same model coefficients and parameters which have been used in previous models and justified on the basis of field measurements). Therefore the results should not be used directly for actual impact assessments.

The circulation model TEA[1] (Westerink, et al., 1984), was used to provide the necessary flow input to the transport model. TEA performs a finite element, frequency-domain solution of the linearized form of the Navier-Stokes equation, and should become the basis for a fully non-linear code, under current development.

TEA is formulated on the basis of triangular elements, with linear elementary expansions, thus dictating the same choice of expansions for

---

[1] Acronym for Tidal Embayment Analysis

velocity and depth in the transport model. The transport model, however, uses quadratic expansions for concentration. These are defined over the same triangular elements by adding three additional (mid-side) nodes.

6.2 Sludge Dumping in Massachusetts Bay

6.2.1 Statement of the Problem and Circulation Analysis

The Metropolitan District Commission of the Commonweath of Massachusetts has been considering several alternatives for disposal of the sludge produced at the Wastewater Treatment Plants of Deer Island and Nut Island. Disposal in Massachusetts Bay is one such alternative. Possible sites include an area just outside of Boston Harbor, where sludge would be conveyed through a submerged discharge, and an area further offshore where dumping would be from a barge. We will simulate the transport of sludge plumes released at locations that roughly correspond to these two possibilities (Site 1 for the submerged discharge, and Site 2 for the barge dumping - see Fig. 6.1).

We will concentrate the analysis on long-term dispersion, trying to assess general tendencies of the plume movement. In particular, will the plume quickly leave the bay towards the ocean, or will it remain in the bay, contributing to a progressive increase of the pollution level? We will consider, for both sites, a single instantaneous sludge source, released at the beginning of the ebb tide, which we will follow for the next six tidal cycles. The source has a Gaussian form, characterized by standard deviations σ_x, σ_y, and total mass M_T.

The above schematization is consistent with our objective. For a given calculation, the source may be considered to result from near field, short-term, dilution of sludge discharged continuously for a few hours. This is particularly meaningful for Site 2 where, for instance, dumping may be concentrated in periods of three to six hours, n tides apart, with n a design parameter.

Clearly the values of σ_x, σ_y should reflect the near field dilution. However, this dilution depends on the mode and actual characteristics of disposal, which have not yet been defined. Therefore, we selected σ_x, σ_y based on possible scenarios; for Site 2, we set σ_x = 8400 m and σ_y = 4200, assuming the barge to describe a long zigzag trajectory along a main axis; for Site 1, we set σ_x = σ_y = 2000 m, assuming either a highly efficient vertical diffuser, or a barge describing a shorter, more circular, motion.

As input for the transport model, we have used circulation patterns obtained with the finite element grid shown in Fig. 6.1. The grid is composed of 360 triangular elements, and has 215 corner nodes (the only ones used for circulation calculations), out of a total of 789 corner plus mid-side nodes (all of which are used for the transport calculations). The maximum difference between the numbers of the nodes within the same element is 19, when corner nodes only are considered, and 75, when all nodes are considered. The circulation is driven both by a steady coastal current and a tidal fluctuation. The tidal forcing is specified by prescribing tidal elevations at the ocean nodes, and driving the system at a frequency corresponding to a period of T = 12.4 hours; tidal elevations vary linearly from Cape Ann to Cape Cod and no

phase shifts are applied. The steady coastal current is simulated by imposing a linear elevation gradient along the ocean boundary, and driving the system at zero frequency. A constant depth of 50 m is assumed over the whole bay.

Calibration of the resulting circulation pattern was brief, and based only on tidal elevation data, available at Boston, Cape Ann and Cape Cod (Westerink, 1984). Therefore, although results (Figs. 6.2 and 6.3) are qualitatively reasonable, given available field data and previous numerical studies, they cannot claim to accurately predict actual circulation. As water circulation is the major transport mechanism for the sludge plume, it is clear that results of the transport model can only be interpreted as estimates.

Sludge from the Wastewater Treatment Plants of Deer Island and Nut Island contains non-degradable components (e.g. heavy metals). As non-degradability constitutes a worst case condition in terms of pollution, a decay coefficient of $\kappa = 0$ was used in our calculations. Sludge does tend to settle, resulting in deposition on the bottom, and consequent loss from the water column. This mechanism is not considered in the present analysis, because it is felt to be secondary to horizontal transport, and not enough information is available for its correct parameterization; however, the model can easily accomodate this mechanism as a sink term.

Isotropic dispersion coefficients were used for all calculations. For Site 1, $D_x = D_y = 0$ while for Site 2 two sets of values were used: $D_x = D_y = 30$ m^2/s and $D_x = D_y = 0$. The 30 m^2/s is in the upper range expected for Massachusetts Bay (as reported by Christodoulou et al., 1974) based on measured sediment plumes.

6.2.2 Results of the Transport Model

Results of the transport model are shown in Figs. 6.4 and 6.5. They are expressed as isoconcentration lines, each of which is associated with a percentage of the maximum concentration of the Gaussian original source,

$$c_{max} = \frac{M_T}{2\pi\, h\sigma_x\sigma_y} \qquad (6.1)$$

where M_T is the total mass of sludge released and h is the flow depth.

These results suggest that Site 2 is clearly preferable to Site 1, as regards sludge dilution. Considering transport by convection alone, results from Fig. 6.4 indicate that, due to the small velocities prevailing near Boston Harbor, the sludge plume released at Site 1 undergoes almost no net drift and very little dilution, even after six tidal cycles. Conversely, the sludge plume released at Site 2 tends to leave the Bay towards the ocean, in a slow net motion. Note, however, that Cape Cod may trap part of the plume inside the Bay, as suggested by Fig. 6.5c and 6.5d; further time of computation would be necessary to check this possibility. Tidal excursion, although still relatively small, is much more efficient in promoting dilution at Site 2 than it was for Site 1.

Fig. 6.5 also illustrates the effect of dispersion, for Site 2. As referred to in Chapter 2, dispersion should be interpreted as a bulk representation of purely convective mechanisms not explicitly represented in the description of the flow field. Although not negligible, especially in the zone of high initial concentrations,

dispersion is seen to be secondary as compared to convection by the part of the flow field explicitly represented in the model; the latter controls the global position of the plume, and promotes a considerable part of its dilution.

The numerical runs that provided the above results were performed on a VAX 1178 computer using a time step of one hour. Tidal circulation calculations using TEA required 2 CPU minutes. Transport calculations with pure convection took 56 CPU minutes, while runs with convection and dispersion took 68 CPU minutes, to simulate 75 prototype hours. Total mass of the sludge plume was preserved within ± 3% accuracy, and no spurious oscillations were observed, even for pure convection. Negative concentrations were found to be restricted, in pure-convection runs, to values of up to 2% of c_{max}, and were concentrated in a small region in the wake of the net motion of the plume. For runs involving convection and dispersion, no significant negative concentrations were observed.

6.3 Thermal Discharge from Brayton Point Generating Station

6.3.1 Background

The previous example of sludge dumping dealt with a passive discharge; i.e., because of the small quantities of effluent, it could be assumed that the discharge did not disturb the ambient circulation. By contrast thermal plumes from electric generating stations which employ once through cooling have significant flow and momentum which may affect the ambient circulation for distance of up to a kilometer or more from the point of discharge. Water temperatures may be affected at even greater distances. A major difficulty arises in trying to model such

discharge plumes numerically due to the large variation in scales. These may range from the order of a meter or so which characterizes the dimensions of the discharge channel to the order of tens of kilometers which may characterize the dimensions of the receiving waterbody which governs such far field processes as tidal flushing and surface heat loss.

One approach to address the dilemma of scales was introduced by Kaufman and Adams (1981) who were interested primarily in the resolution of induced velocities and temperatures in the so-called intermediate field, i.e., that region extending from several hundred meters to a kilometer or so from the point of discharge. Recognizing that intermediate field behavior was influenced by near field processes (occurring at smaller scales) and far field processes (occurring at larger scales) and that all the regions could not be adequately resolved simultaneously, a hybrid approach was employed. Using the 2-D finite element circulation and dispersion models CAFE and DISPER, the intermediate and far fields were simulated numerically, while near field mixing was represented using inner boundary conditions along a transition circle corresponding to the edge of the near field. The location of the transition circle, volumetric dilution, lateral and vertical entrainment rates and the layer depth of the far field were computed from analytical formulae describing the near field mixing of surface discharges. In this manner, the effect of the near field on the far field could be realistically modeled.

Several calculations were presented for both the Millstone Point Nuclear Station on Long Island Sound and the Brayton Point Generating Station on Mt. Hope Bay (part of Narragansett Bay). While basically successful in producing 2-D descriptions of intermediate and far field

velocity and temperature, the approach was limited by excessive computer times dictated by the small grid sizes and time steps required by the two models. The present example corresponds to the three unit discharge from the Brayton Point Generating Station and includes the same basic schematizations as introduced previously.

6.3.2 Statement of the Problem and Circulation Analysis

The station is located in Somerset, Massachusetts at the northern end of Mt. Hope Bay which connects with Narragansett Bay to the south. Fig. 6.6 shows the finite element discretization of Mt. Hope Bay used for the circulation analysis. The grid contains 684 triangular elements containing 411 corner nodes.

Ambient circulation is driven primarily by tidal forcing at the six southern nodes (entrance to Narragansett Bay) where tidal amplitudes of 2.95 ft were specified. In addition to the tide, an inflow of 435 cfs from the Tauton River, to the northeast of the site, was simulated as a constant normal flux. In order to correspond with previous calculations, simulations were performed with zero wind speed; however, they could easily be run with non-zero speeds.

Induced circulation was generated by prescribing fluxes along the transition circle. See Fig. 6.7 for greater detail. Flux into the domain represents the diluted flow from three generating units. The combined condenser flow rate is 1380 cfs and the volumetric dilution, accounting for a shallow water condition, is 5.1; hence the diluted flow rate is $5.1 \times 1380 = 7000$ cfs which was distributed as a normal flux over the central elements south of the actual discharge. See Fig. 6.7. The horizontal entrainment factor is 1.3 which gives rise to an outflow of $1.3 \times 1380 = 1790$ cfs distributed along the outer elements of

the transition circle. The intake flow rate of 1380 cfs was simulated as a normal flux along the east side of the discharge peninsula (above the transition circle).

The radius of the transition circle was 1000 ft and the depth of the intermediate/far field plume was 11.5 ft. The difference between flow discharged into the domain and withdrawn from the domain by horizontal entrainment and the station intake is presumed to downwell (and, subsequently to enter the near field via vertical entrainment). The downwelling was simulated as a normal flux out of the domain through elements along the southeastern edge of the domain. Further details on the schematization may be found in Kaufman and Adams (1981).

Circulation patterns were produced by prescribing 12.4 hr tidal forcing and steady state plant generation (near field flux conditions). Figs. 6.8 to 6.10 depict circulation patterns for two phases of the tide. As noted by Westerink et al (1984) the expected jet-like behavior at the edge of the near field is not fully simulated by TEA. This is due mainly to the fact that the current version of TEA does not include the non-linear momentum terms needed to simulate jet behavior. TEA drives the discharge only by elevation gradients which accounts for the rapid spreading of the jet as best illustrated in Figs. 6.9 and 6.10.

6.3.3 Temperature Predictions

Temperature simulations with the transport model require 6-noded elements. The grid of Fig. 6.6 contained an excessive number of nodes so only the northern portion of the grid was used as depicted in Fig. 6.11. This smaller grid contains 468 elements and 1037 nodes with a maximum difference in node number per element of 80.

The dependent variable in the transport calculation was depth-average excess temperature. Thus initial temperatures in the domain correspond to a background temperature of zero and the average diluted discharge temperature entering the domain is 2.9°F (condenser temperature rise of 14.8 °F divided by volumetric dilution of 5.1). For these calculations, surface heat exchange was neglected, i.e. $\kappa = 0$, but linearized heat exchange could easily be incorporated. Two different sets of isotropic horizontal dispersion coefficients were used, $D_x = D_y = 10\ m^2/s$ and $D_x = D_y = 0$.

Calculations were made for one tidal cycle. Fig. 6.12 shows excess temperature contours for the two tidal phases corresponding to the velocities plotted in Figs. 6.8-6.10.

The calculated contours show reasonable agreement, in terms of shape and area, with measured contours for three units (Kaufman and Adams, 1981, pp. 104-105). In general, the calculated plumes are somewhat wider and shorter than corresponding measurements; however, as discussed previously, this is associated with the high lateral spreading of the circulation model. In agreement with the measurements, but in contrast with the previous calculations based on CAFE and DISPER, the present calculations are noteworthy in being able to simulate sharp temperature gradients (fronts) at the plume edges and in not predicting significant intake circulation at any stage of the tide.

Finally, the computed isotherms illustrate sensitivity to the horizontal dispersion coefficients. The larger of the two sets of coefficients ($10\ m^2/s$) is the same as used by Kaufman and Adams (1981). However, their choice was dictated by the desire to avoid

wiggles in the computed temperature field. The smaller value of zero dispersion is associated with pure convection. Based on a formula presented by Christodoulou et al (1976), Kaufman and Adams (1981) calculate that the true "physical" dispersion coefficient varies throughout the domain but is generally less than 1 m^2/s and thus closer to the case of pure convection. Comparison of the two calculations in Fig. 6.12 indicates considerable sensitivity reinforcing the need for more accurate determination of dispersion coefficients.

The numerical runs that provided the above results were performed on a VAX 1178 using a time step of 30 minutes. Tidal circulation calculations required 4 CPU minutes. Transport runs with pure convection took 34 CPU minutes, while runs with convection and dispersion took 44 CPU minutes to simulate 12.4 prototype hours.

7. CONCLUSIONS AND AREAS FOR FUTURE RESEARCH

7.1 Summary

We have formulated and tested an Eulerian-Lagrangian method that solves the 2-D, unsteady transport equation by the combined use of the finite element method and the method of characteristics.

The method shows very satisfactory performance. In comparison with analytical solutions, the numerical model introduces little numerical damping and diffusion (providing that adequate spatial discretization is ensured) and is free from spurious oscillations. Mass and phase tend to be preserved almost exactly.

Illustrative prototype applications of the method to pollutant transport in coastal (shallow) waters demonstrate great promise. Costs can be kept moderate, by appropriate (and rather unrestricted) choice of the time step. Moreover, the method is able to address problems in the full range between pure diffusion and pure convection without spurious oscillations or excessive numerical damping and diffusion.

The facts that little numerical diffusion is introduced by the method, even for pure convection problems, and that no input of artificial diffusion is required to avoid spurious oscillations, constitute a significant achievement, which should lead to a renewed interest in properly understanding and quantifying ocean dispersion. Indeed dispersion can now be simulated for its own sake, instead of being used as a stabilizer for the numerical solution (as has often been the case in Eulerian methods).

7.2 Areas of Future Research

Future work could be useful in the following areas:

(1) Optimal Time Step

The trade-off between accuracy and cost is rather different, in the present method (and in other ELM), than in conventional Eulerian methods.

Indeed, in Eulerian methods, both accuracy and cost increase monotonically as the number of time steps, N, increases (i.e., as the time step, Δt, decreases). Therefore, except for round-off errors, better accuracy always implies an increased cost.

In the present method, however, the dependence of the accuracy on N is a function of the relative importance of convection and diffusion, as measured by Pe. Fig. 7.1a illustrates qualitatively such dependence. For diffusion problems, optimal accuracy is obtained as N goes to infinity (i.e., Δt goes to zero) as is the case in Eulerian methods. For convection problems, though, leading errors per time step are essentially independent of the actual time step, and therefore, optimal accuracy is obtained as N goes to 1 (i.e., as Δt goes to T). For convection-diffusion problems, optimal accuracy is obtained for a value of N that decreases (i.e., for a value of Δt that increases) as Pe increases.

Costs associated with the solution of the convection equation are almost independent of N (and thus Δt). Indeed, for a given problem and spatial discretization, cost is essentially a funcion of the total computational time, T, and of the accuracy desired for the backtracking

of particles along the characteristic lines. Costs associated with diffusion, however, vary linearly with N. Fig. 7.1b shows the qualitative dependence of costs on N for diffusion, convection and convection-diffusion problems; note that costs are independent of Pe, except for the limiting cases Pe = 0 and Pe = ∞, where the program skips over convection and diffusion calculations, respectively.

Clearly, the value of N (and thus, Δt) that gives maximum accuracy for a given cost is much closer to the value that gives optimal accuracy independent of cost for convection-dominated problems than it is for diffusion-dominated problems.

The above discussion suggests that the cost-efficiency of the method depends on an appropriate selection of the time step, which could be based, for a given type of problem, on curves of the form shown in Fig. 7.1a. Also, it is suggested that cost-efficiency could be increased further either (i) by defining, within a run, time steps that vary in time, and lead to optimal accuracy for the instantaneous value of Pe; or (ii) by defining different time steps for diffusion and for convection, the former being a fraction of the latter. The diffusion time step should approach the convection time step as Pe increases.

(2) Optimal Interpolation

Another issue deserving further analysis is the optimum order of the expansions for concentration. Unlike most conventional formulations, an increase of order (e.g., increasing from quadratic to cubic expansions) may prove cost-effective due to the fact that, for convection-dominated problems, leading errors come from pure interpolation procedures.

For any given order of expansions, it is highly recommended that triangular and quadrilateral elements be used simultaneously. Quadrangles are more accurate than triangles of comparable order, and should be used over most of the domain; triangles should be used only in zones where a fine representation of complex geometries is necessary (in which case quadrangles become cumbersome).

(3) Validation Tests

Extensive validation of the transport model, based on field and/or physical model data is deemed essential. Such validation is not intended as a test for the numerical formulation, which can be assessed more effectively by solution of problems with exact solution. Emphasis should rather be placed on identification and, when possible, correction of limitations of the formulation of the governing equations.

Issues to address include evaluation of the depth-averaged assumption (both for stratified and unstratified flows), quantification of dispersion coefficients (taking into account both the dispersive characteristics of prototype and the finite element discretization of the domain), and simulation of near field dilution (for discharges in the full range between negligible to strong initial momentum).

(4) Coupling with Circulation Model

The need for a model that provides the transport model with accurate input on circulation is easily understandable, given that convection is often the major transport mechanism. When strong non-linearities are not present in the prototype, TEA is appropriate, showing good accuracy and very low cost. Furthermore TEA yields results

as a continuous function of time which is helpful for accurate tracking of particles along the characteristic lines.

However, when non-linear effects are important (e.g., near capes or near discharges with significant momentum), a model solving the non-linear Navier-Stokes equations is required. Such model is now under parallel development at MIT, as an improvement of TEA, and should be used in the validation effort for the transport model.

The present work suggests that TEA (or other circulation models to be coupled with the transport model) might want to use quadratic expansions for velocities and elevations. Such a change would improve compatibility with regard to the transport model, allowing cost-efficient grids to be established for computation of both circulation and transport. Also, it should represent a significant improvement for the circulation model alone, in regards to local mass preservation and general accuracy.

Fluxes represent natural boundary conditions in the finite element formulation of TEA; as a consequence, some leakage through land boundaries is unavoidable. The importance of the leakage, in terms of water and pollutant balances, should be assessed and corrective measures introduced as necessary. Such measures may include (i) definition of a flux correction procedure for land boundaries to apply prior to the transport calculations, and (ii) specification of fluxes as essential boundary conditions in the formulation of TEA.

REFERENCES

Book, D.L., Boris, J.P. and Hain, K., "Flux-Corrected Transport II: Generalization of the Method", J. of Comp. Phys., Vol. 18, 248-283, 1975.

Cheng, R.T., Casull, V. and Milford, S., "Eulerian-Lagrangian Solution of the Convection-Diffusion Equation in Natural Coordinates", submitted for publication.

Christie, I., Griffiths, D.F., Mitchell, A.R. and Zienkiewicz, O.C., "Finite Element Methods for Second Order Differential Equations with Significant First Derivatives", Int. J. Num. Meth. Engrg., Vol. 10, 1389-1396, 1976.

Christodoulou, G.C., Connor, J.J., and Pearce, B.R., "Mathematical Modeling of Dispersion in Stratified Waters", Report No. 219, R.M. Parsons Laboratory for Water Resources and Hydrodynamics, Massachusetts Institute of Technology, October 1976.

Christodoulou, G.C., Leimkuhler, W.F. and Ippen, A.T., "Mathematical Models of the Massachusetts Bay. Part III: A Mathematical Model for the Dispersion of Suspended Sediments in Coastal Waters", Report No. 179, R.M. Parsons Laboratory for Water Resources and Hydrodynamics, Massachusetts Institute of Technology, January 1974.

Daily, J.W. and Harleman, D.R.F., Fluid Dynamics, Addison-Wesley Publishing Company, Inc., Reading, Massachusetts, U.S.A., 1966.

Glass, J. and Rodi, W., "A Higher Order Numerical Scheme for Scalar Transport", Comp. Meth. in Appl. Mech. and Eng., Vol. 31, 337-358, 1982.

Hasbani, Y., Livne, E. and Bercovier, M., "Finite Elements and Characteristics Applied to Advection-Diffusion Equations", Computer and Fluids, Vol. 11, No. 2, 71-83, 1983.

Heinrich, J.C., Huyakorn, P.S., Zienkiewicz, O.C. and Mitchell, A.R., "An 'Upwind' Finite Element Scheme for Two-Dimensional Convective-Transport Equation", Int. J. Num. Meth. Engrg., Vol. 11, 131-143, 1977.

Heinrich, J.C. and Zienkiewicz, O.C., "Quadratic Finite Element Schemes for Two-Dimensional Convective Transport Problems", Int. J. Num. Meth. Engrg., Vol. 11, 1831-1844, 1977.

Holly, F.M., Jr. and Preissmann, A., "Accurate Calculation of Transport in Two Dimensions", Journal of the Hydraulics Division, ASCE, Vol. 103, No. HY11, 1259-1278, Nov. 1977.

Holly, F.M., Jr. and Polatera, J.M., "Dispersion Simulation in 2-D Tidal Flow", to appear in Journal Hydr. Engrg., ASCE, 1984.

Hughes, T.R., "A Simple Scheme for Developing Upwind Finite Elements", Int. J. Num. Meth. Engrg, Vol. 12, 1359-1365, 1979.

Hughes, T.R. and Brooks, A., "A Multi-Dimensional Upwind Scheme with No Crosswind Diffusion", Proc. A.S.M.E. Specialty Conference, New York, 1979.

Kaufman, J.T. and Adams, E.E., "Coupled Near and Far Field Thermal Plume Analysis Using Finite Element Techniques", Report No. MIT-EL 81-036, Energy Laboratory, Massachusetts Institute of Technology, October 1981.

Kelly, D.W., Nakazawa, S., Zienkiewicz, O.C. and Heinrich, J.C., "A Note on Upwinding and Anisotropic-Balancing Dissipation in Finite Element Approximations to Convective Diffusion Problems", Int. J. Num. Meth. Engrg, Vol. 15, 1705-1711, 1980.

Leimkuhler, W.F., "A Two-Dimensional Finite Element Dispersion Model", Civil Engineer Thesis, M.I.T., 1974.

Neuman, S.P., "An Eulerian-Lagrangian Scheme for the Dispersion-Convection Equation Using Conjugate Space-Time Grids", Journal of Comp. Phys., Vol. 41, 270-279, 1981.

Neuman, S.P. and Sorek, S., "Eulerian-Lagrangian Methods for Advection-Dispersion", in Finite Elements in Water Resources, (Ed. K.P. Mole et al), Vol. 4, pp. 14.41-14.68, 1982.

O'Neill, K. and Lynch, D.R., "Effective and Highly Accurate Solution of Diffusion and Convection-Diffusion Problems using Moving, Deformable Coordinates", in Proc. 3rd Int. Conf. on Fin. Elem. in Wat. Res., Univ. of Mississippi, Oxford, 1980, Vol. 1, pp. 3.67-3.76.

Onishi, Y., "Sediment-Contaminant Transport Model", Journal of the Hydraulics Division, ASCE, Vol. 107, HY79, 1089-1107, September 1981.

Roache, P., Computational Fluid Dynamics, Hermosa Publishers, 1982.

Varoglu, E. and Finn, W.L., "Space-Time Finite Elements Incorporating Characteristics for the Burgers Equation", Int. J. for Num. Meth. Engrg., Vol. 16, 171-184, 1980.

Westerink, J.J., Connor, J.J., Stolzenbach, K.D., Adams, E.E. and Baptista, A.M., "TEA: A Linear Frequency Domain Finite Element Model for Tidal Embayment Analysis", Report No. MIT-EL 84-012, Energy Laboratory and R.M. Parsons Laboratory for Water Resources and Hydrodynamics, M.I.T., February 1984.

Westerink, J.J., Private communication, Massachusetts Institute of Technology, 1984.

Figures

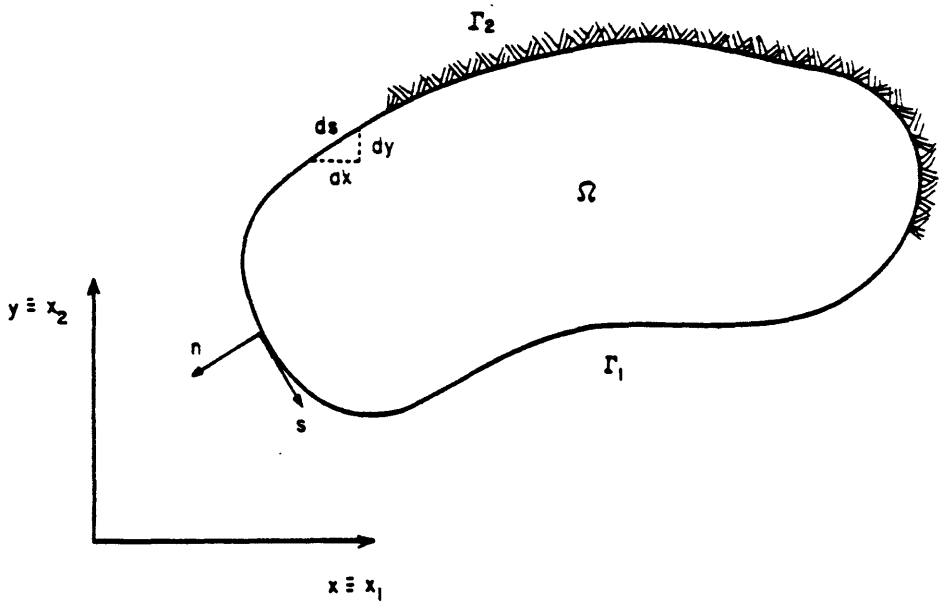

Fig. 2.1 Statement of the transport problem. Definition sketch.

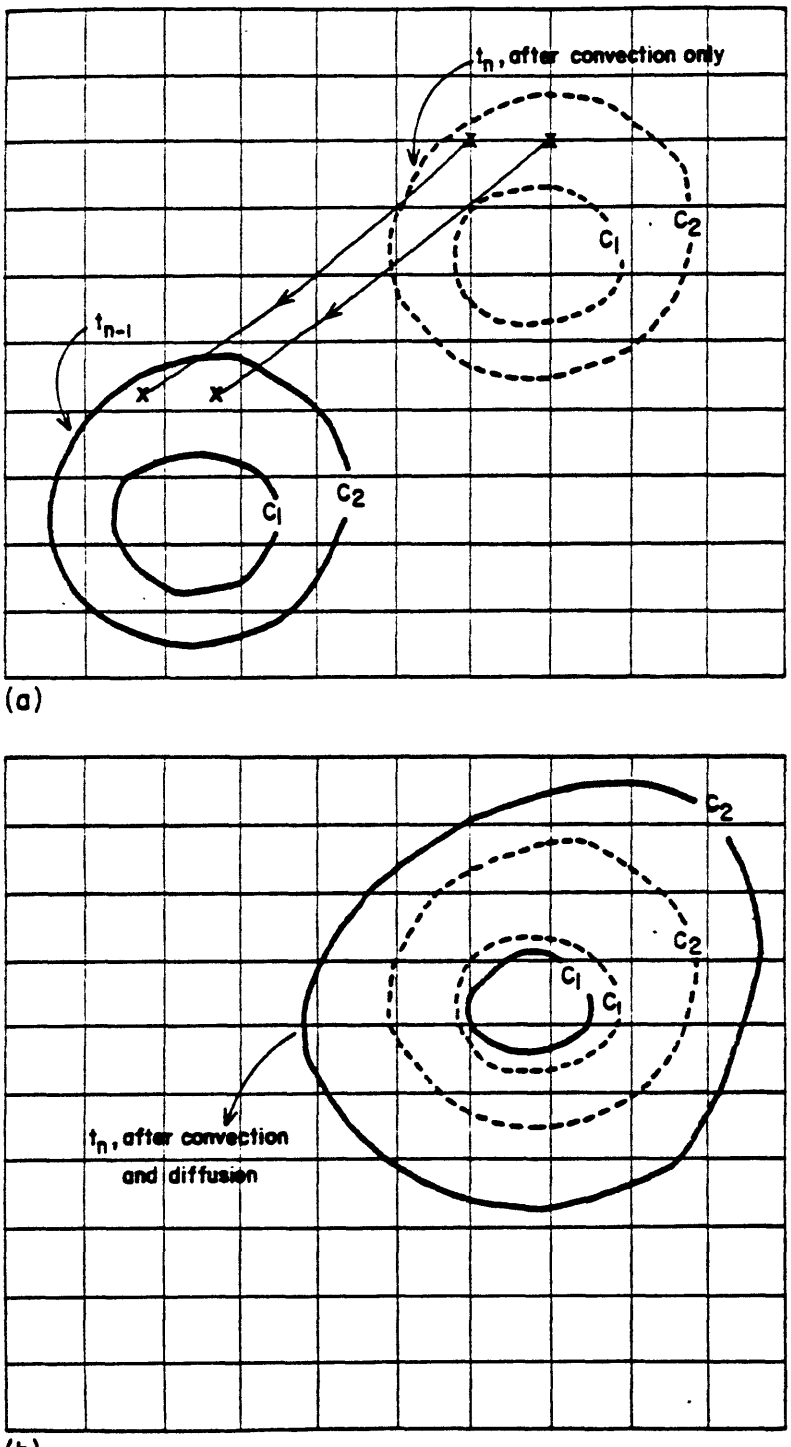

Fig. 3.1 General solution procedure of Eulerian-Lagrangian methods. Illustrative sketch.

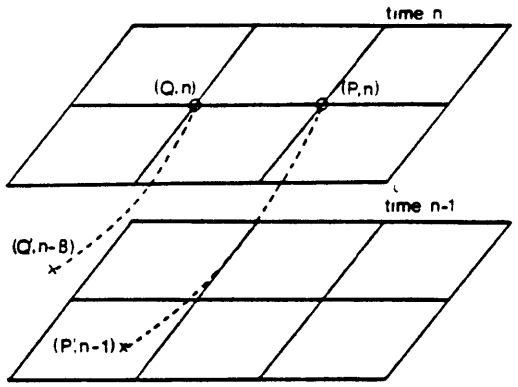

Fig. 4.1 Solution of the convection equation. Illustrative sketch.

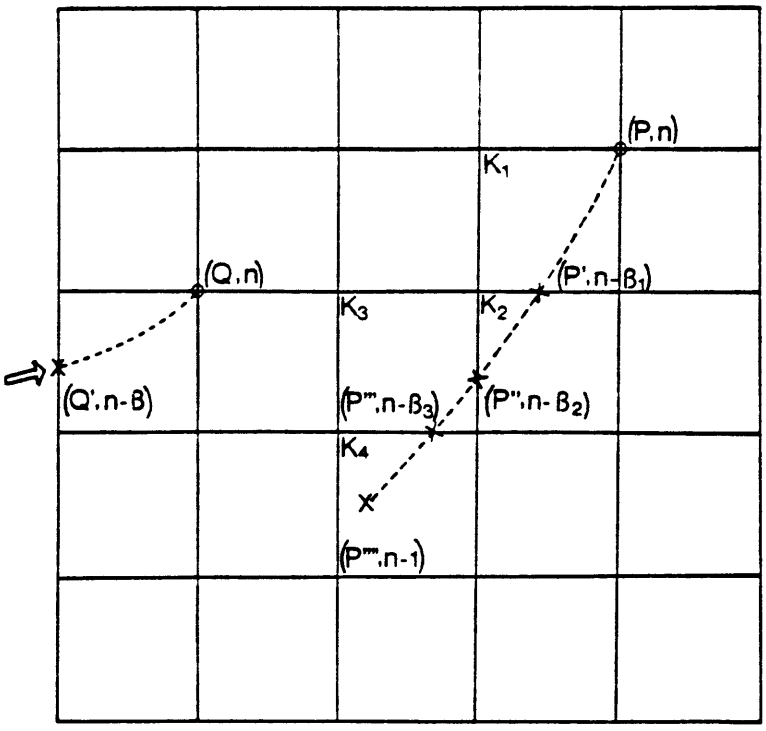

Fig. 4.2 Tracking algorithm. Illustrative sketch.

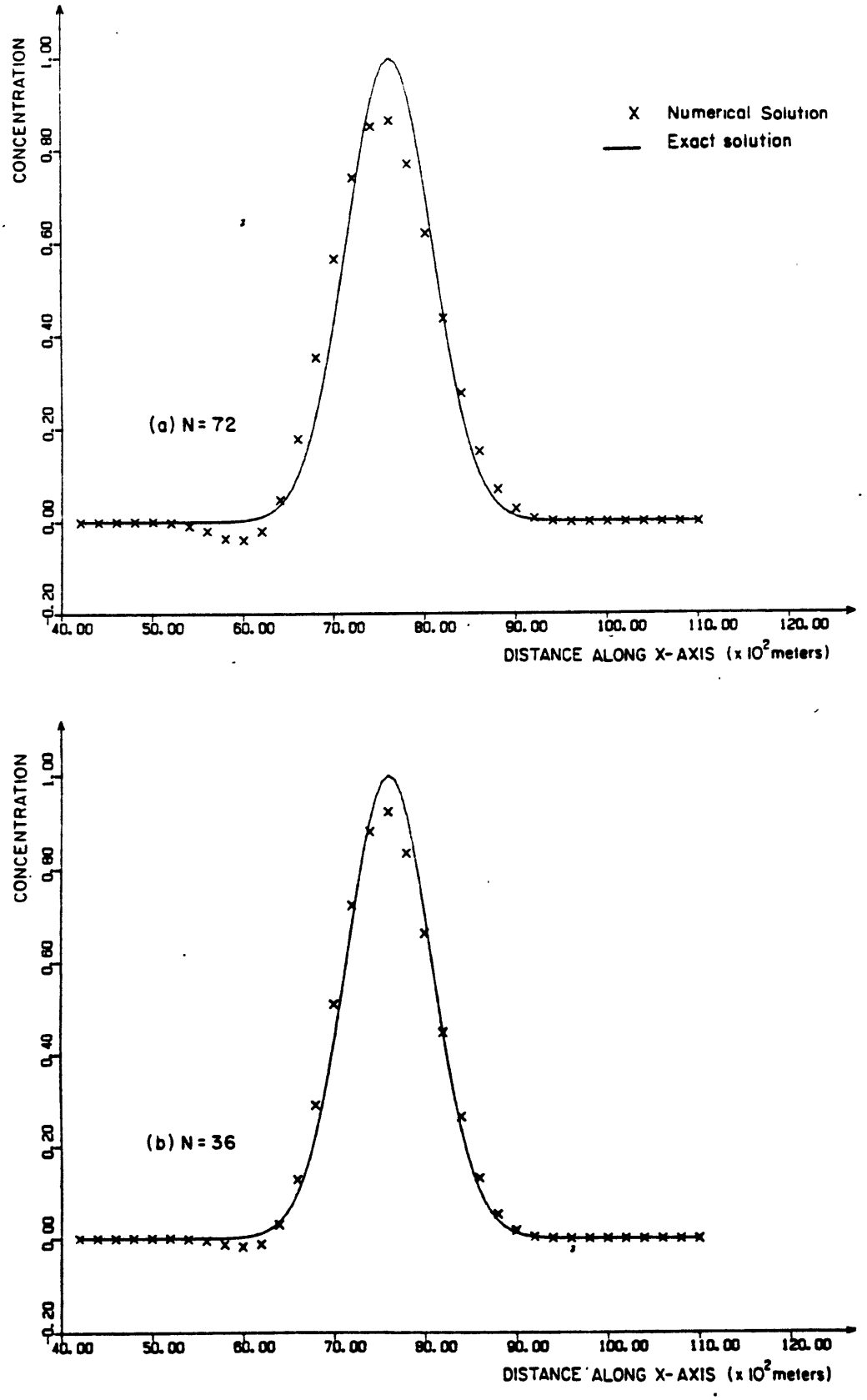

Fig. 5.1 Convection in a steady uniform flow. Numerical solutions for different values of N ($t \equiv T = 9216$ s; $M = 7$).

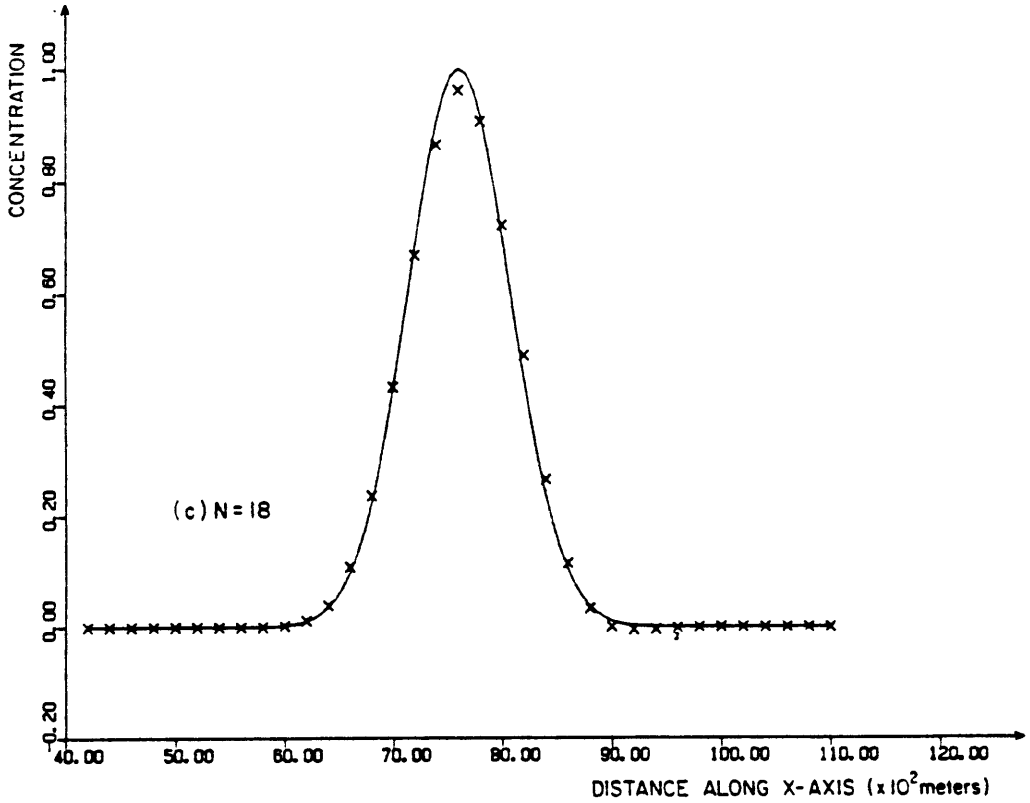
CONCENTRATION
1.00
0.80
0.60
0.40
0.20
0.00
-0.20
(c) N = 18
40.00
50.00
60.00
70.00
80.00
90.00
100.00
110.00
120.00
DISTANCE ALONG X-AXIS (x 10² meters)

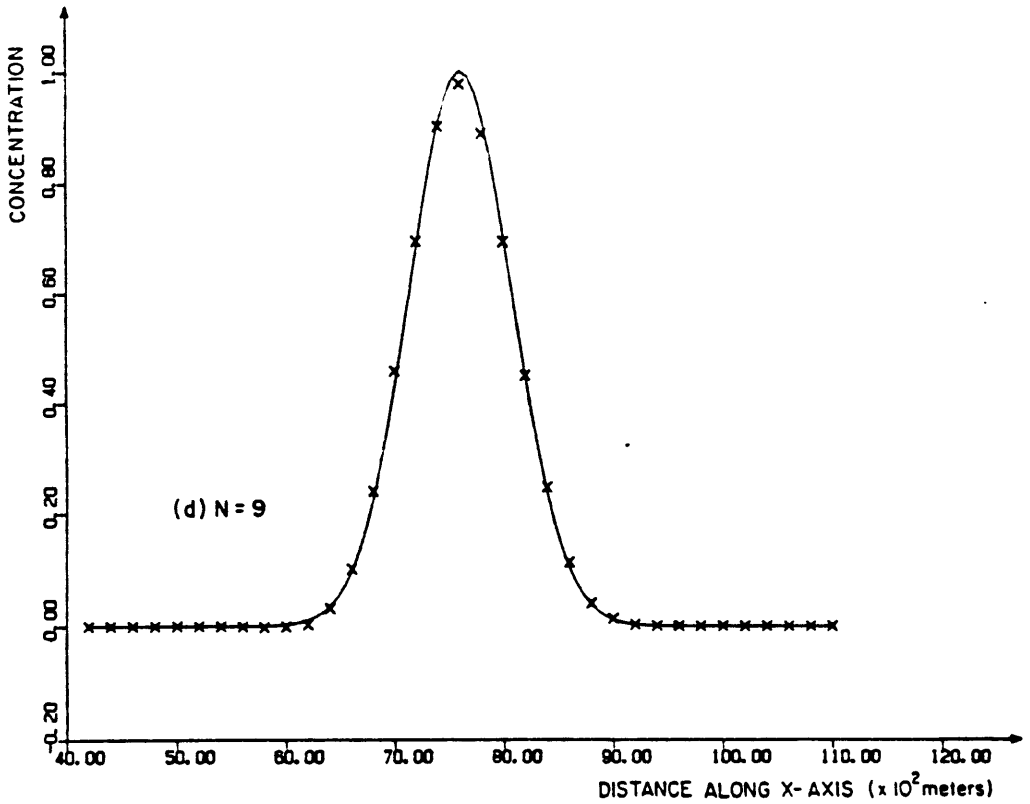
CONCENTRATION
1.00
0.80
0.60
0.40
0.20
0.00
-0.20
(d) N = 9
40.00
50.00
60.00
70.00
80.00
90.00
100.00
110.00
120.00
DISTANCE ALONG X-AXIS (x 10² meters)

Fig. 5.1 (cont.)

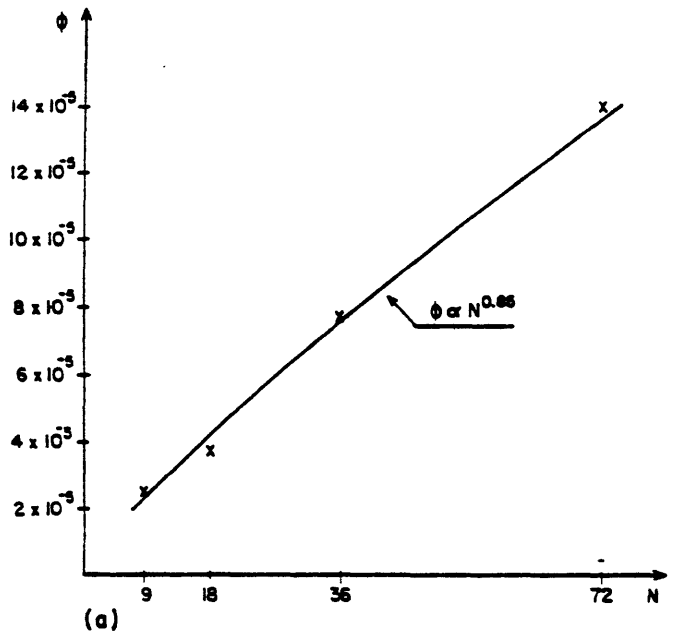

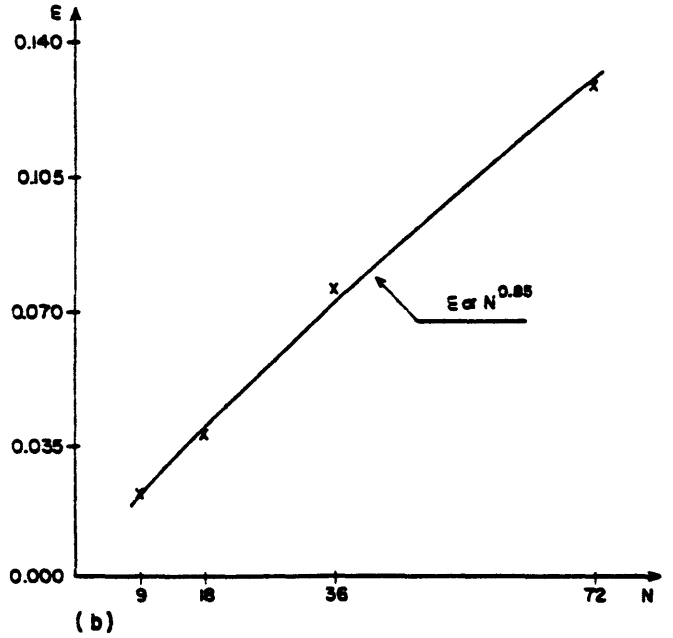

Fig. 5.2 Convection in a steady uniform flow. Error measures as a function of N ($t \equiv T = 9216$ s; $M = 7$).

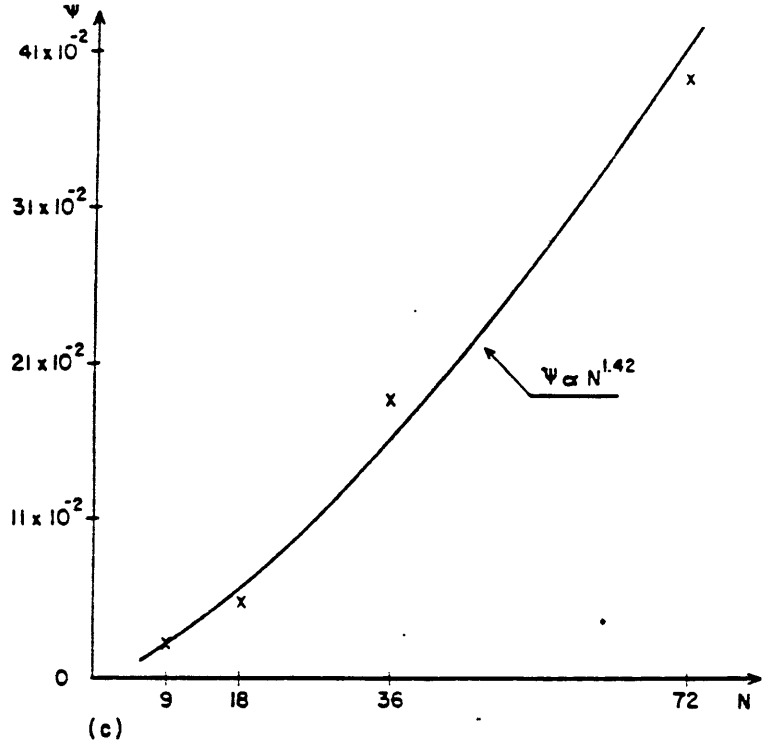
Ψ
41 x 10^-2
31 x 10^-2
21 x 10^-2
11 x 10^-2
0
Ψ α N^1.42
9
18
36
72
N
(c)

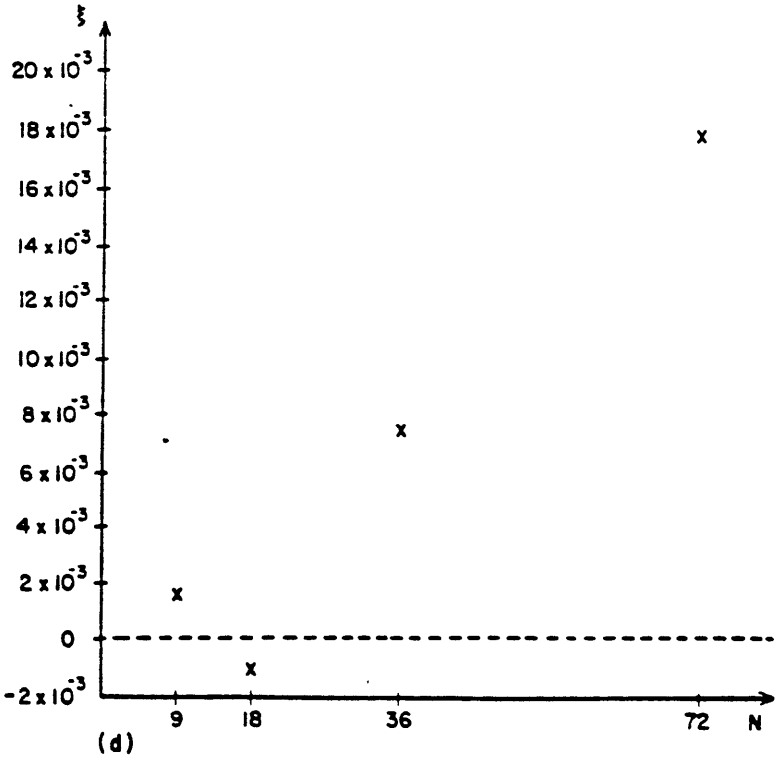
ξ
20 x 10^-3
18 x 10^-3
16 x 10^-3
14 x 10^-3
12 x 10^-3
10 x 10^-3
8 x 10^-3
6 x 10^-3
4 x 10^-3
2 x 10^-3
0
-2 x 10^-3
9
18
36
72
N
(d)

Fig. 5.2 (cont.)

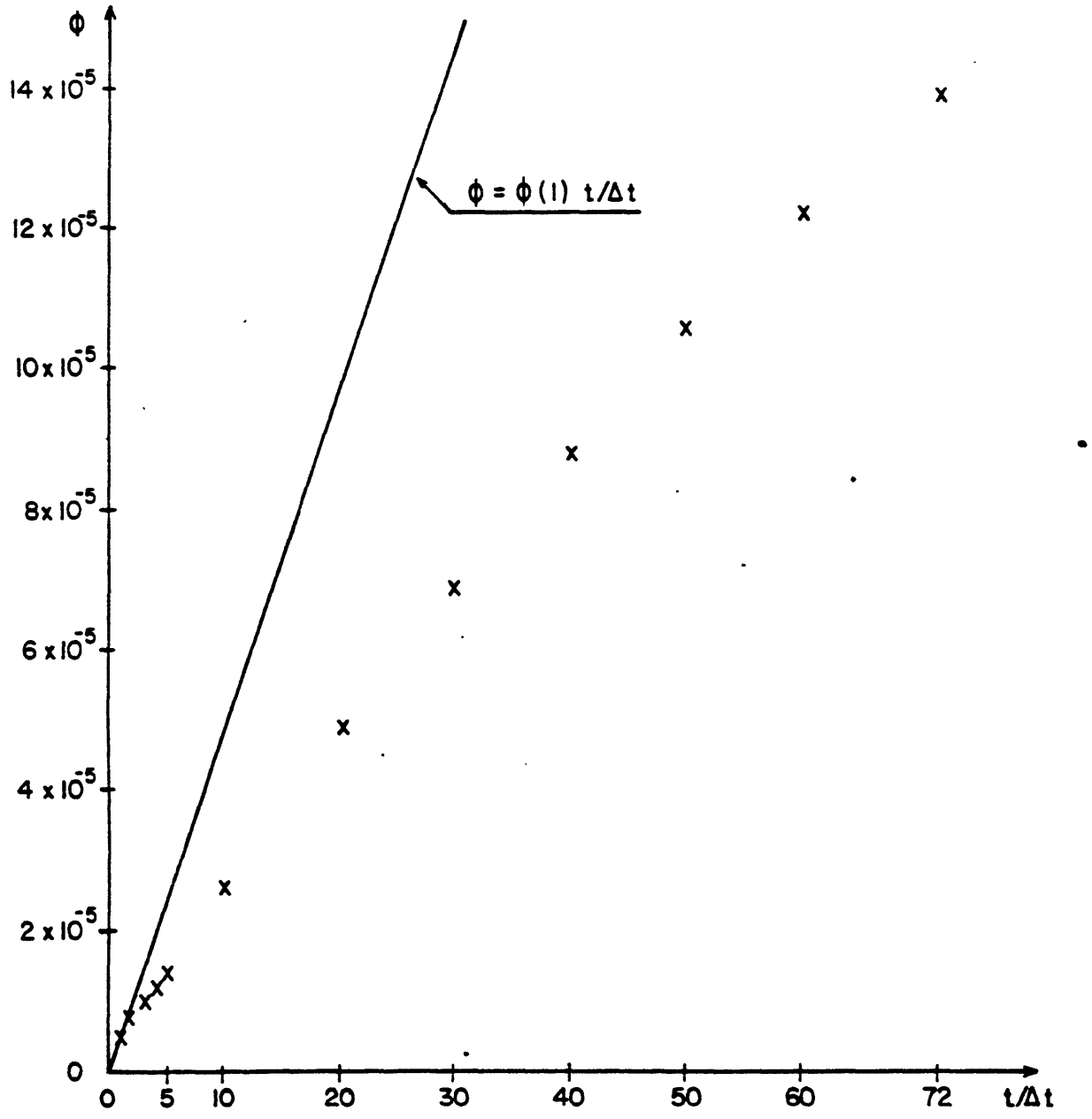

Fig. 5.3 Convection in a steady uniform flow. Evolution of the L-2 error norm with time (M = 7; N = 72; T = 9216 s).

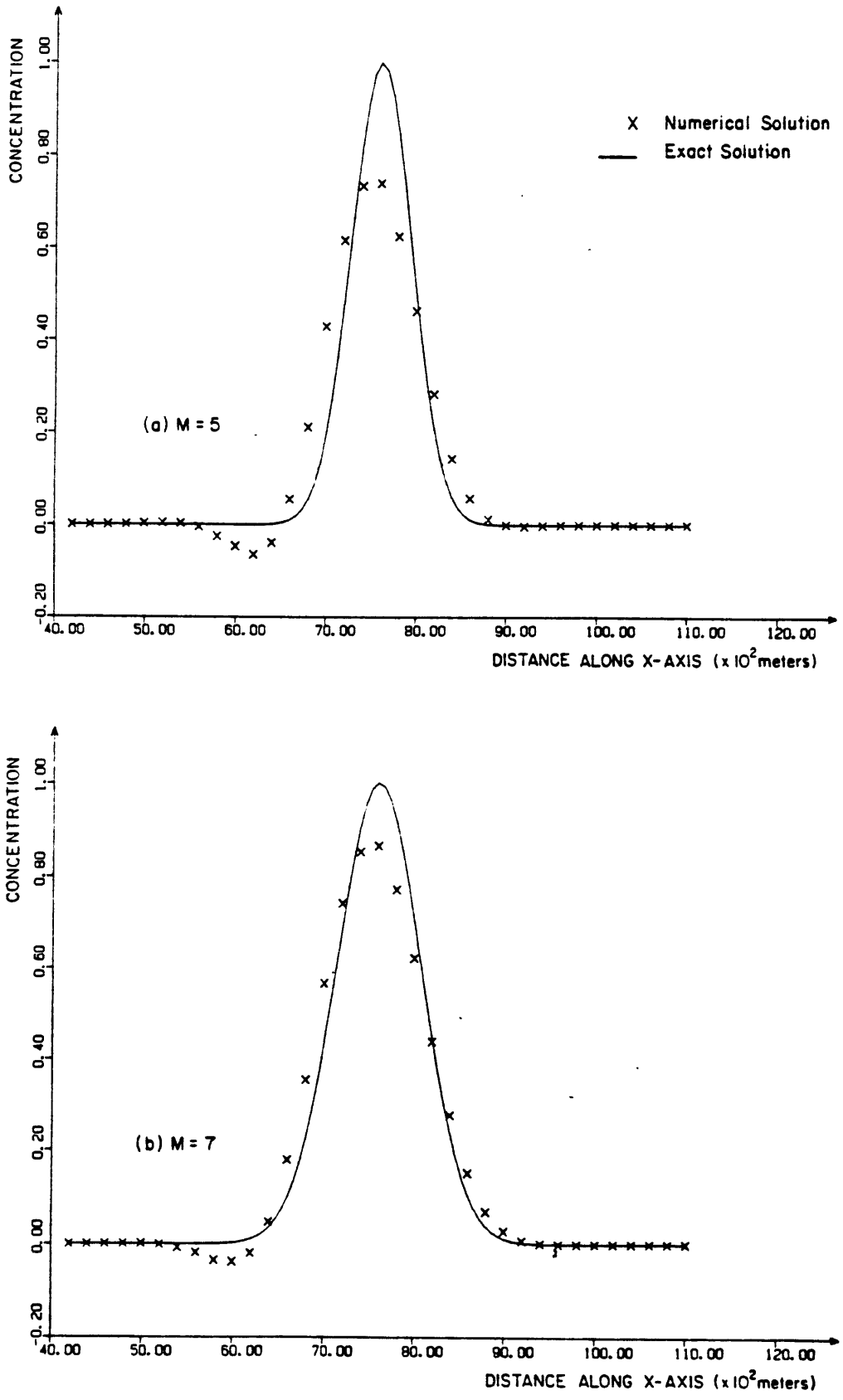

Fig. 5.4 Convection in a steady uniform flow. Numerical solutions for different values of M ($t \equiv T = 9216$ s; $N = 72$).

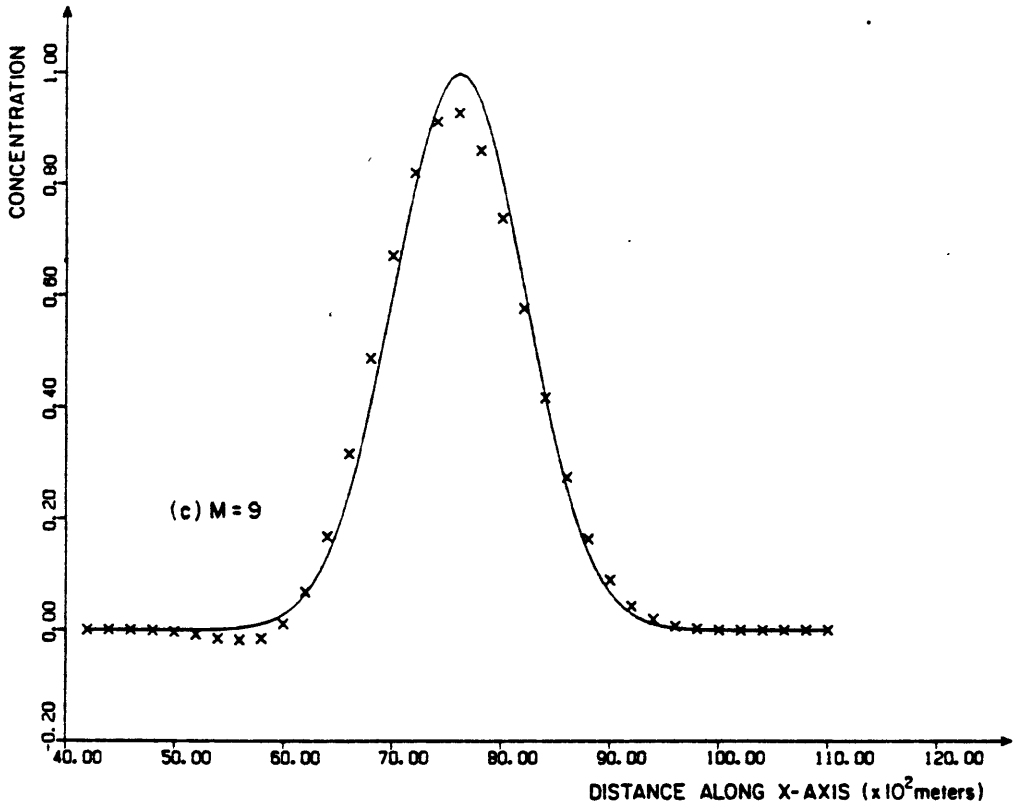
CONCENTRATION
1.00
0.80
0.60
0.40
0.20
0.00
-0.20
(c) M = 9
40.00
50.00
60.00
70.00
80.00
90.00
100.00
110.00
120.00
DISTANCE ALONG X-AXIS (x10²meters)

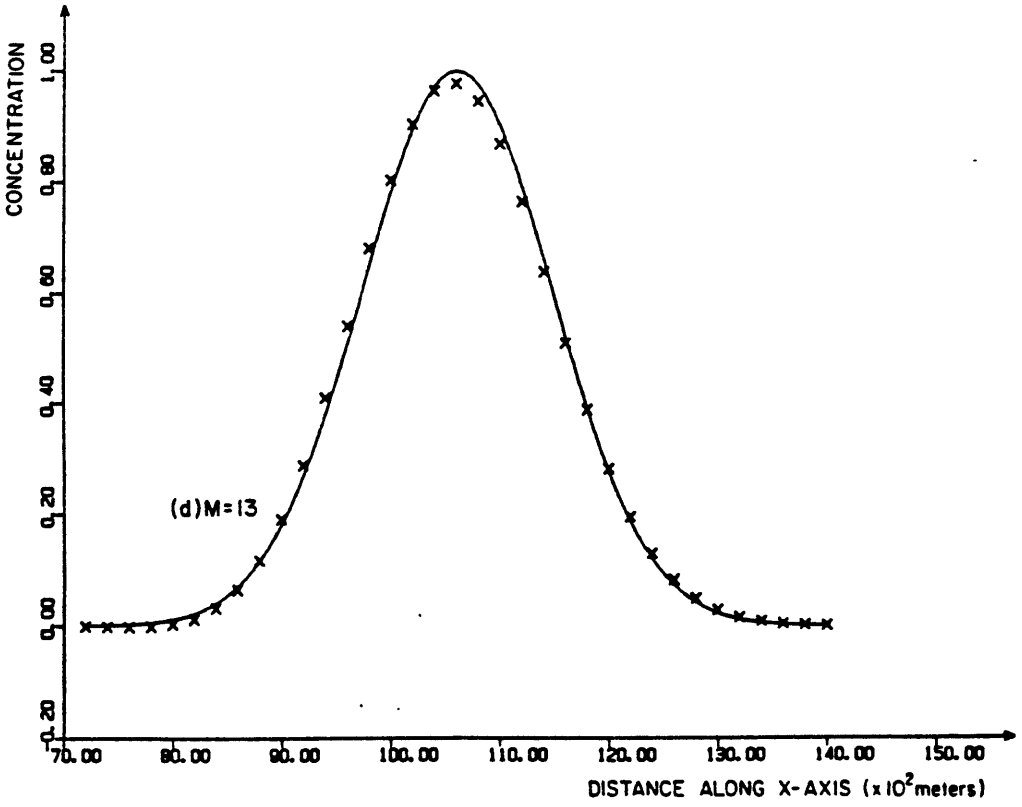
CONCENTRATION
1.00
0.80
0.60
0.40
0.20
0.00
-0.20
(d)M=13
70.00
80.00
90.00
100.00
110.00
120.00
130.00
140.00
150.00
DISTANCE ALONG X-AXIS (x10²meters)

Fig. 5.4 (cont.)

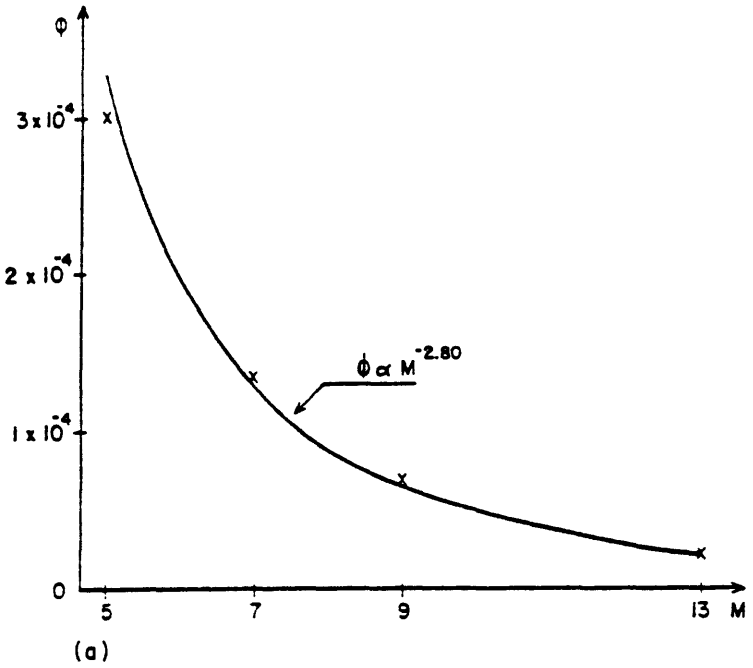

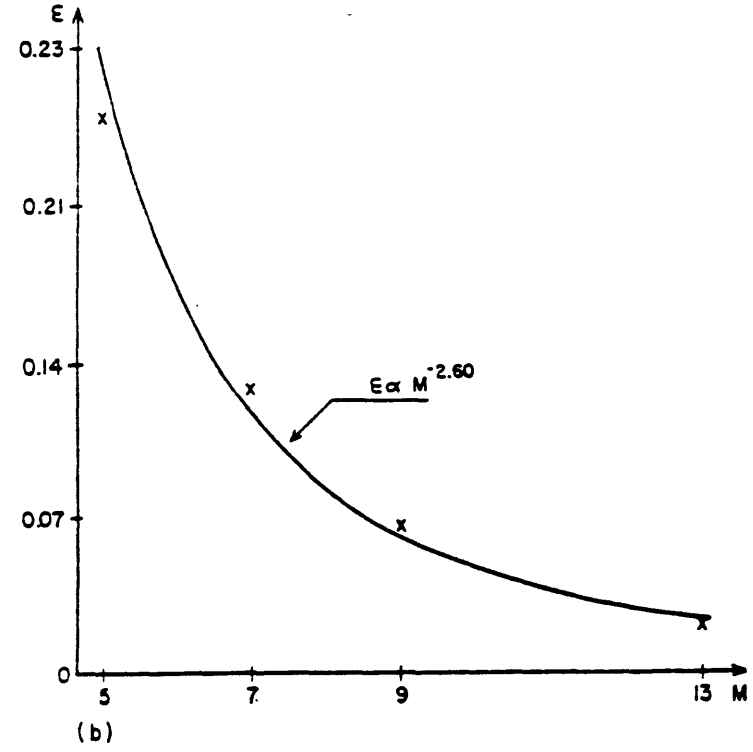

Fig. 5.5 Convection in a steady uniform flow. Error measures as a function of M ($t \equiv T = 9216$ s; $N = 72$).

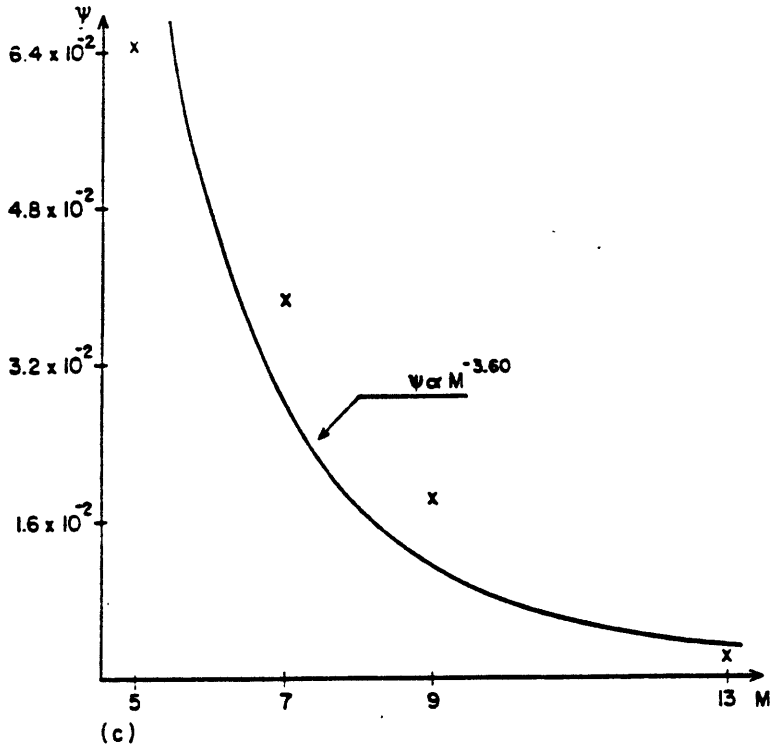
ψ
6.4 x 10^-2
4.8 x 10^-2
3.2 x 10^-2
1.6 x 10^-2
ψ α M^-3.60
5
7
9
13 M
(c)

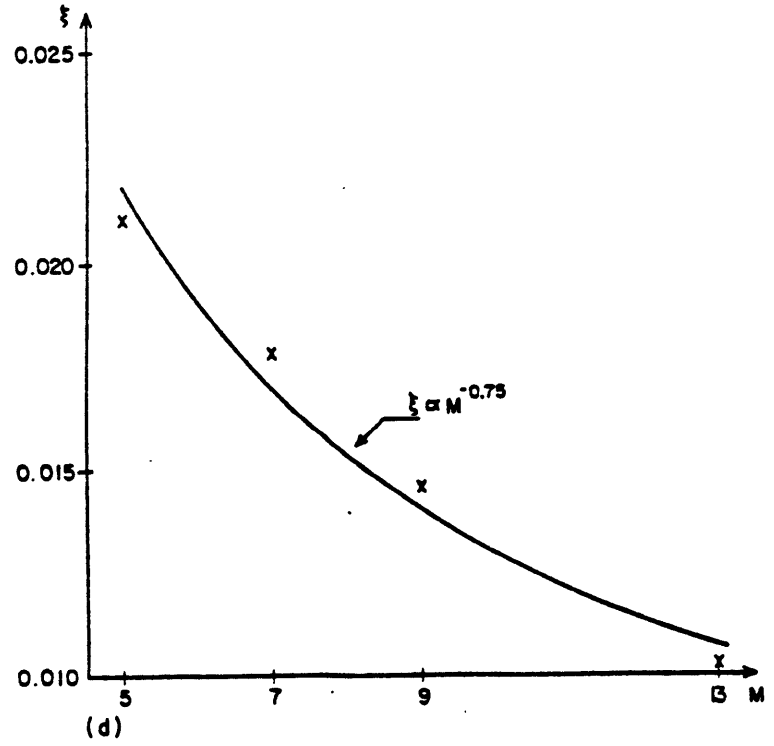
ξ
0.025
0.020
0.015
0.010
ξ α M^-0.75
5
7
9
13 M
(d)

Fig. 5.5 (cont.)

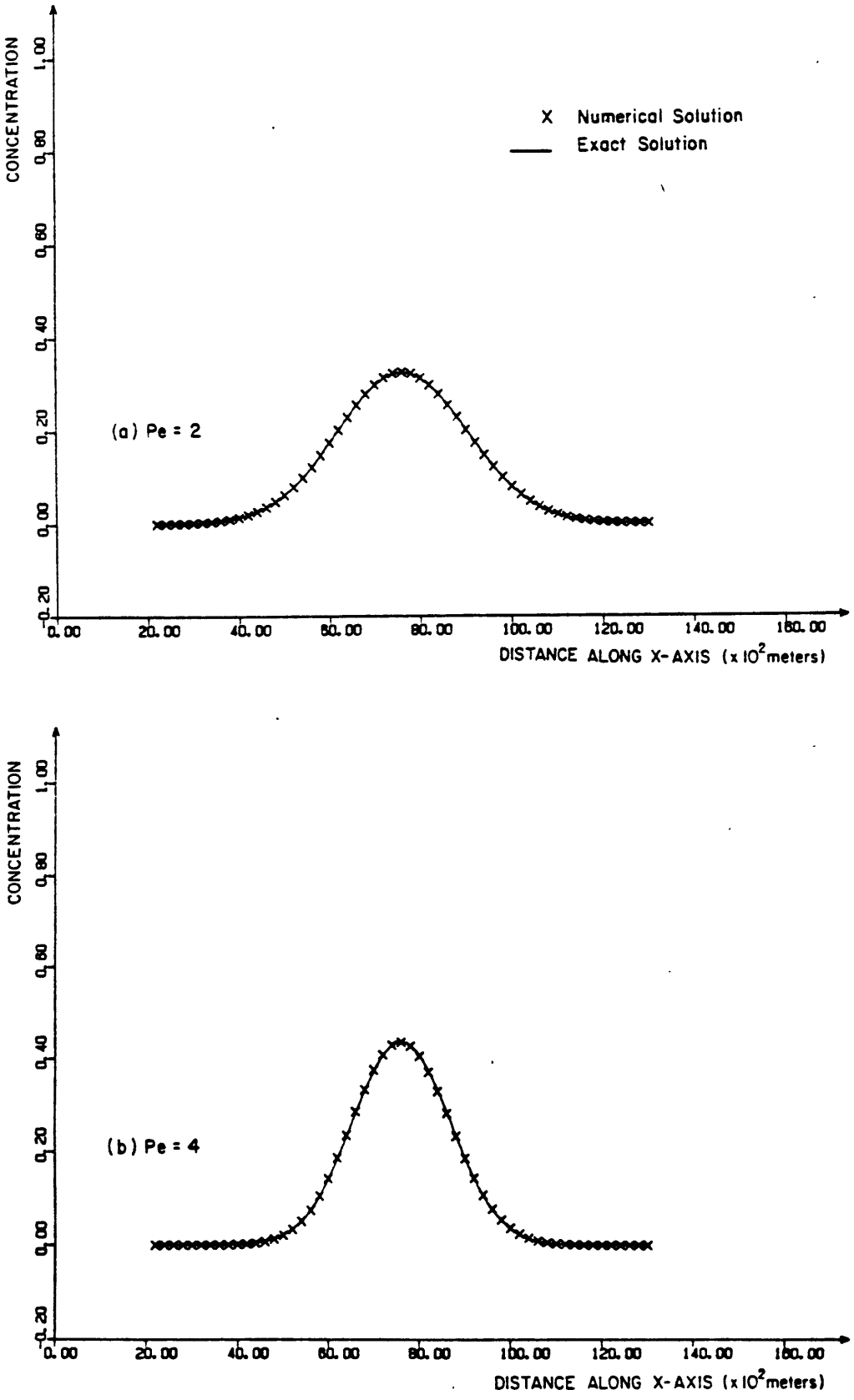

Fig. 5.6 Convection and diffusion in a steady uniform flow. Numerical solutions for different values of Pe ($t \equiv T = 9216$ s; $M = 7$; $N = 72$).

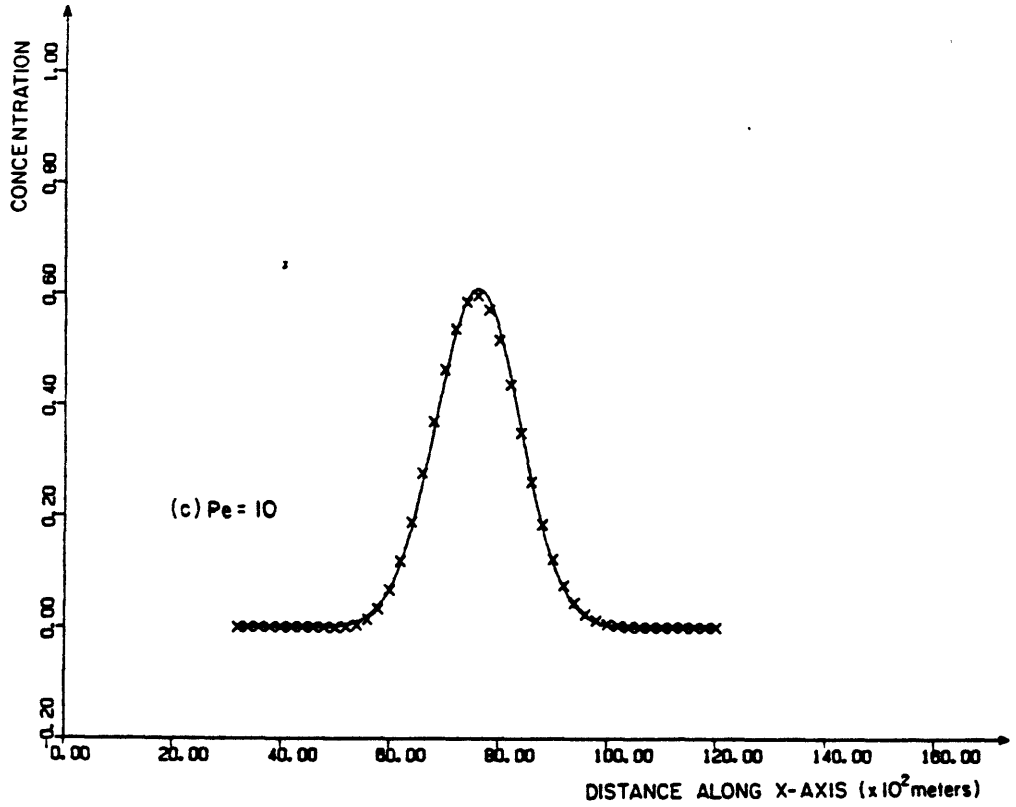
CONCENTRATION
1.00
0.80
0.60
0.40
0.20
0.00
-0.20
(c) Pe = 10
0.00
20.00
40.00
60.00
80.00
100.00
120.00
140.00
160.00
DISTANCE ALONG X-AXIS (x 10² meters)

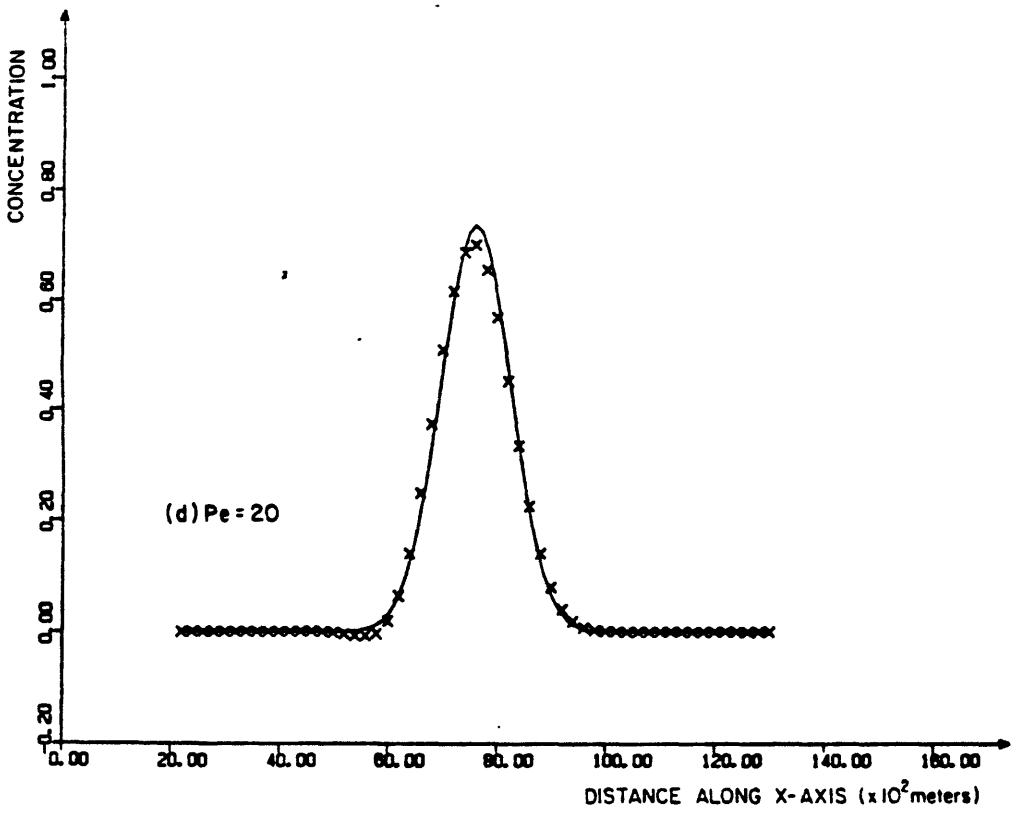
CONCENTRATION
1.00
0.80
0.60
0.40
0.20
0.00
-0.20
(d) Pe = 20
0.00
20.00
40.00
60.00
80.00
100.00
120.00
140.00
160.00
DISTANCE ALONG X-AXIS (x 10² meters)

Fig. 5.6 (cont.)

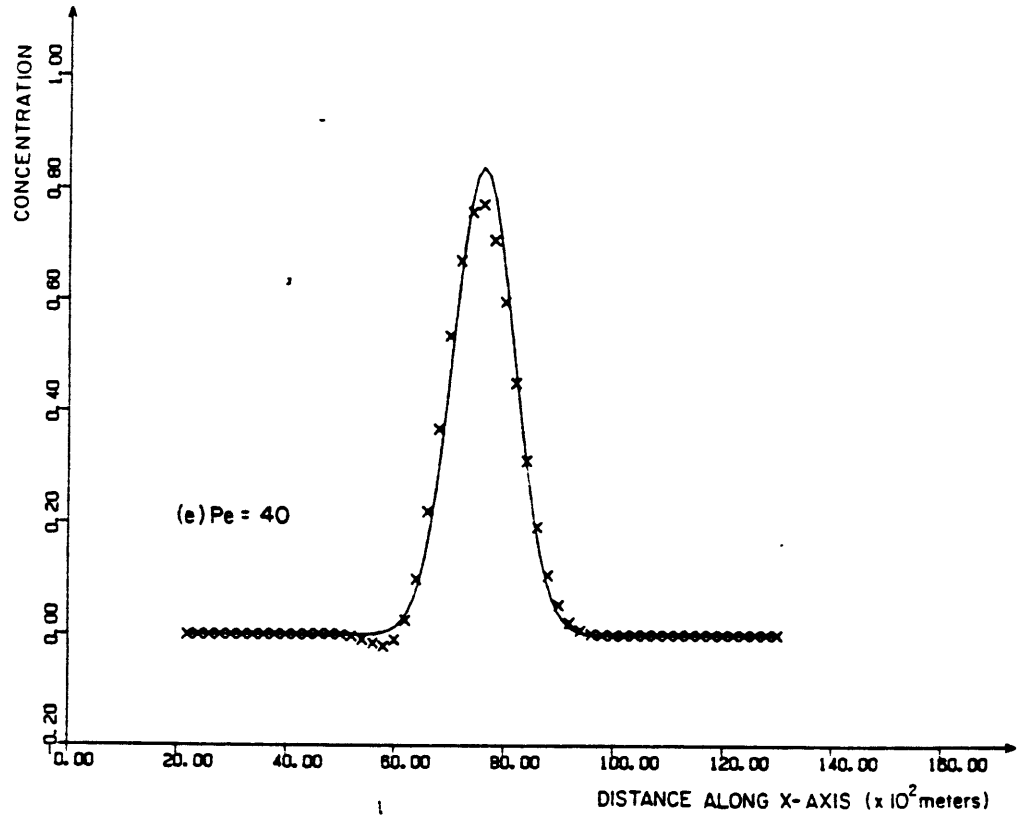
CONCENTRATION
1.00
0.80
0.60
0.40
0.20
0.00
-0.20
(e) Pe = 40
0.00
20.00
40.00
60.00
80.00
100.00
120.00
140.00
160.00
DISTANCE ALONG X-AXIS (x 10² meters)

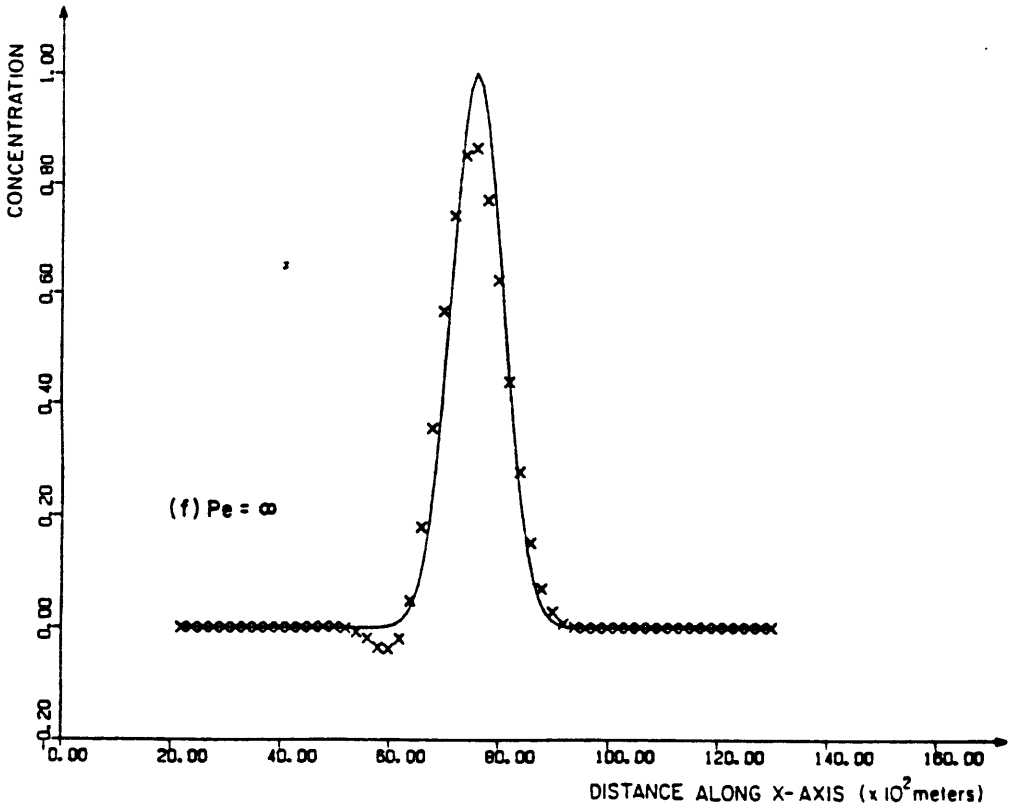
CONCENTRATION
1.00
0.80
0.60
0.40
0.20
0.00
-0.20
(f) Pe = ∞
0.00
20.00
40.00
60.00
80.00
100.00
120.00
140.00
160.00
DISTANCE ALONG X-AXIS (x 10² meters)

Fig. 5.6 (cont.)

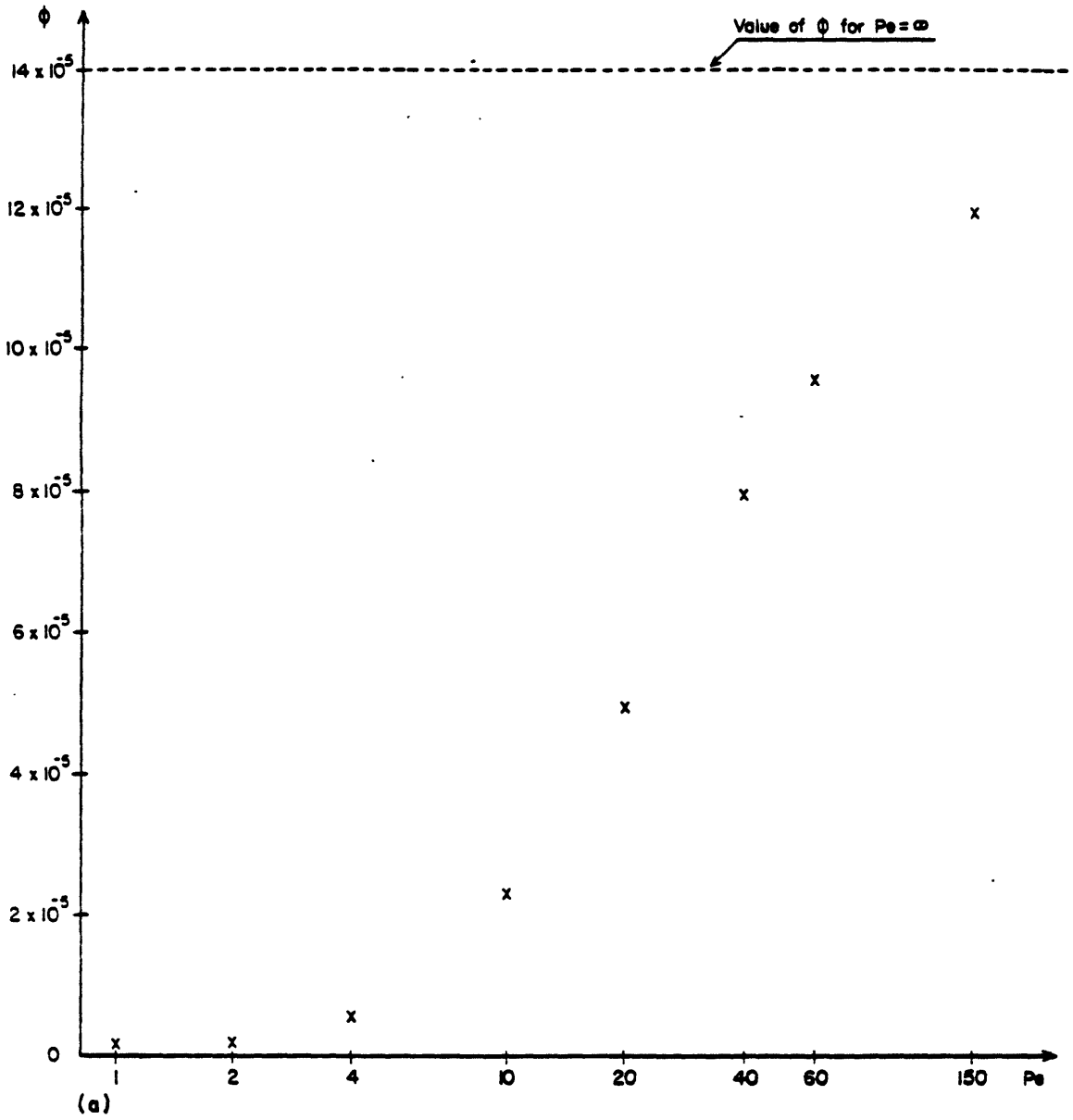

Fig. 5.7 Convection and diffusion in a steady uniform flow. Error measures as a function of Pe ($t \equiv T = 9216$ s; $M = 7$; $N = 72$).

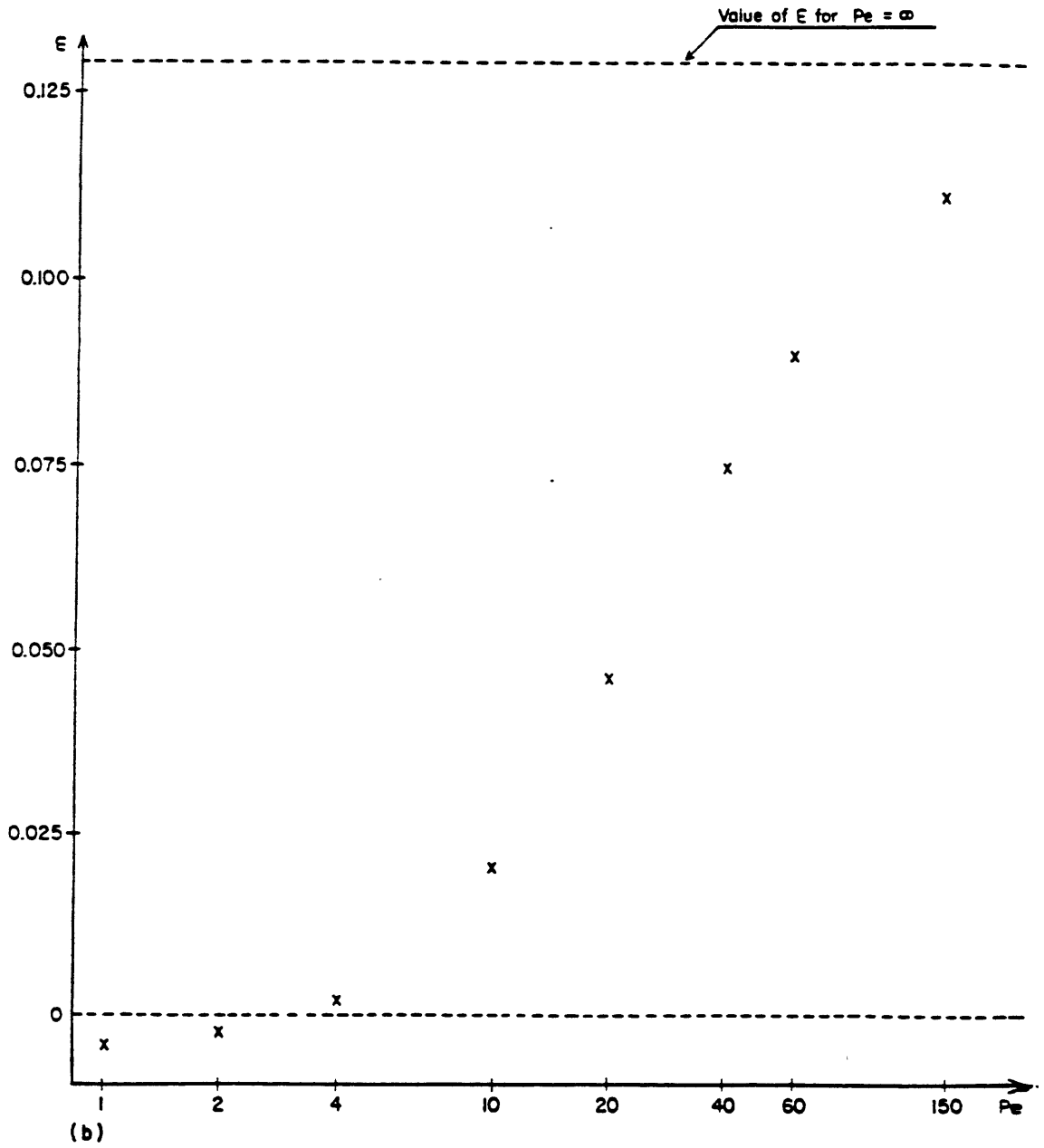
Value of E for Pe = ∞
E
0.125
0.100
0.075
0.050
0.025
0
1
2
4
10
20
40
60
150
Pe
(b)

Fig. 5.7 (cont.)

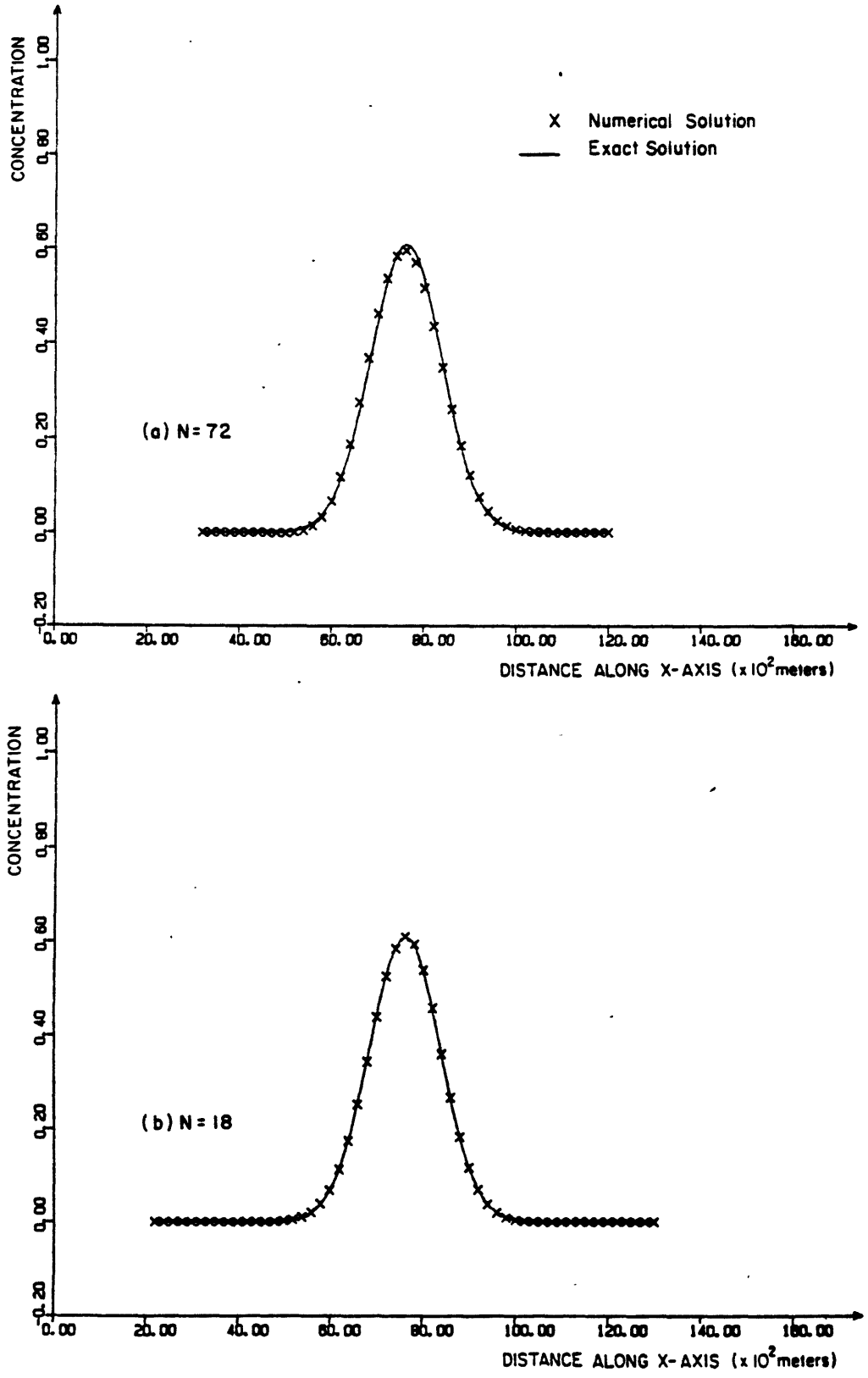

Fig. 5.8 Convection and diffusion in a steady uniform flow. Numerical solutions for different values of N ($t \equiv T = 9216$ s; $M = 7$; $N = 72$).

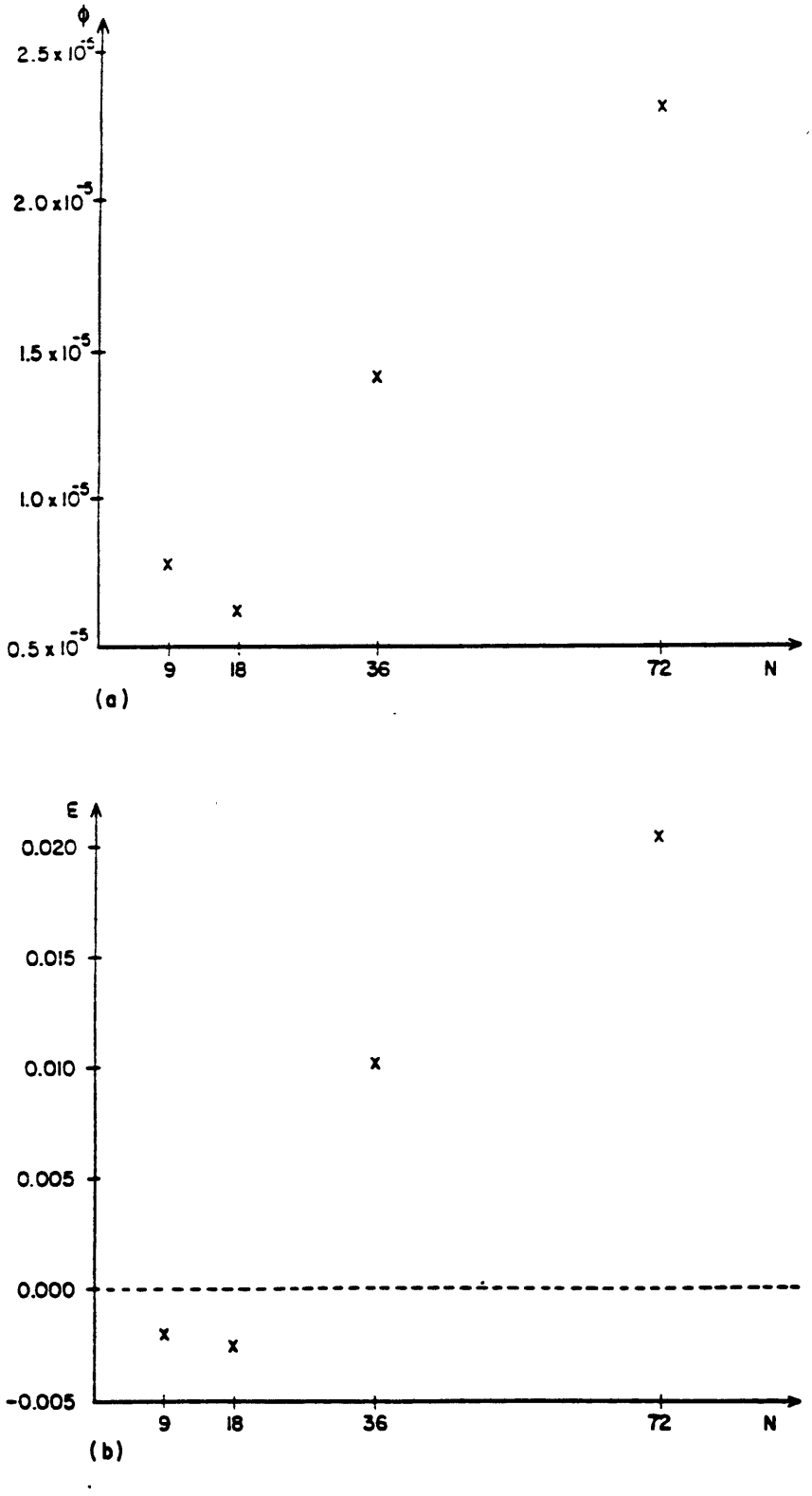

Fig. 5.9 Convection and diffusion in a steady uniform flow. Error measures as a function of N ($t \equiv T = 9216$ s; $M = 7$; $Pe = 10$).

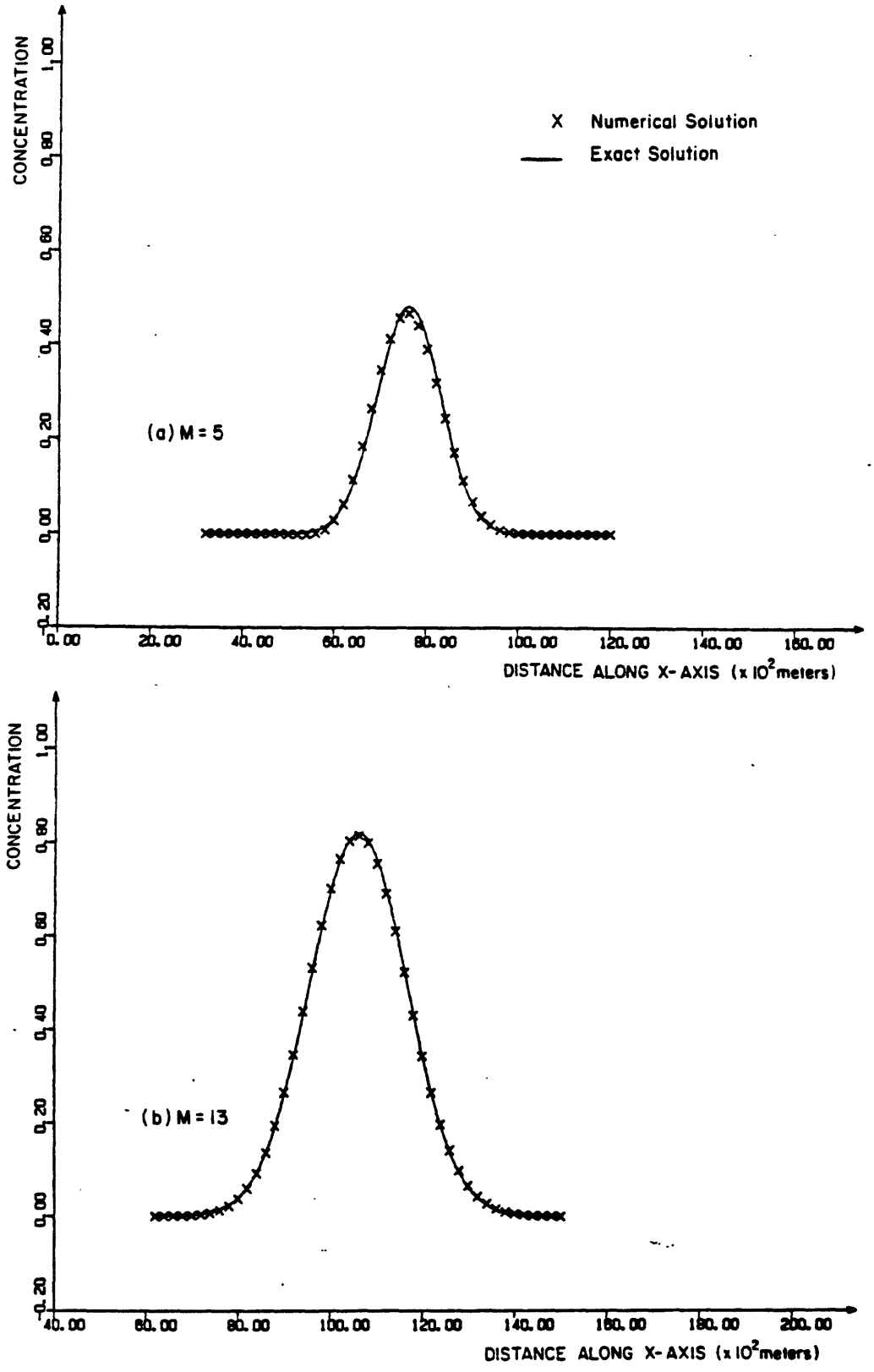

Fig. 5.10 Convection and diffusion in a steady uniform flow. Numerical solutions for different values of M ($t \equiv T = 9216$ s; $N = 72$; $Pe = 10$).

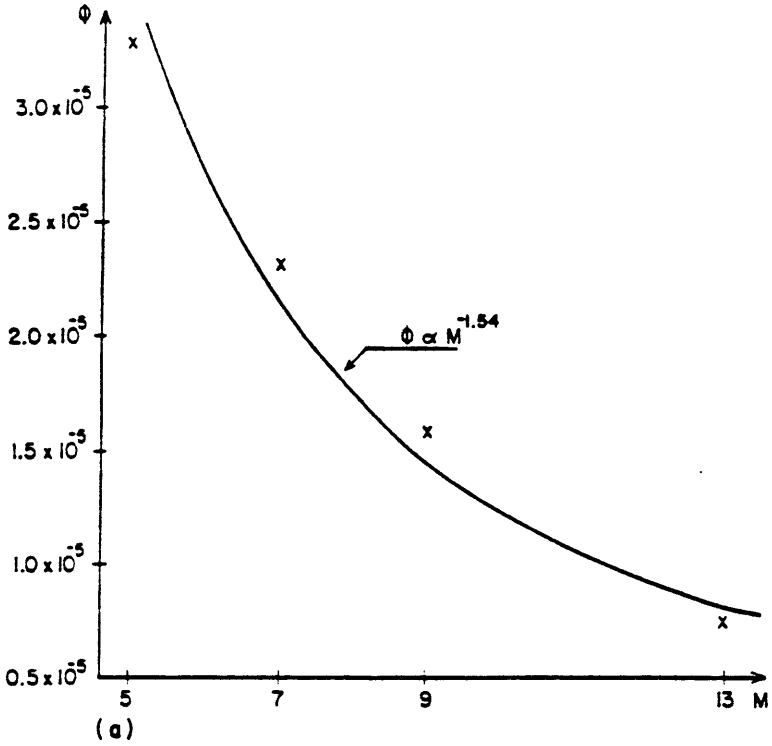

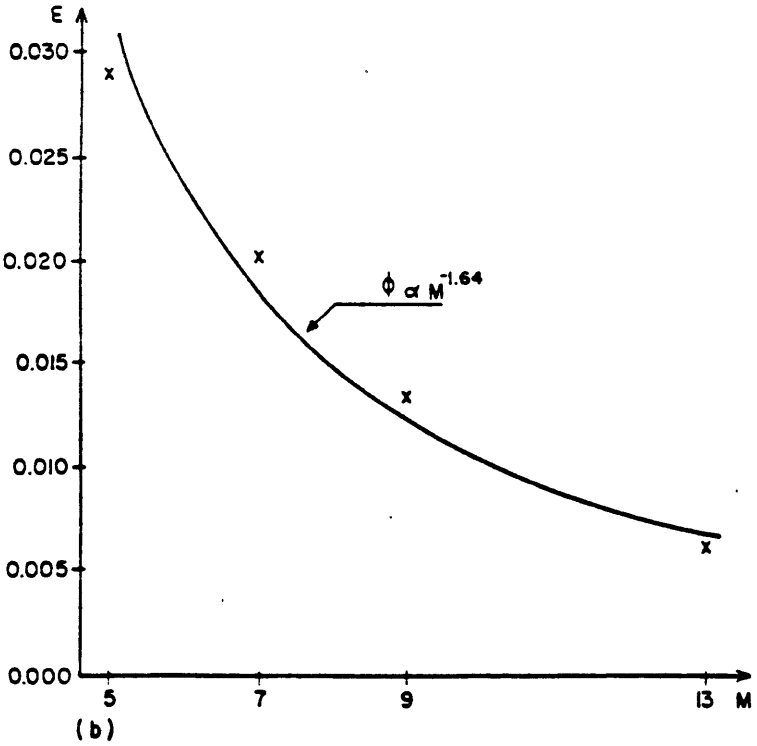

Fig. 5.11 Convection and diffusion in a steady uniform flow. Error measures as a funcion of M ($t \equiv T = 9216$ s; $N = 72$; $Pe = 10$).

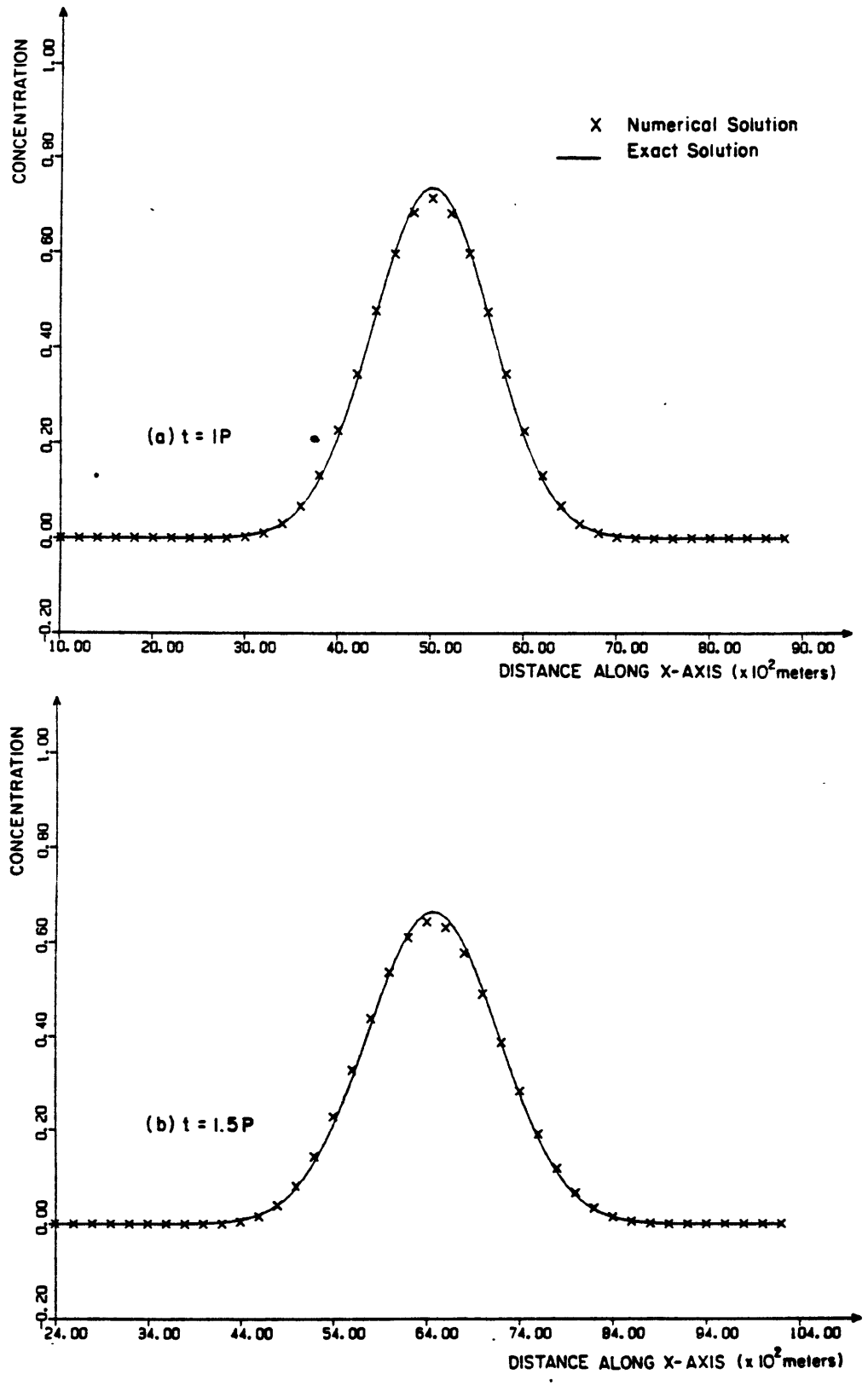

Fig. 5.12 Convection and diffusion in a sinusoidal uniform flow. Numerical solutions at different times (M = 7, N = 288, T = 36864; Pe_{max} = 20).

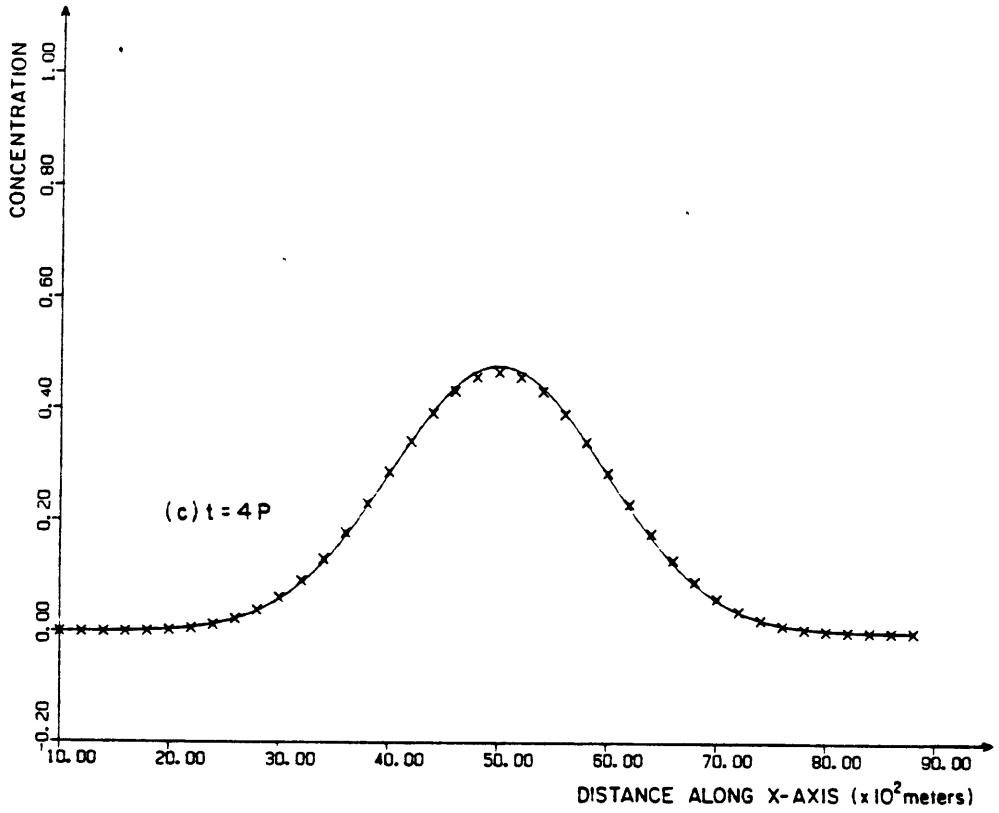
CONCENTRATION
1.00
0.80
0.60
0.40
0.20
0.00
-0.20
(c) t = 4P
10.00
20.00
30.00
40.00
50.00
60.00
70.00
80.00
90.00
DISTANCE ALONG X-AXIS (x 10² meters)

Fig. 5.12 (cont.)

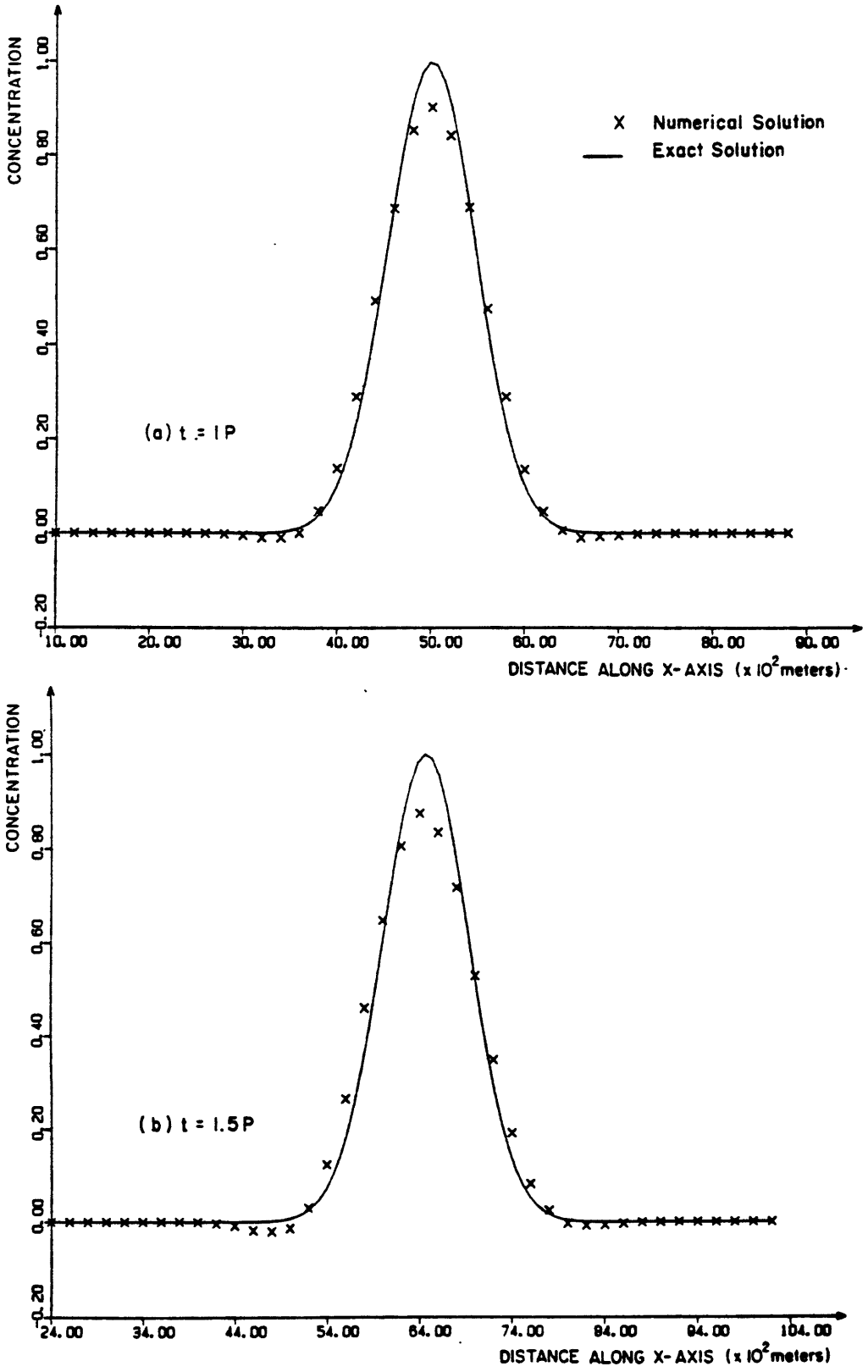

Fig. 5.13 Convection and diffusion in a sinusoidal uniform flow. Numerical solutions at different times (M = 7, N = 288, T = 36864, $Pe_{max} = \infty$).

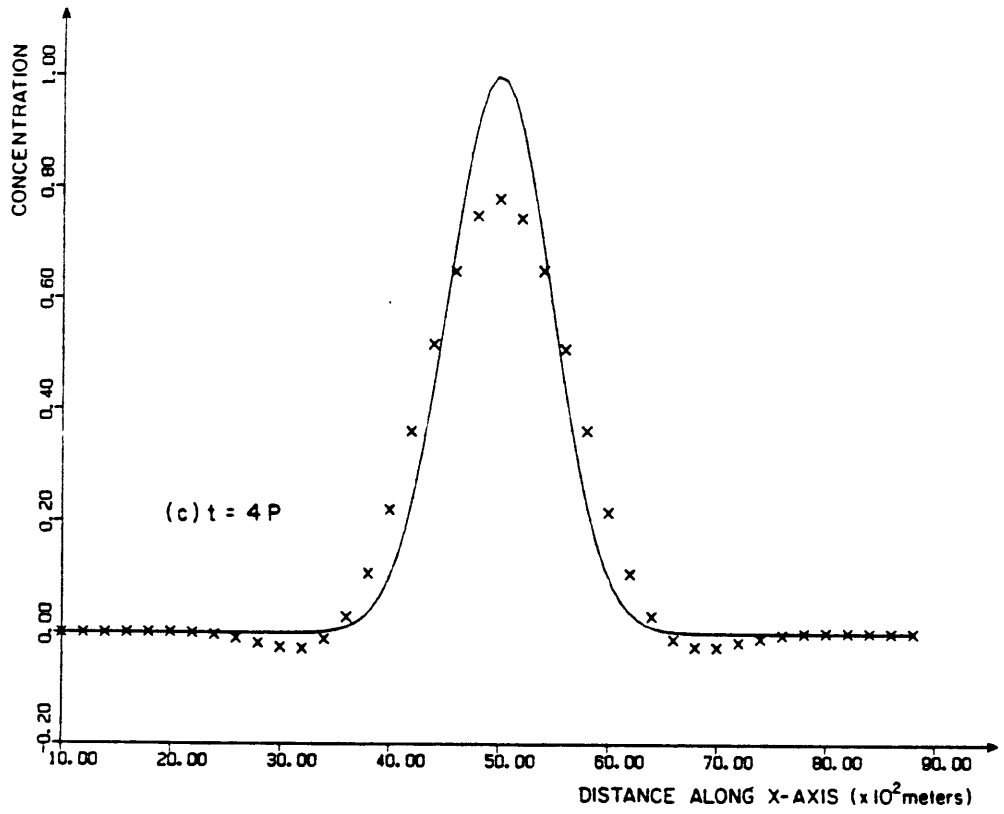
CONCENTRATION
1.00
0.80
0.60
0.40
0.20
0.00
-0.20
(c) t = 4 P
10.00
20.00
30.00
40.00
50.00
60.00
70.00
80.00
90.00
DISTANCE ALONG X-AXIS (x 10² meters)

Fig. 5.13 (cont.)

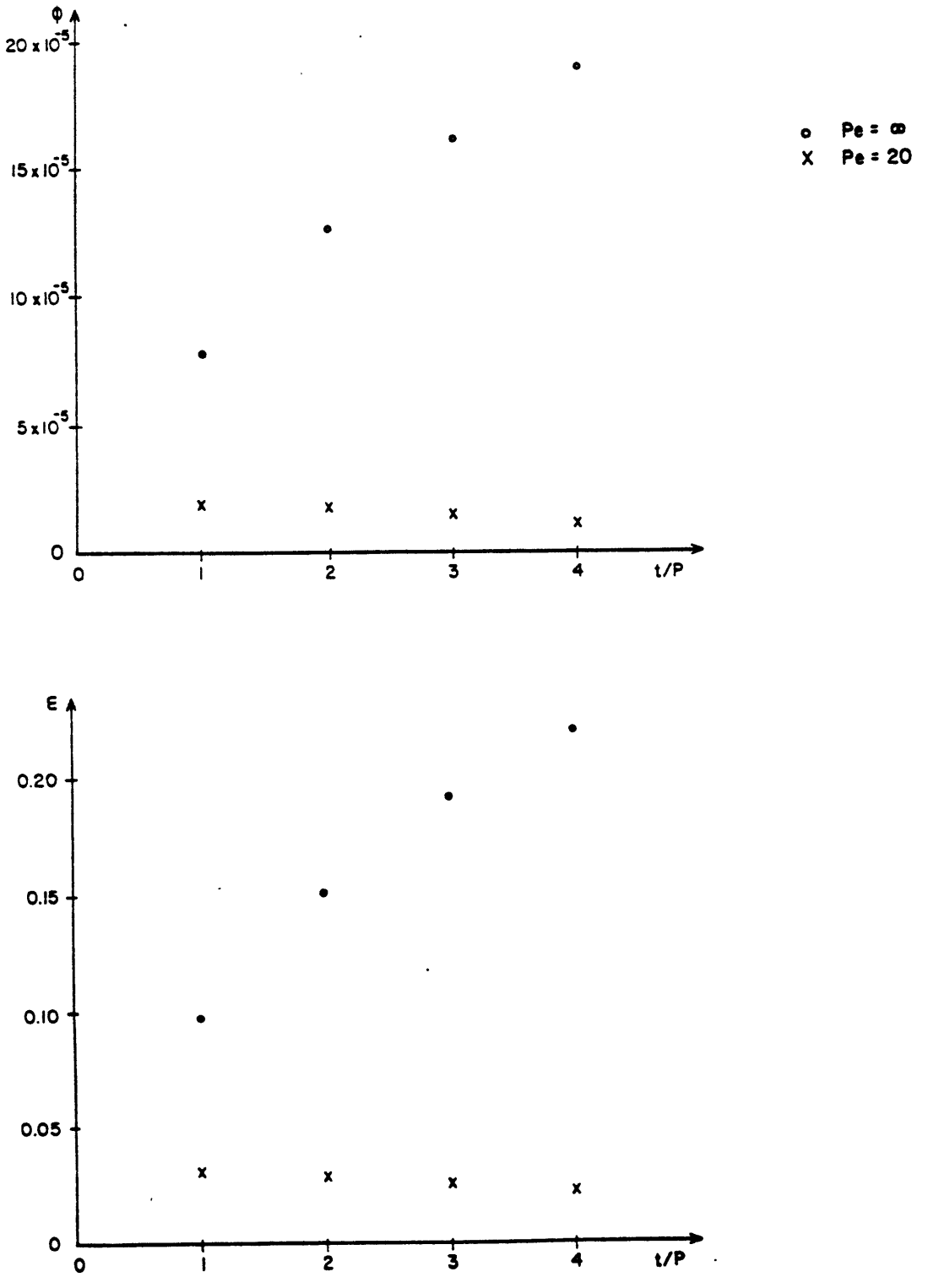

Fig. 5.14 Convection and diffusion in a sinusoidal uniform flow. Error measures as a function of time.

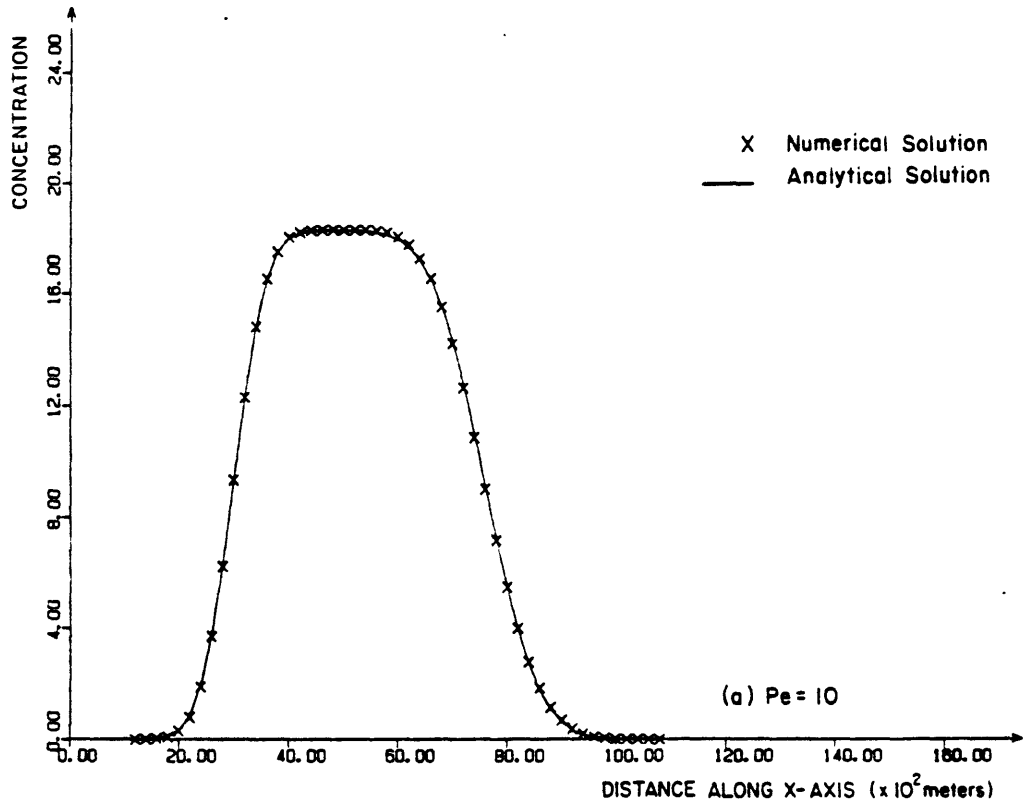

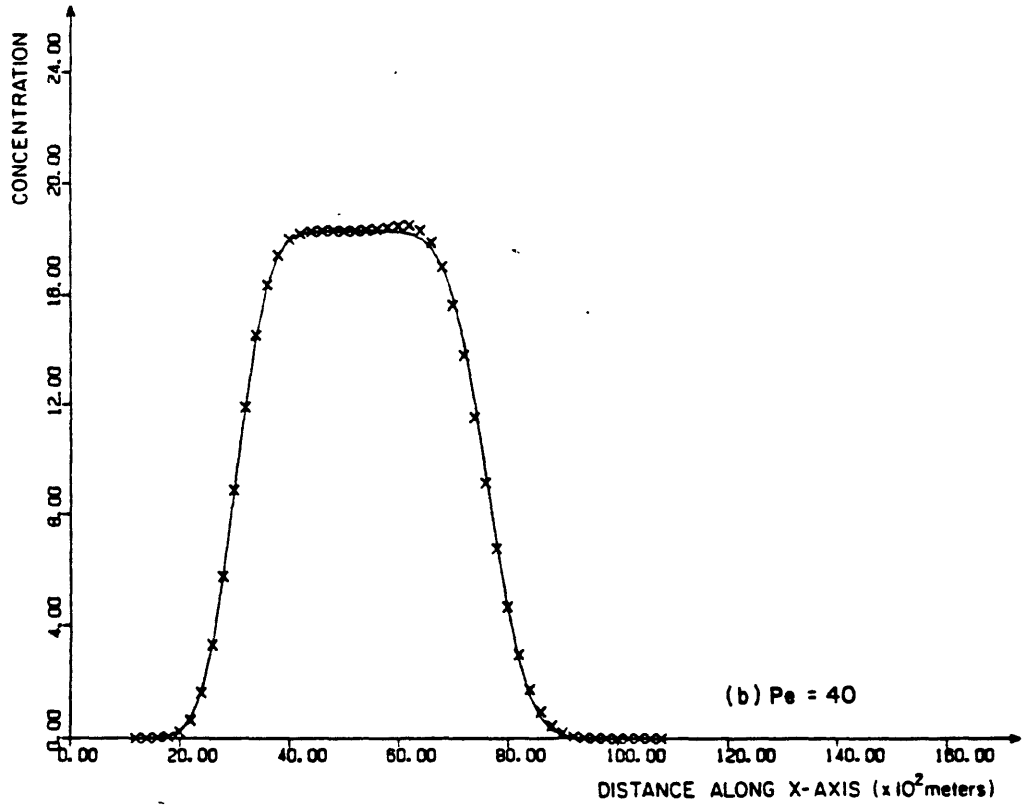

Fig. 5.15 Convection and diffusion of a continuous source in a steady uniform flow. Numerical solutions for different values of Pe ($t \equiv T = 9216$ s; $M = 7$; $N = 72$).

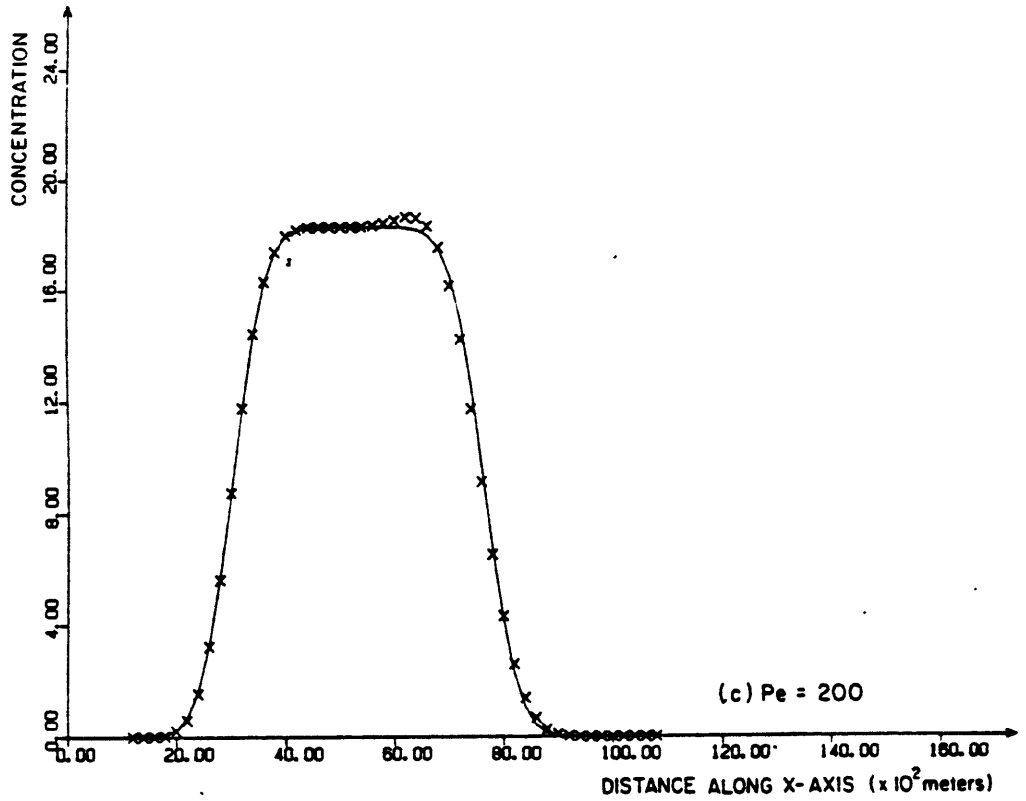
CONCENTRATION
0.00
4.00
8.00
12.00
16.00
20.00
24.00
0.00
20.00
40.00
60.00
80.00
100.00
120.00
140.00
160.00
(c) Pe = 200
DISTANCE ALONG X-AXIS (x 10² meters)

Fig. 5.15 (cont.)

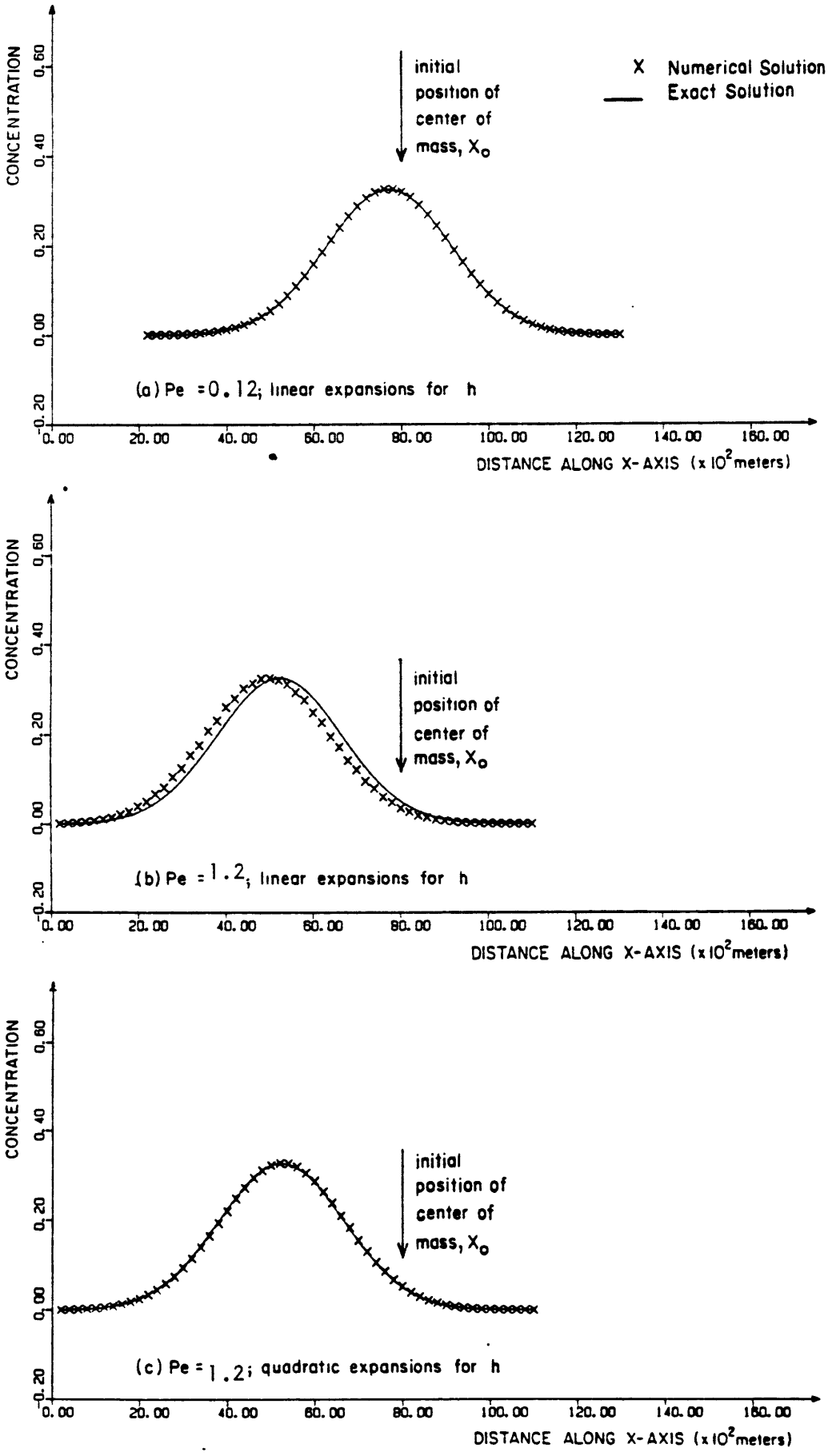

Fig. 5.16 Diffusion in a depth-variable medium. Numerical solutions ($t \equiv T = 9216$ s; $M = 7$; $N = 72$).

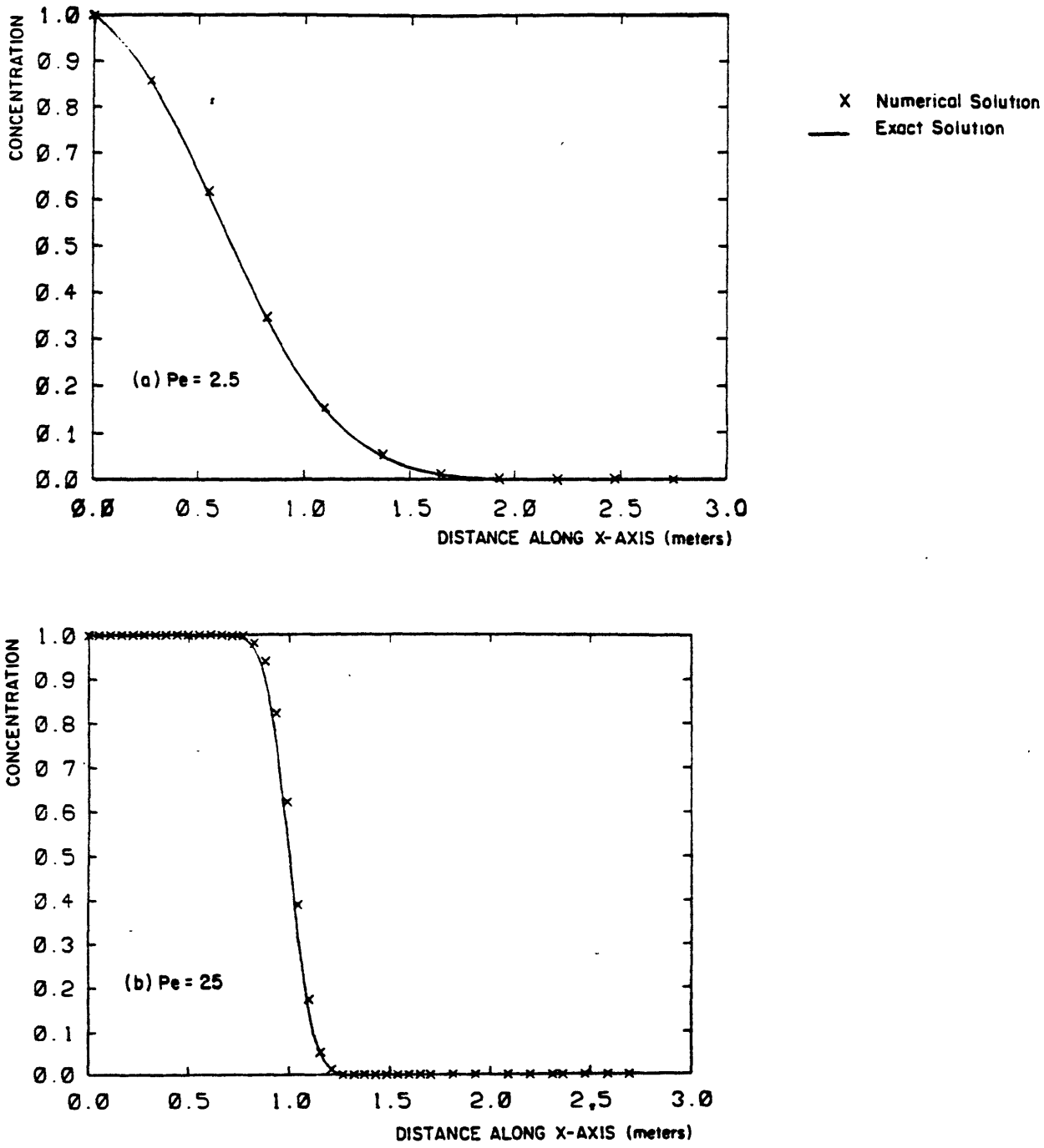

Fig. 5.17 Advancing front. Numerical solution for different Pe.

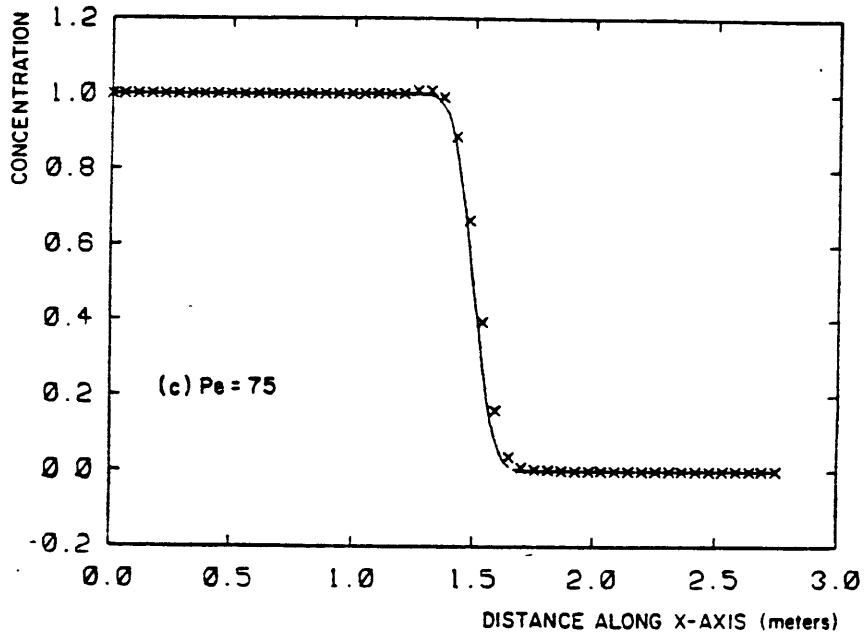
CONCENTRATION
1.2
1.0
0.8
0.6
0.4
0.2
0 0
-0.2
(c) Pe = 75
0.0
0.5
1.0
1.5
2.0
2.5
3.0
DISTANCE ALONG X-AXIS (meters)

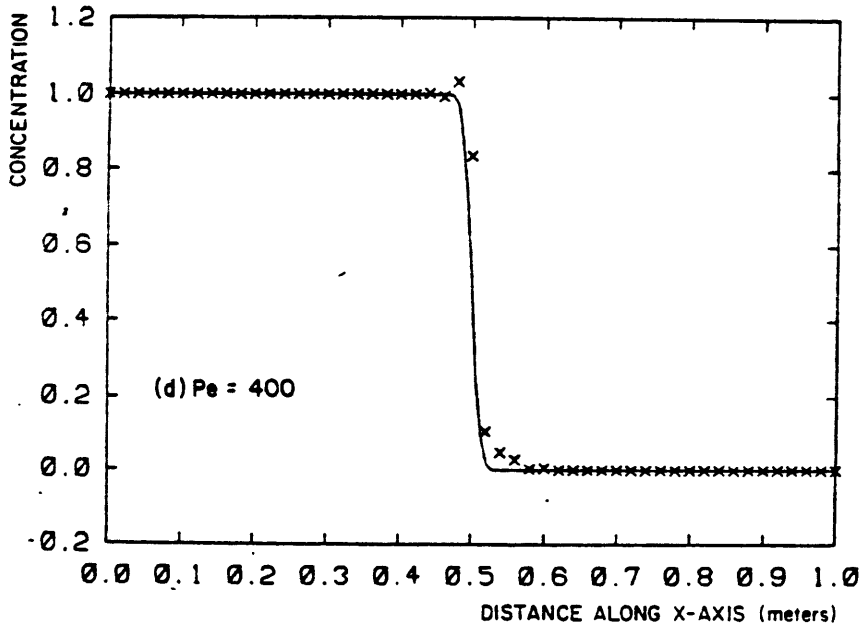
CONCENTRATION
1.2
1.0
0.8
0.6
0.4
0.2
0.0
-0.2
(d) Pe = 400
0.0 0.1 0.2 0.3 0.4 0.5 0.6 0.7 0.8 0.9 1.0
DISTANCE ALONG X-AXIS (meters)

Fig. 5.17 (cont.)

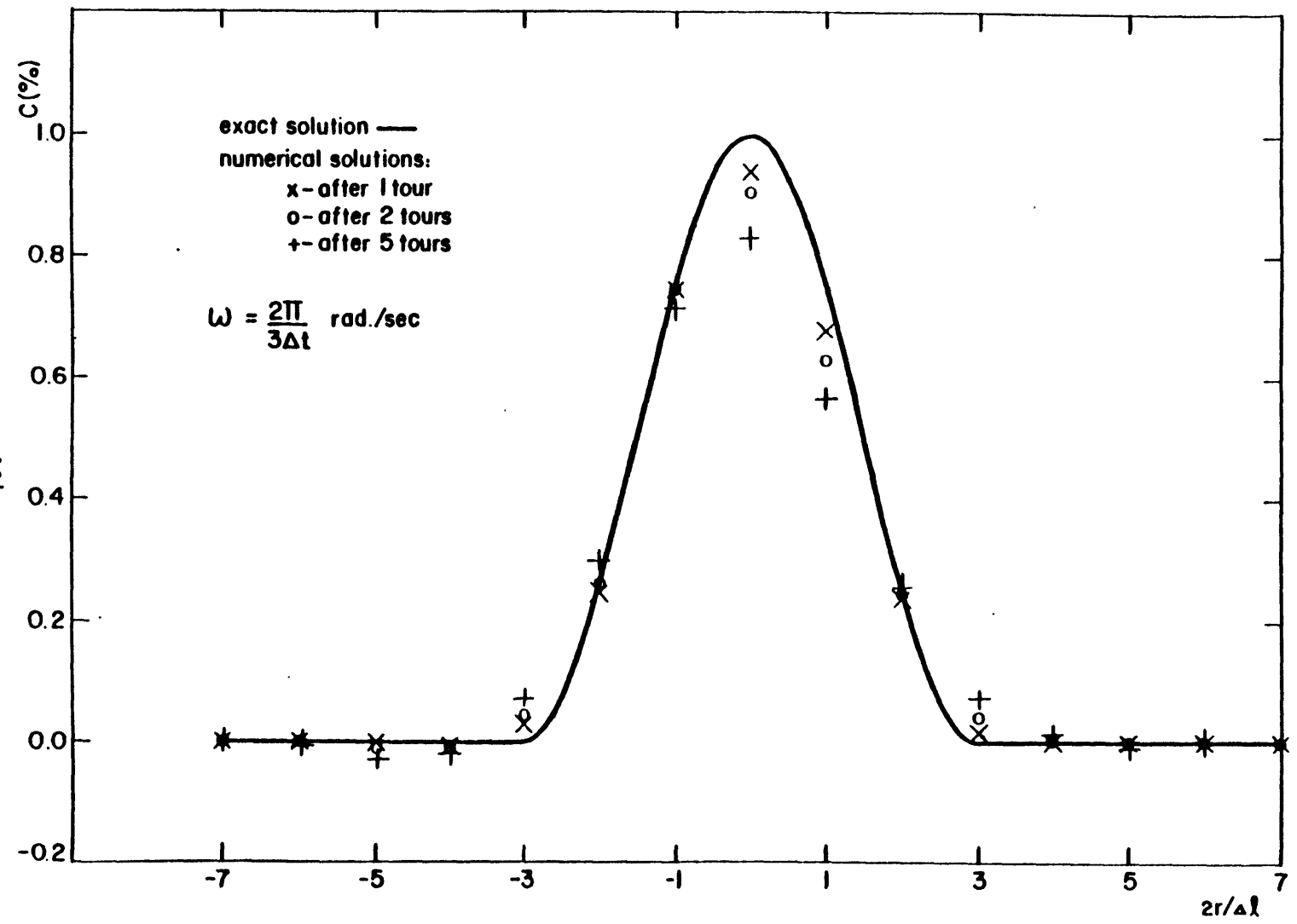

Fig. 5.18 Convection in a flow in rigid-body rotation.

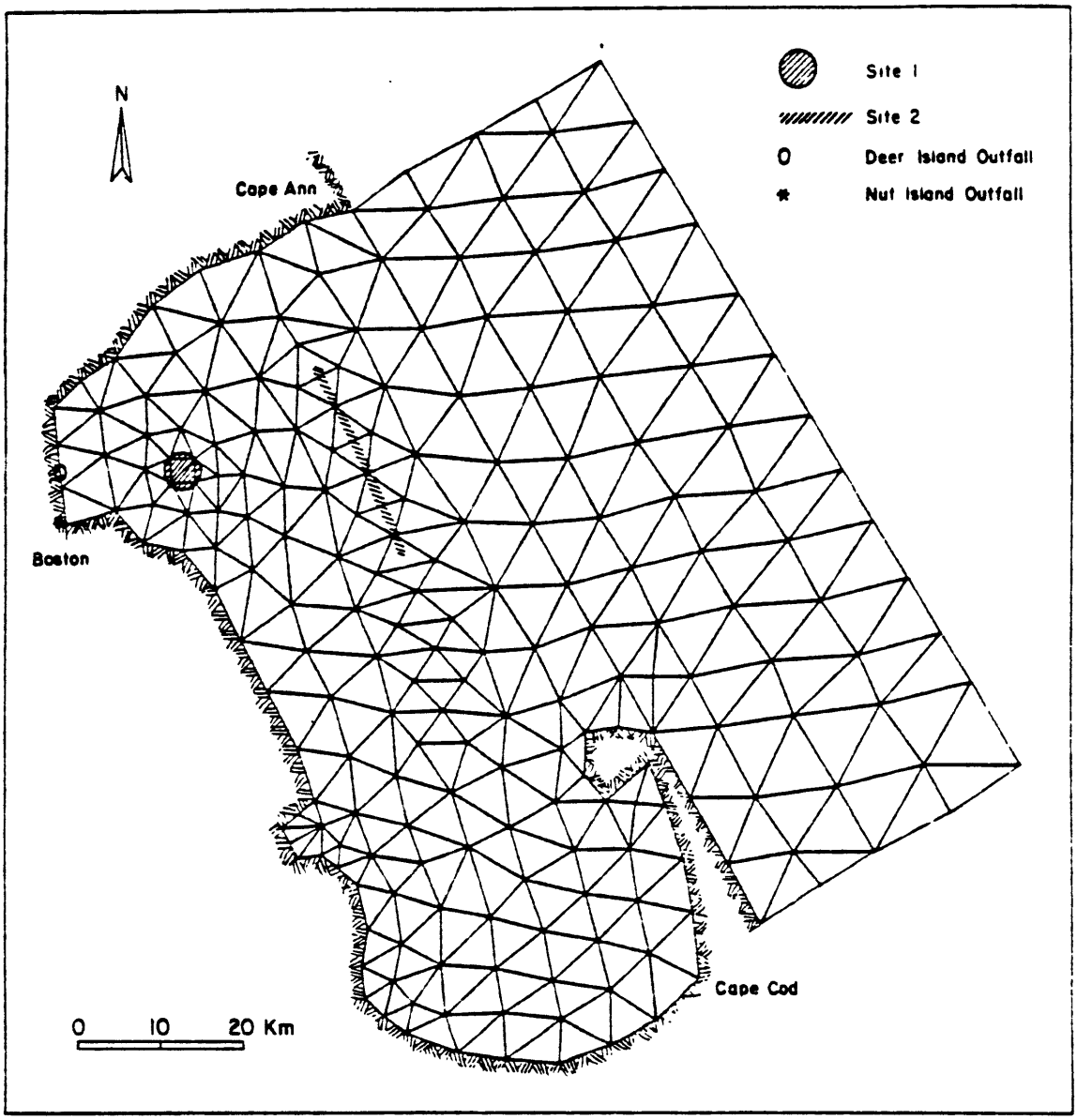

Fig. 6.1 Massachusetts Bay. Finite Element Grid.

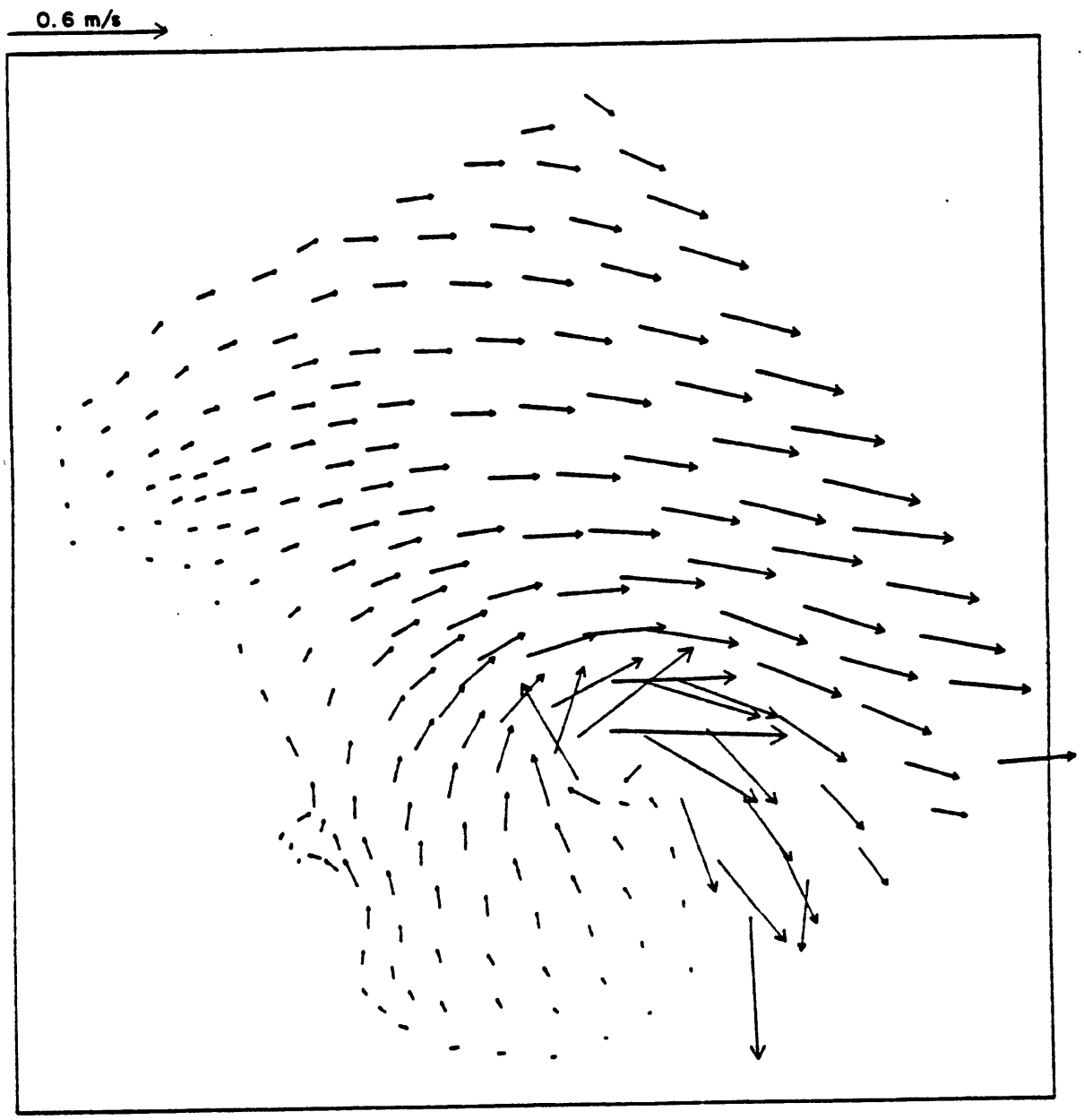

Fig. 6.2 Massachusetts Bay. Velocity field at maximum ebb.

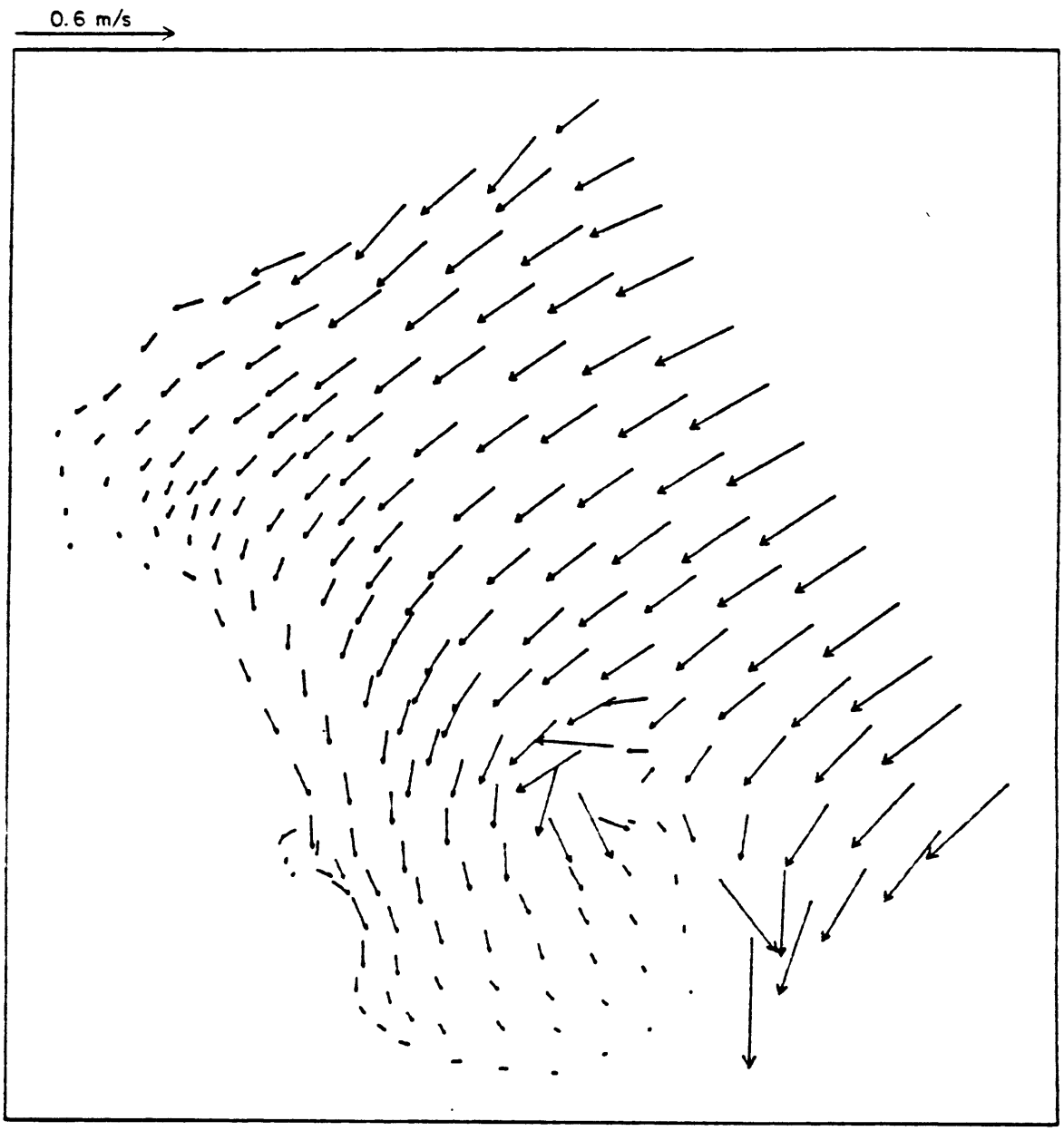

Fig. 6.3 Massachusetts Bay. Velocity field at maximum flood.

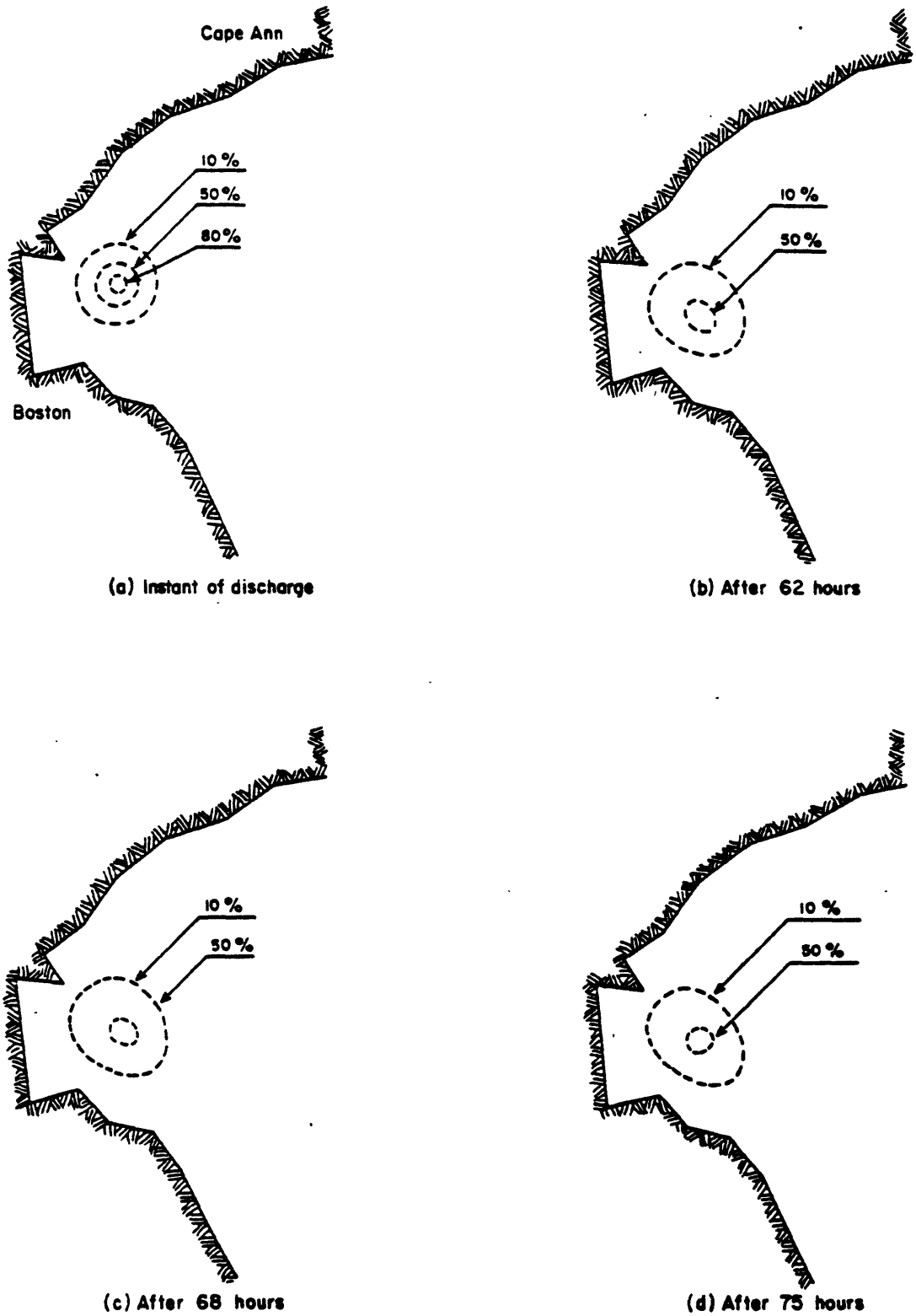

Fig. 6.4 Massachusetts Bay. Sludge plumes for discharge at Site 1.

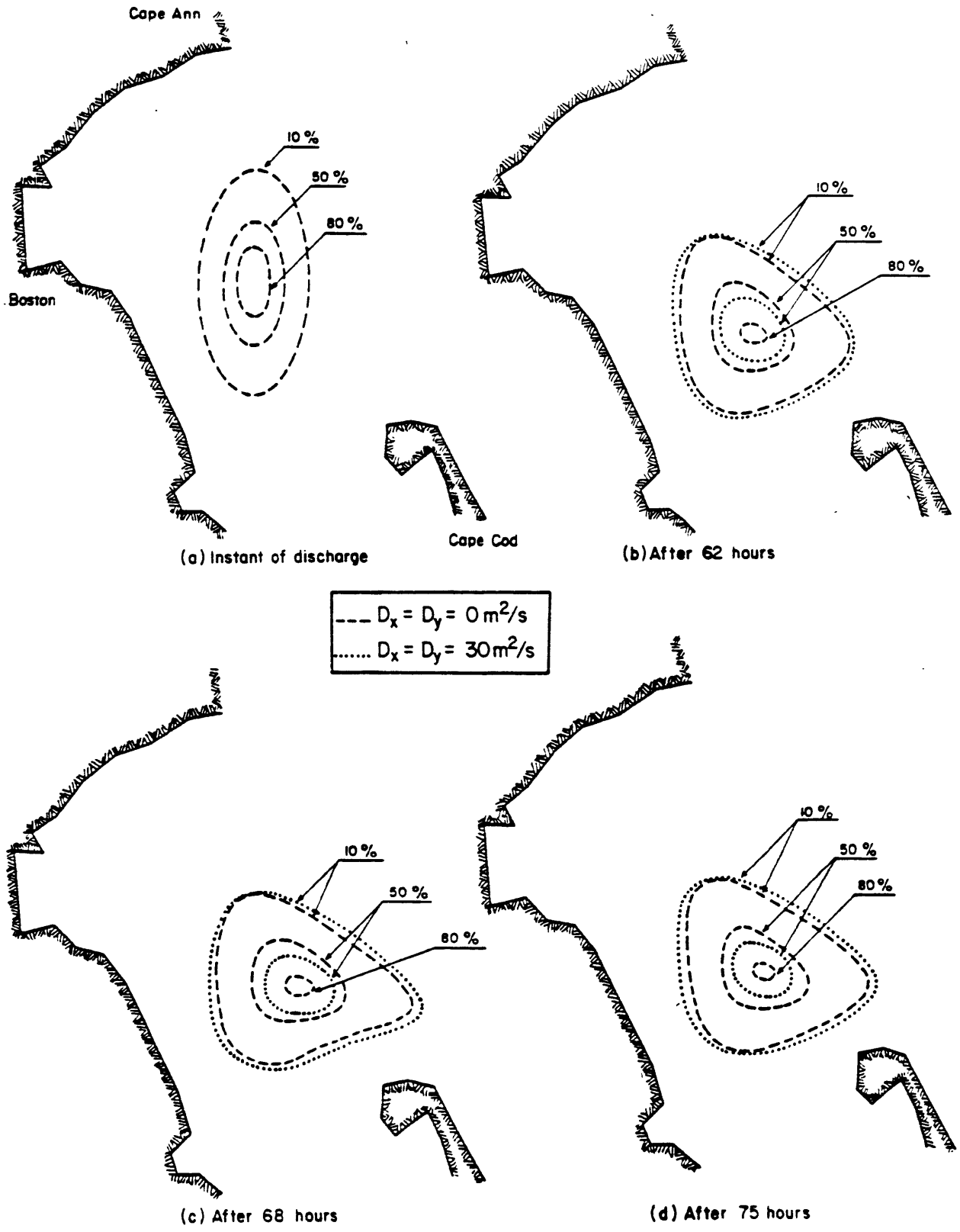

Fig. 6.5 Massachusetts Bay. Sludge plumes for discharge at Site 2.

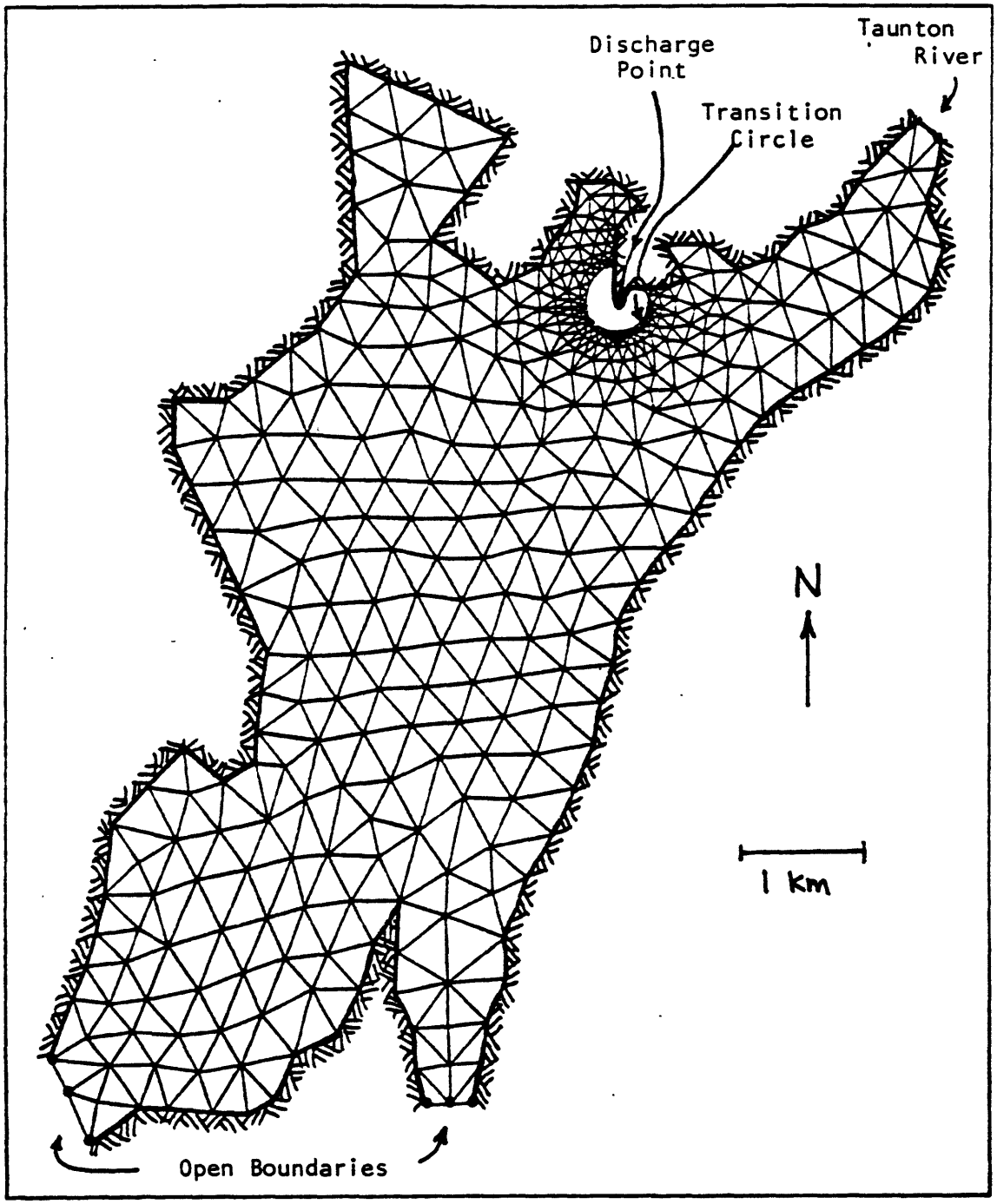

Fig. 6.6 Brayton Point. Complete finite element grid for Mt. Hope Bay.

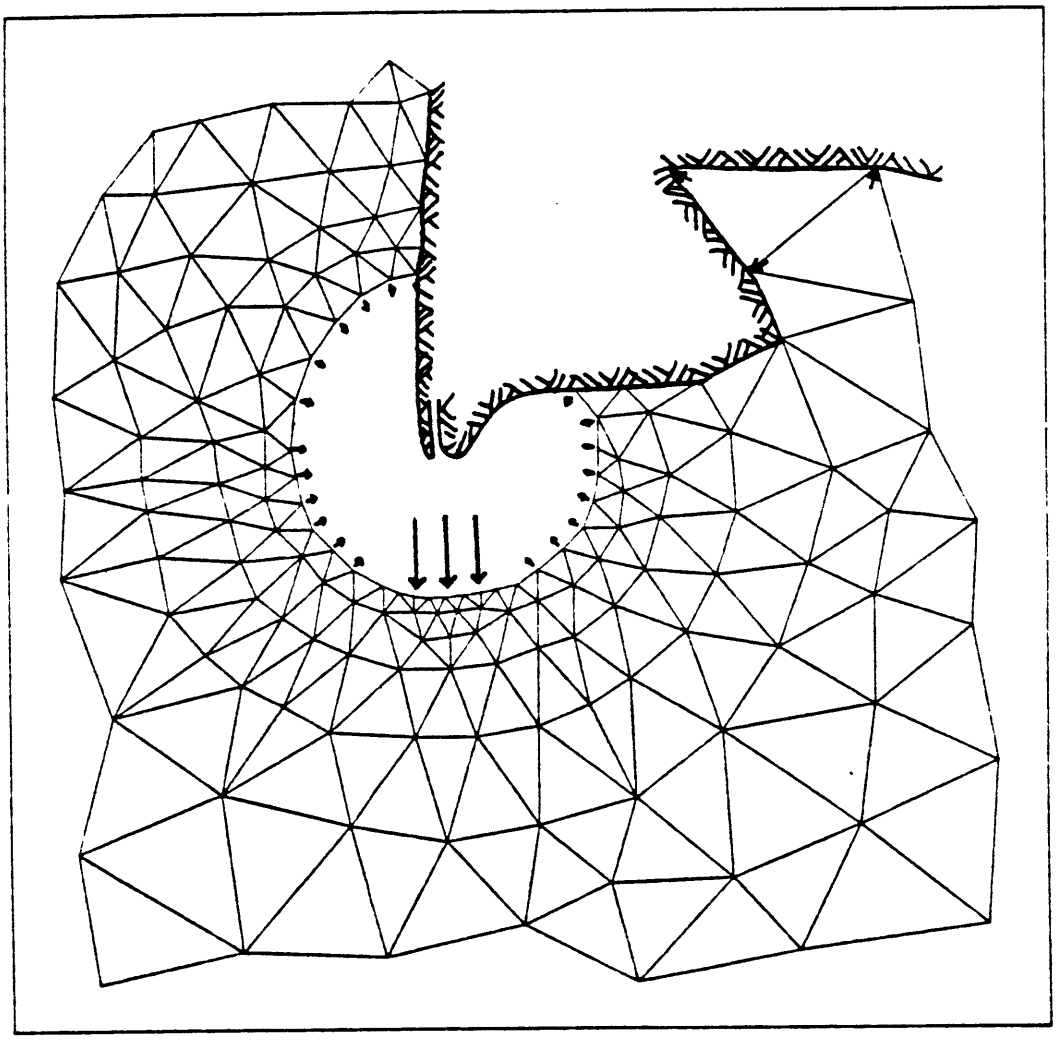

Fig. 6.7 Brayton Point. Detail of the finite element grid near the discharge.

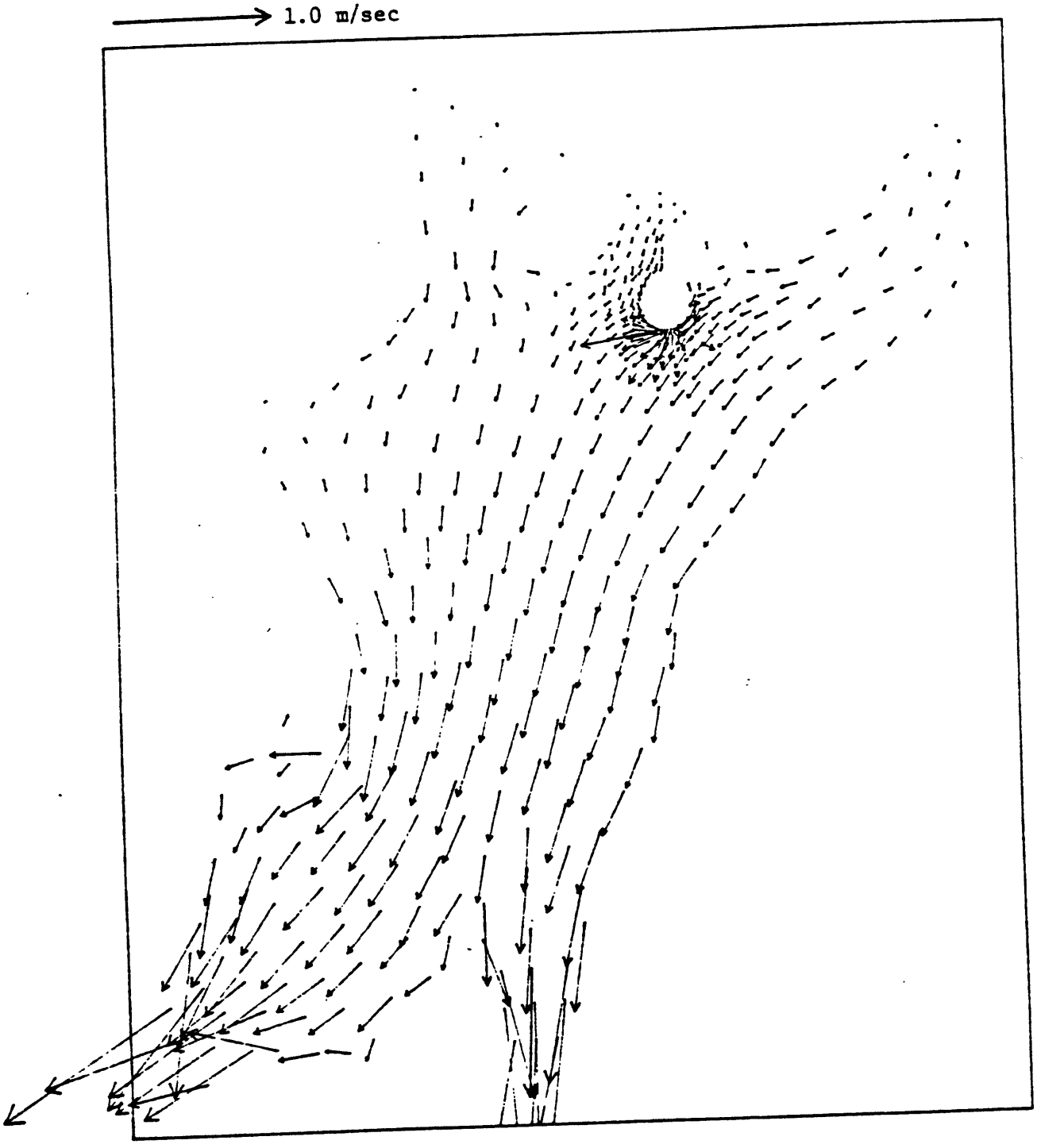

Fig. 6.8 Brayton Point. Circulation computed by TEA at maximum ebb.

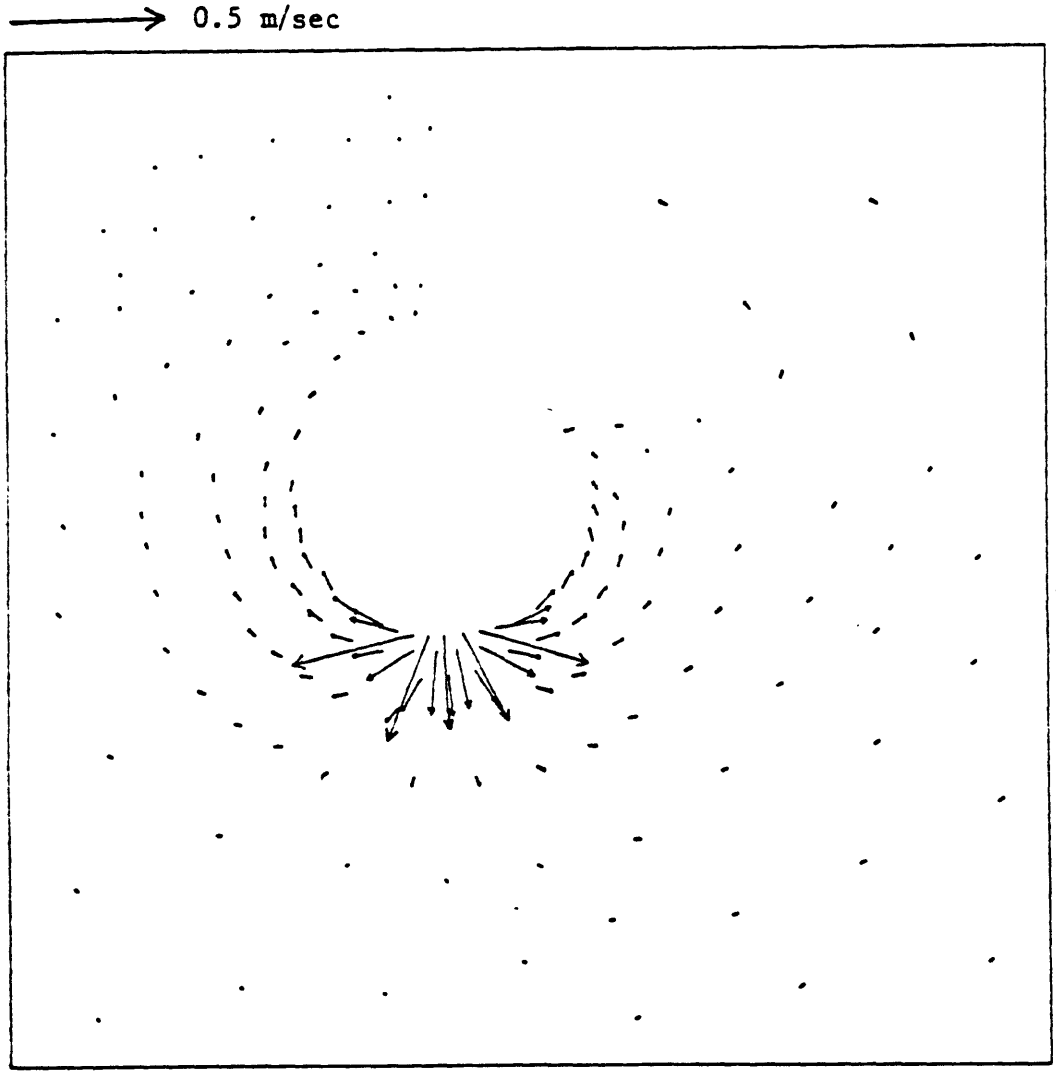

Fig. 6.9 Brayton Point. Detail of circulation computed by TEA at high tide.

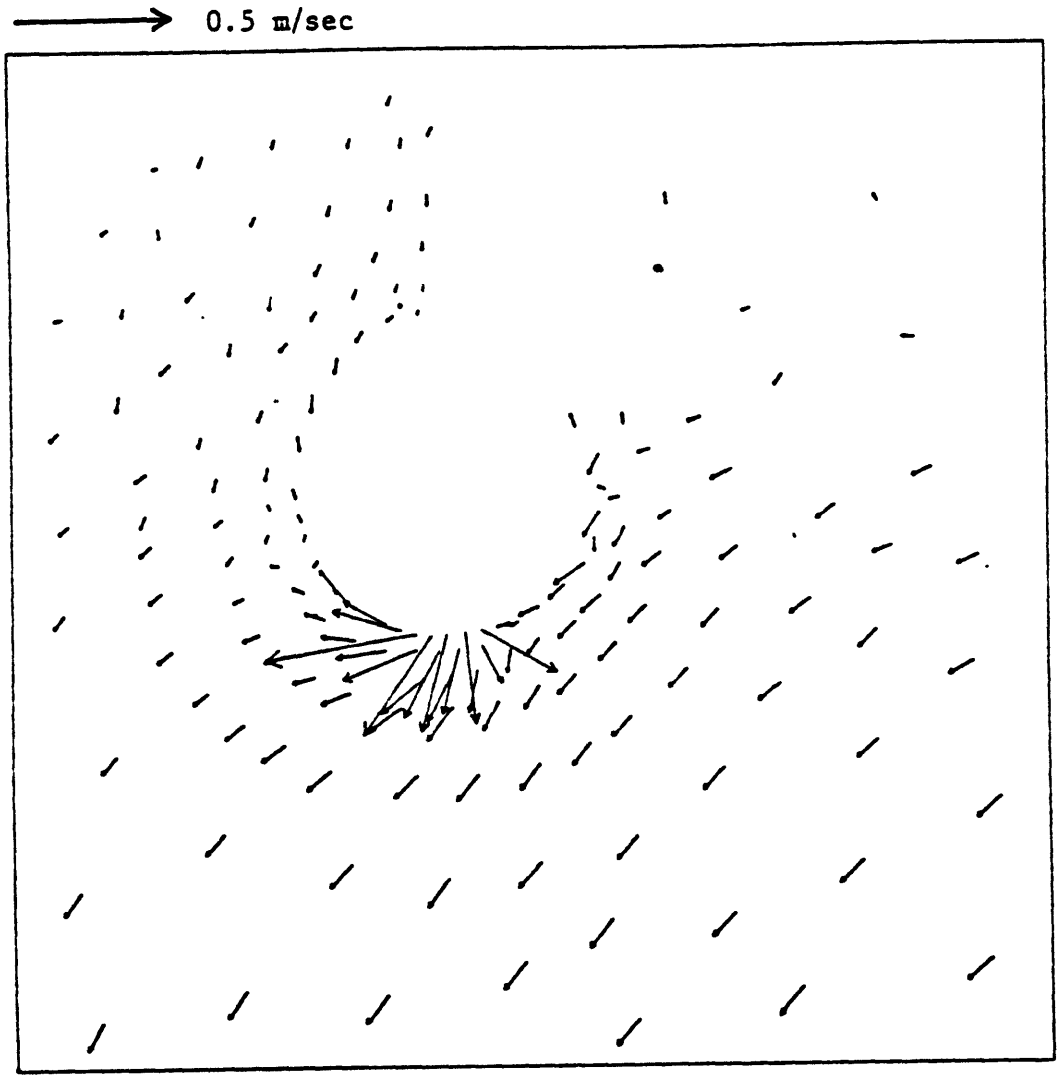

Fig. 6.10 Brayton Point. Detail of circulation computed by TEA at maximum ebb.

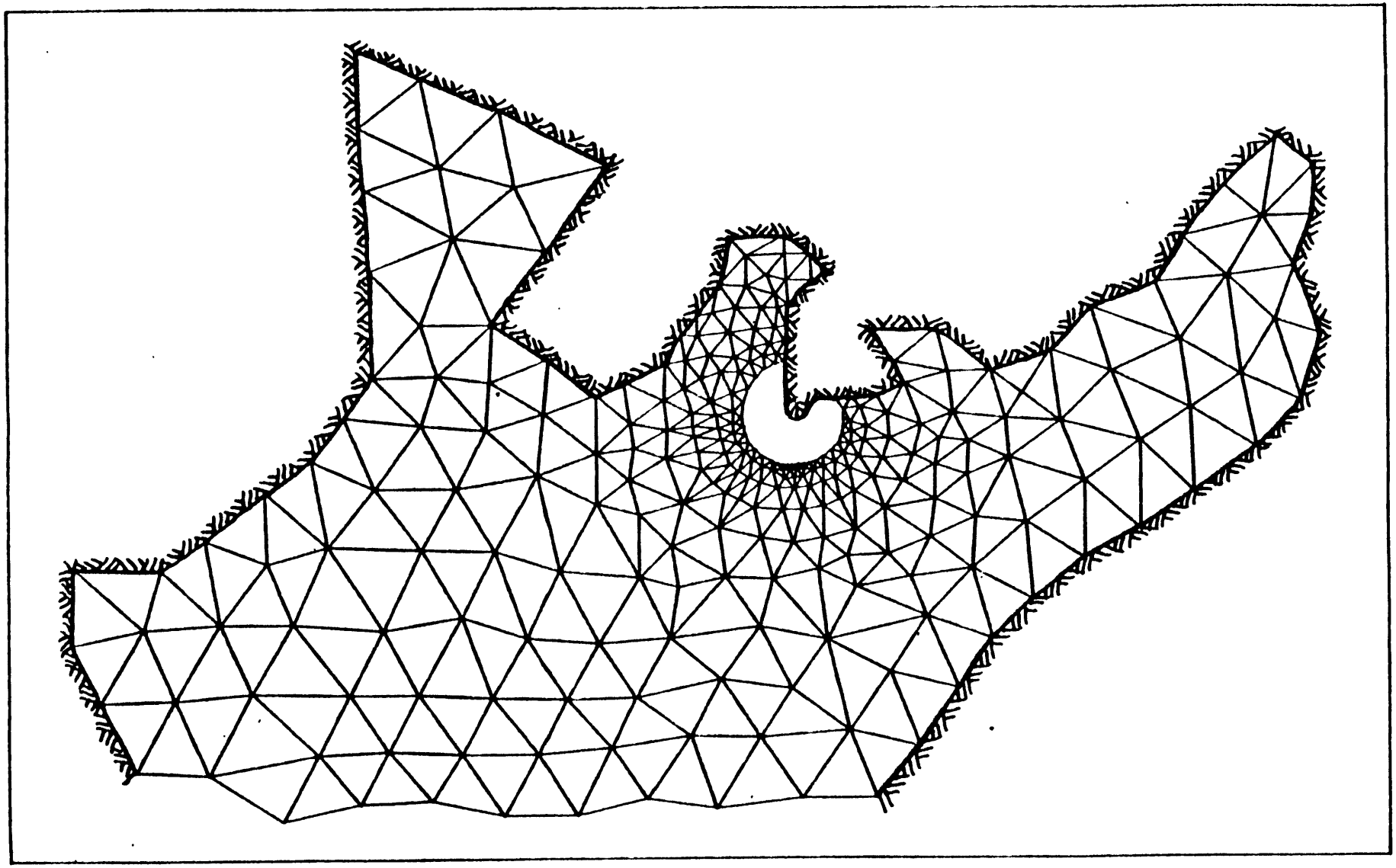

Fig. 6.11 Brayton Point. Finite element grid used for transport calculations.

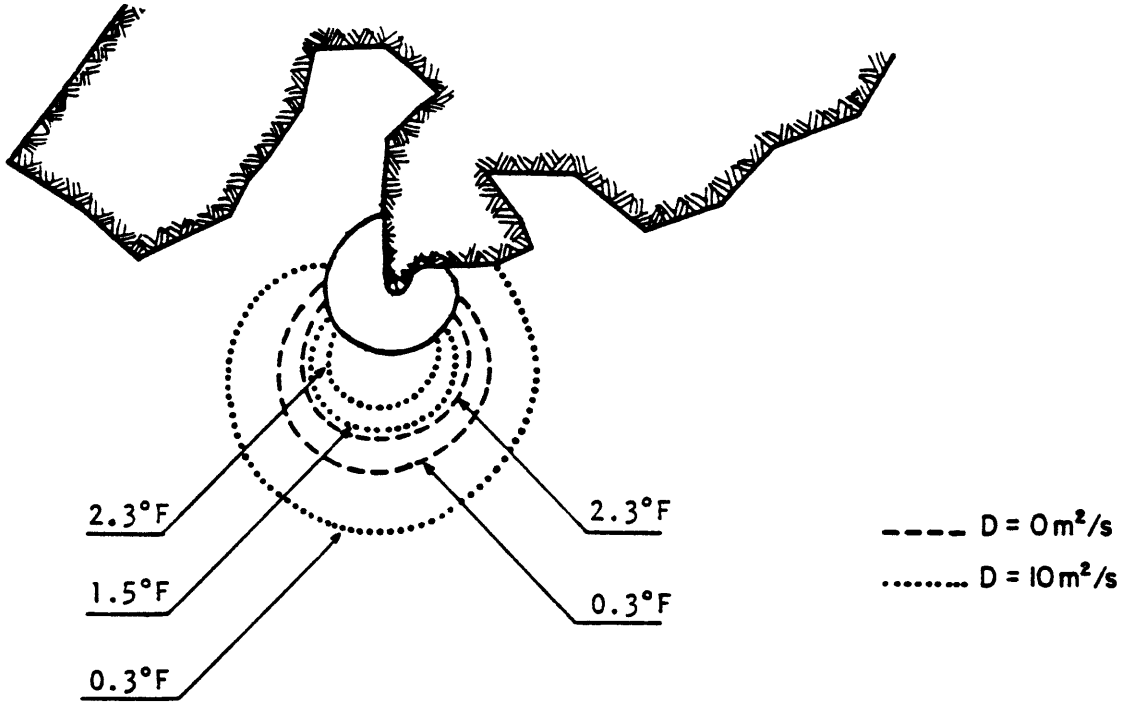

(a) 3 hours after maximum flood (approximately high tide)

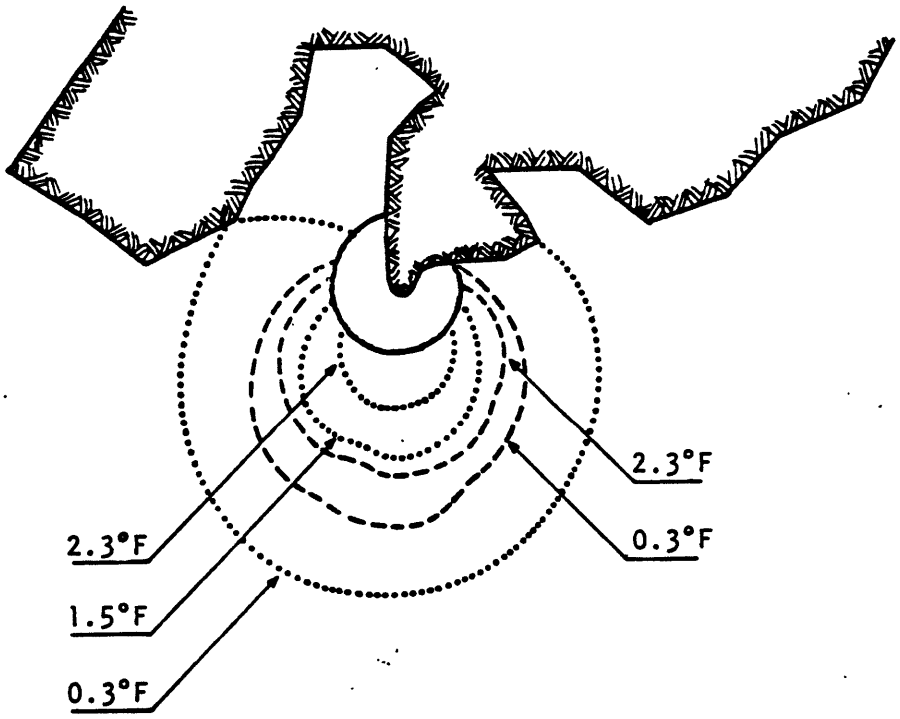

(b) 6 hours after maximum flood (approximately maximum ebb)

Fig. 6.12 Brayton Point. Excess temperature computed at high tide and maximum ebb

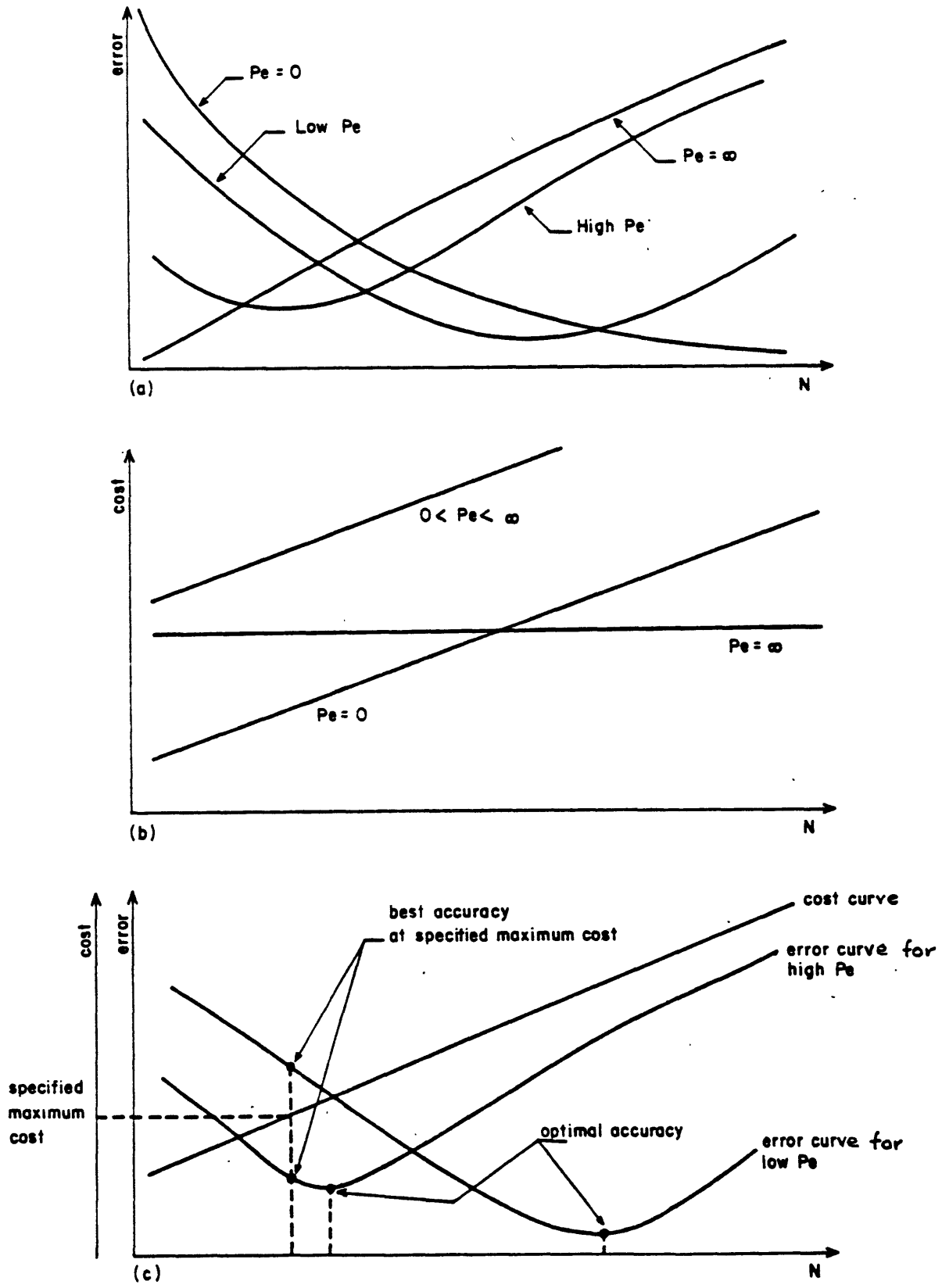

Fig. 7.1 Optimal time step. Illustrative sketches.

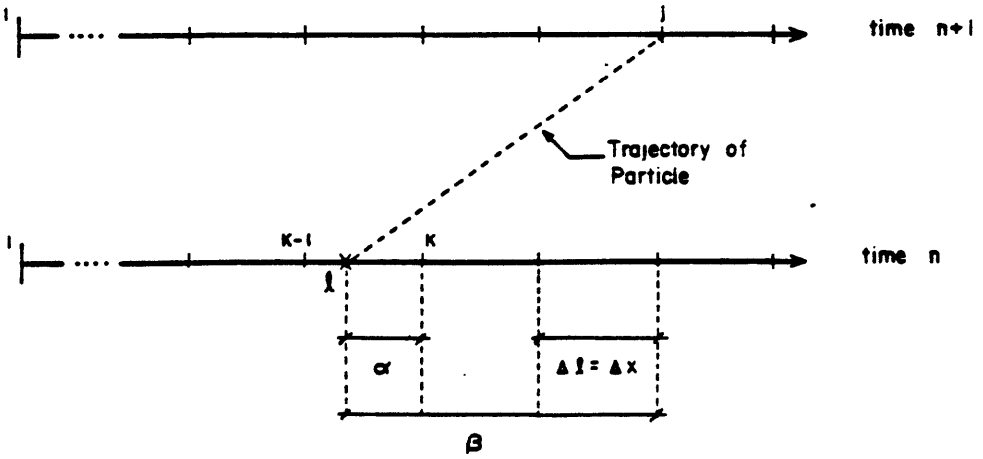

Fig. A.1 Linear discretization scheme.

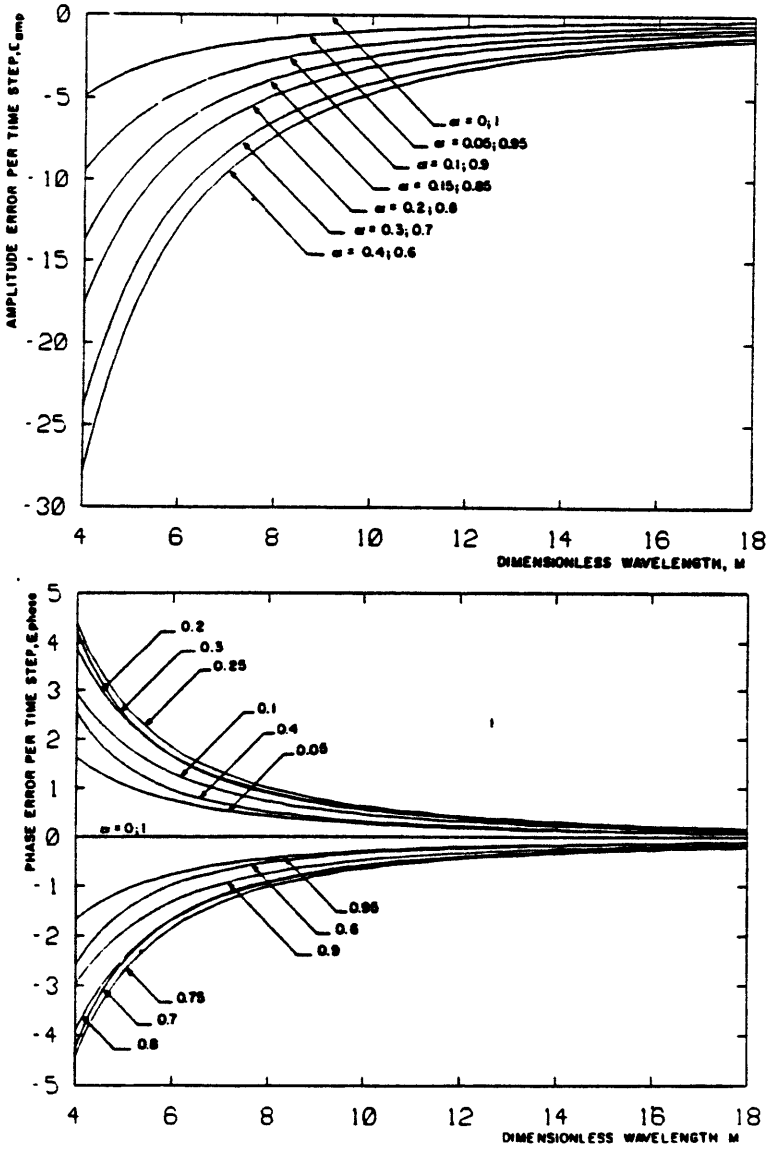

Fig. A.2 Amplitude and phase errors per time step, for 1-D linear expansions.

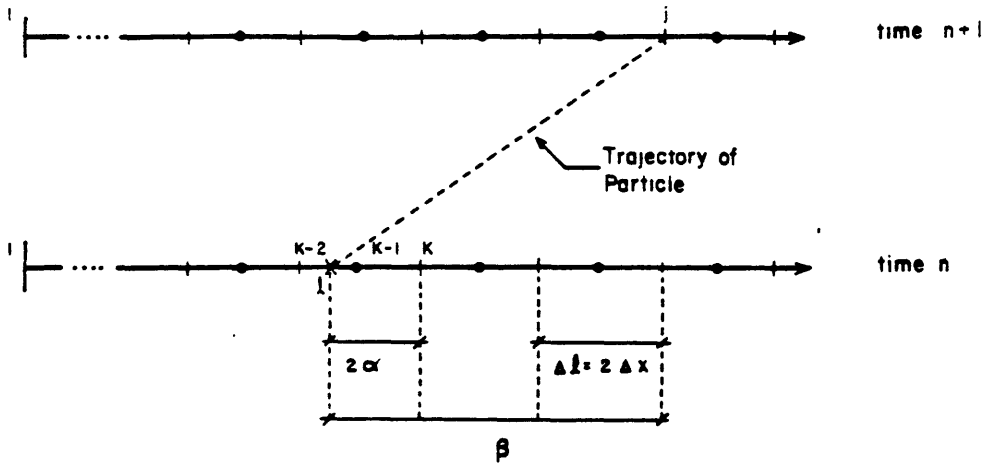

Fig. A.3 Quadratic discretization scheme.

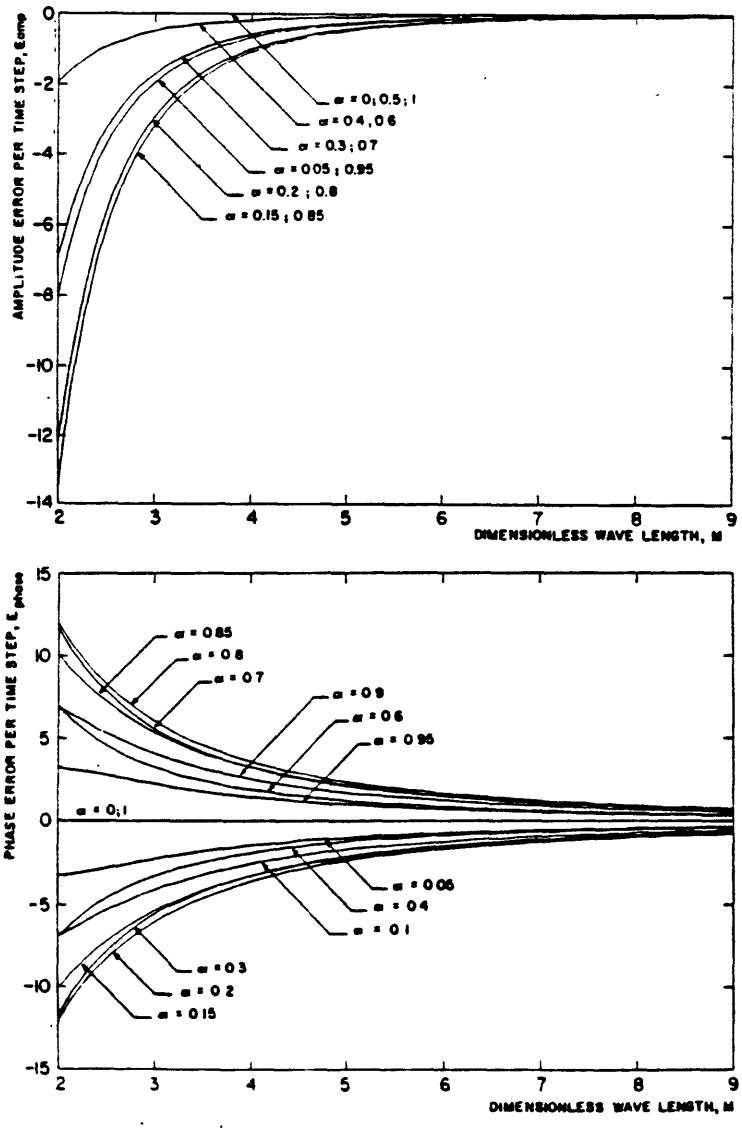

Fig. A.4 Amplitude and phase errors per time step, for 1-D quadratic expansions.

Tables

Table 5.1 - Definition of error measures

Symbol	Description	Definition	Comments	Value for Exact Solution
ϕ	L-2 error norm normalized by the total mass	$\phi(t) = \frac{1}{m(t)}\left\{\int_{\Omega}[c^{nu}(x,y,t) - c^{ex}(x,y,t)]^2 dxdy\right\}^{1/2}$	Integral measure of the overall error of the numerical solution	0
ε	Error in the peak concentration normalized by the exact peak concentration	$\varepsilon(t) = \frac{c^{ex}_{max}(t) - c^{nu}_{max}(t)}{c^{ex}_{max}(t)}$	Point measure of the artifical damping of the numerical solution (numerical damping)	0
ψ	Absolute value of the maximum negative concentration, normalized by the exact peak concentration	$\psi(t) = \left\lvert \frac{c^{nu}_{max,neg}(t)}{c^{ex}_{max}(t)} \right\rvert$	Point measure of the spurious oscillations in the numerical solution (wiggles)	0
ξ	Error in the position of the peak concentration	$\xi(t) = 1 - \frac{x^{nu}_{max}(t)}{x^{ex}_{max}(t)}$	Point measure of the phase shift introduced in the numerical solution	0
μ_o	0th moment of the concentration profile, normalized by the exact value	$\mu_o(t) = \frac{1}{m(t)} \int_{\Omega} c^{nu}(x,y,t)\, dxdy$	Integral measure of mass preservation	1

Table 5.1 - cont.

Symbol	Description	Definition	Comments	Value for Exact Solution
μ_x μ_y	Error in the 1st moments of the concentration profile, normalized by their exact values	$\mu_x(t) = 1 - \dfrac{\int_\Omega x c^{nu}(x,y,t)\,dxdy}{\int_\Omega x c^{ex}(x,y,t)\,dxdy}$ $\mu_y(t) = 1 - \dfrac{\int_\Omega y c^{nu}(x,y,t)\,dxdy}{\int_\Omega y c^{ex}(x,y,t)\,dxdy}$	Integral measures of the phase shifts introduced in the numerical solution	0
μ_{xx} μ_{yy}	Centered 2nd moments of the concentration profile, normalized by the exact value	$\mu_{xx}(t) = \dfrac{\int_\Omega [x - E^{nu}(x)]^2 c^{nu}(x,y,t)\,dxdy}{\int_\Omega [x - E^{ex}(x)]^2 c^{ex}(x,y,t)\,dxdy}$ $\mu_{yy}(t) = \dfrac{\int_\Omega [y - E^{nu}(y)]^2 c^{nu}(x,y,t)\,dxdy}{\int_\Omega [y - E^{ex}(y)]^2 c^{ex}(x,y,t)\,dxdy}$	Integral measure of the artifical spreading of the numerical solution (numerical spreading)	1

Table 5.2 - Convection in a steady uniform flow. Characteristics of the runs

Parameter \ Run	1	2	3	4	5	6	7
u (m/s)	0.5						
'mass', m (m)	$\sqrt{2\pi}\,\sigma_{ox}$						
σ_{ox}^2 (m^2)	2.17778×10^5				1.11111×10^5	3.6×10^5	7.51111×10^5
x_o (m)	3000						5000
L (m)	16000						
W (m)	800						
M	7	7	7	7	5	9	13
$\Delta\ell$ (m)	400						
Δt (s)	128	256	512	1024	128		
$Cu = \frac{u\Delta t}{\Delta\ell}$	0.16	0.32	0.64	1.28	0.16		
$Pe = \frac{u\Delta\ell}{D}$	∞						

Table 5.3 - Convection in a steady uniform flow. Error measures as a function of N ($t \equiv T = 9216$ s; $M = 7$)

Run	N	ϕ	ε	ψ	ξ	μ_o	μ_x	μ_{xx}
1	72	1.399×10^{-4}	0.1287	0.0384	0.0178	0.99998	0.00000	1.00002
2	36	0.773×10^{-4}	0.0762	0.0178	0.0074	1.00002	0.00000	1.00000
3	18	0.369×10^{-4}	0.0377	0.0049	-0.0011	0.99999	0.00000	0.99994
4	9	0.250×10^{-4}	0.0227	0.0022	0.0017	0.99997	0.00000	1.00000

Table 5.4 - Convection in a steady uniform flow. Error measures as a function of M ($t \equiv T = 9216$ s; $N = 72$).

Run	N	ϕ	ϵ	ψ	ξ	μ_o	μ_x	μ_{xx}
5	5	3.027×10^{-4}	0.2505	0.0647	0.0210	1.00003	0.00000	0.99991
1	7	1.399×10^{-4}	0.1287	0.0384	0.0178	0.99998	0.00000	1.00002
6	9	0.695×10^{-4}	0.0671	0.0184	0.0145	0.99998	0.00000	0.99997
7	13	0.218×10^{-4}	0.0219	0.0021	0.0103	0.99998	0.00000	1.00001

Table 5.5 - Convection and diffusion in a steady uniform flow.
Characteristics of the runs.

Run / Parameter	8	9	10	11	12	13	14	15	16	17	18
u (m/s)	0.5										
D (m^2/s)	100	50	20	10	5	20					
'mass', m (m)	$\sqrt{2\pi}\,\sigma_{ox}$										
σ_{ox}^2 (m^2)	2.1778×10^5								1.11111×10^5	3.60000×10^5	7.51111×10^5
x_o (m)	3000										6000
L (m)	16000										
W (m)	800										
M	7								5	9	13
$\Delta\ell$ (m)	400										
Δt (s)	128					256	512	1024	128		
$Cu = \frac{u\Delta t}{\Delta\ell}$	0.16					0.32	0.64	1.28	0.16		
$Pe = \frac{u\Delta\ell}{D}$	2	4	10	20	40	10					

Table 5.6 - Convection and diffusion in a steady uniform flow. Error measures as a function of Pe ($t \equiv T = 9216$ s; $M = 7$; $N = 72$)

Run	Pe	ϕ	ε	ψ	ξ	μ_o	μ_x	μ_{xx}
8	2	0.208×10^{-5}	-0.0026	0.0000	0.0017	0.99997	0.00001	0.99993
9	4	0.565×10^{-5}	0.0020	0.0000	0.0017	1.00003	0.00000	1.00003
10	10	2.320×10^{-5}	0.0203	0.0016	0.0092	0.99997	0.00000	0.99999
11	20	4.954×10^{-5}	0.0459	0.0107	0.0126	0.99997	0.00000	1.00000
12	40	7.960×10^{-5}	0.0742	0.0250	0.0150	1.00002	0.00000	1.00001
1	∞	13.990×10^{-5}	0.1287	0.0384	0.0178	0.99998	0.00000	1.00002

Table 5.7 - Convection and diffusion in a steady uniform flow. Error measures as a function of N ($t \equiv T = 9216$ s; $M = 7$; $Pe = 10$).

Run	N	ϕ	ϵ	ψ	ξ	μ_o	μ_x	μ_{xx}
10	72	2.32×10^{-5}	0.0203	0.00160	0.0092	0.99997	0.00000	0.99999
13	36	1.42×10^{-5}	0.0103	0.00026	0.0049	1.00003	0.00000	0.99999
14	18	0.62×10^{-5}	-0.0025	0.00000	-0.0090	0.99999	0.00000	1.00000
15	9	0.77×10^{-5}	-0.0020	0.00000	0.0000	0.99998	0.00000	0.99999

Table 5.8 - Convection and diffusion in a steady uniform flow. Error measures as a function of M ($t \equiv T = 9216$ s; N = 72, Pe = 10).

Run	M	ϕ	ε	ψ	ξ	μ_o	μ_x	μ_{xx}
16	5	3.27×10^{-5}	0.0290	0.00449	0.01060	1.00004	0.00000	0.99997
10	7	2.32×10^{-5}	0.0203	0.00160	0.00920	0.99997	0.00000	0.99999
17	9	1.59×10^{-5}	0.0135	0.00025	0.00777	0.99998	0.00000	1.00001
18	13	0.75×10^{-5}	0.0061	3.05×10^{-7}	0.00535	1.00002	0.00000	1.00001

Table 5.9 - Convection and diffusion in a sinusoidal flow.
Characteristics of the runs.

Parameter / Run	U_{max} (m/s)	P (s)	D (m^2/s)	'mass', m (m)	σ_{ox}^2 (m^2)	x_o (m)	L (m)	W (m)	M	$\Delta\ell$ (m)	Δt (s)	Cu_{max}	Pe_{max}
19	0.5	9216	10	$\sqrt{2\pi}\ \sigma_{ox}$	2.17778×10^5	8000	16000	800	7	400	128	0.16	20
20			0										∞

Table 5.10 - Convection and diffusion in a sinusoidal flow.
Error measures as a function of time.
(M = 7; N = 288; T = 36866 s)

Run	t (sec)	t/P	ϕ	ϵ	ψ	ξ	μ_o	μ_x	μ_{xx}
19	9216	1.0	2.04×10^{-5}	0.0306	0.0007	0.0009	1.00002	0.00000	1.00002
(Pe=20)	13824	1.5	2.16×10^{-5}	0.0313	0.0016	0.0058	1.00001	0.00021	1.00000
	18432	2.0	1.76×10^{-5}	0.0292	0.0006	0.0003	1.00000	0.00000	1.00002
	27648	3.0	1.45×10^{-5}	0.0259	0.0004	0.0001	1.00002	0.00000	1.00003
	36864	4.0	1.21×10^{-5}	0.0229	0.0002	0.0001	1.00000	0.00000	0.99999
20	4608	0.5	6.23×10^{-5}	0.0509	0.0114	0.0083	0.99999	0.00190	0.99998
(Pe=∞)	9216	1.0	7.83×10^{-5}	0.0978	0.0034	0.0034	1.00001	0.00001	1.00004
	18432	2.0	12.63×10^{-5}	0.1521	0.0014	0.0014	0.99999	0.00000	0.99996
	27648	3.0	16.14×10^{-5}	0.1908	0.0009	0.0009	1.00001	0.00000	0.99996
	36864	4.0	18.90×10^{-5}	0.2207	0.0006	0.0006	1.00006	0.00000	1.00010

Table 5.11 - Convection and diffusion of a continuous source in a steady uniform flow. Characteristics of the runs.

Parameter / Run	U (m/s)	D (m^2/s)	$\dot{m}$ (m/s)	σ_{ox}^2 (m^2)	x_o (m)	L (m)	W (m)	M	$\Delta\ell$ (m)	Δt (s)	Cu	Pe
21	0.5	20	$\frac{\sqrt{2\pi}\,\sigma_{ox}}{\Delta t}$	2.17778×10^5	3000	16000	800	7	400	128	0.16	10
22		5										40
23		1										200

Table 5.12 - Convection and diffusion of a continuous source in a steady uniform flow. Error measures as a function of Pe ($t \equiv T = 9216$ s; $M = 7$, $N = 72$).

Run	Pe	ϕ	μ_o	ψ
21	10	2.64×10^{-6}	0.99999	0.0000
22	40	6.73×10^{-6}	0.99996	0.0000
23	200	9.62×10^{-6}	0.99995	0.0001

Table 5.13 - Diffusion in a depth-variable steady flow.
Characteristics of the runs.

Parameter / Run	D (m^2/s)	h_o (m)	a (m^{-1})	'mass', m (m)	σ_{ox}^2 (m^2)	x_o (m)	L (m)	W (m)	M	$\Delta\ell$ (m)	Δt (s)	Cu	Pe	Interpolation functions for depth, h
24	100	3	0.0003	$\sqrt{2\pi}\sigma_{ox}$	2.17778×10^5	8000	16000	800	7	400	128	0.16	0.12	linear
25			0.003										1.2	linear
26			0.003										1.2	quadratic

Table 5.14 - Advancing front. Characteristics of the runs.

Run	u (m/s)	D (m^2/s)	L (m)	W (m)	$\Delta\ell$ (m)	Δt (s)	Cu	Pe
27	0.05	0.011	2.75	1.10	0.55	1	0.09	2.5
28	0.10	0.44×10^{-3}	2.75	0.22	0.11	1	0.91	25
29	0.15	0.22×10^{-3}	2.75	0.22	0.11	1	1.36	75
30	10^4	1	1.00	0.08	0.04	10^{-5}	2.5	400

Appendix

APPENDIX

FORMAL ACCURACY ANALYSIS OF THE SOLUTION OF CONVECTION IN THE CASE OF A HARMONIC WAVE

A.1 Introduction

We consider the problem of a 1-D harmonic wave (e.g., representing concentrations) being convected by a uniform flow, between times n and n+1, a time step, Δt, apart.

The exact solution is the displacement, following the flow, of the undisturbed wave. Formal comparison of this with the numerical solution obtained by the method described in §4.4 enables the analysis of the accuracy of the method.

As discussed in the text, the method includes the backtracking of particles along characterisitc lines, and the interpolation for concentrations at the foot of each characteristic line. The present analysis assumes that the backtracking is performed exactly; therefore, observed errors result from the interpolation procedure alone.

Two 1-D spatial discretization schemes will be considered, one based on 2-noded elements (over which linear expansions apply), and the other on 3-noded elements (over which quadratic expansions apply).

A.2 Linear Expansion

Consider the linear spatial discretization scheme illustrated in Fig. A.1. At time n+1, the value at node j of a harmonic wave of unit

amplitude may be expressed as:

$$c_{j,n+1} = \exp\{i[\lambda j - \phi_{n+1}]\} \tag{A.1}$$

where λ is a dimensionless wave number, defined as $\lambda = 2\pi\Delta\ell/L$; ϕ_{n+1} is a phase shift, defined as $\phi_{n+1} = \phi_o + \frac{1}{L}\int_o^{t_{n+1}} u\,dt$; $\Delta\ell$ is the element length (constant over the domain); and L is the wavelength.

As convection alone is being considered, the exact value of the harmonic at (j,n+1) is equal to the value of the same harmonic at (ℓ,n) where ℓ is the position, at time n, of the particle that is at node j, at time n+1. Therefore

$$c_{j,n+1} = c_{\ell,n} = \exp\{i[\lambda\ell - \phi_n]\} \tag{A.2}$$

or, as $\ell = j-\beta \equiv K-\alpha$,

$$c_{j,n+1} = \exp(-i\lambda\alpha)\,\exp\{i(\lambda K - \phi_n)\} \tag{A.3}$$

where α is the decimal part of the dimensionless displacement, β, of a particle between instants n and n+1 (Fig A.1); note that, in the case of a steady flow, β coincides with the Courant number, $Cu = u\Delta t/\Delta\ell$.

Now, if the harmonic wave is known only at time n, and we use the method described in §4.4 to compute values at time n+1, we obtain (because linear expansions apply over each element)

$$c^{nu}_{j,n+1} = c^{nu}_{\ell,n} = (1-\alpha)\,c_{K,n} + \alpha\,c_{K-1,n} \tag{A.4}$$

Eq. (A.4) may be expanded using the definition of $c_{K,n}$ and $c_{K-1,n}$. We obtain, after rearrangement

$$c_{j,n+1} = \{(1-\alpha) + \alpha \exp(-i\lambda)\} \exp\{i(\lambda K - \phi_n)\} \tag{A.5}$$

Comparison of Eqs. A.3 and A.5 shows that the interpolation required to find $c^{nu}_{j,n+1}$ introduces errors in both the amplitude and the phase of the wave. Normalized measures of such errors may be defined as

$$\varepsilon_{amp} = \frac{\left|c^{nu}_{j,n+1}\right| - \left|c_{j,n+1}\right|}{\left|c_{j,n+1}\right|} \tag{A.6}$$

$$\varepsilon_{phase} = \frac{\arg\{c^{nu}_{j,n+1}\} - \arg\{c_{j,n+1}\}}{\lambda} \tag{A.7}$$

Introducing Eqs. A.3 and A.5 into the above equations, expanding and rearranging, we obtain

$$\varepsilon_{amp} = \{[1-\alpha(1-\cos\lambda)]^2 + (\alpha\sin\lambda)^2\}^{1/2} - 1 \tag{A.8}$$

$$\varepsilon_{phase} = \frac{1}{\lambda}\left\{\arctan\left[\frac{-\alpha\sin\lambda}{1-\alpha(1-\cos\lambda)}\right] + \lambda\alpha\right\} \tag{A.9}$$

The amplitude and phase errors, given by Eqs. A.8 and A.9 are shown in Fig. A.2 as a function of the dimensionless wave length $M = L/\Delta\ell \equiv 2\pi/\lambda$, for different values of α.

A.3 Quadratic Expansion

Consider now the quadratic discretization illustrated in Fig. A.3. Following the same approach as in §A.2, we find

$$\varepsilon_{amp} = \left\{ [a\sin(2\lambda) + b\sin\lambda]^2 + [a\cos(2\lambda) + b\cos\lambda + d]^2 \right\}^{1/2} - 1 \qquad (A.10)$$

$$\varepsilon_{phase} = \frac{1}{\lambda} \left\{ \arctan\left[- \frac{a\sin(2\lambda) + b\sin\lambda}{a\cos(2\lambda) + b\cos\lambda + d} \right] + 2\alpha\lambda \right\} \qquad (A.11)$$

with

$$a = (2\alpha-1)/2d \qquad (A.12)$$

$$b = 4\lambda(1-\alpha) \qquad (A.13)$$

$$c = (1-2\alpha)(1-\alpha) \qquad (A.14)$$

The amplitude and phase errors given by Eqs. A.10 and A.11 are shown in Fig. A.4, as a function of the dimensionless wavelength, M, for different values of α.